

Design of High-Capacity Fiber-Optic Transport Systems



by

Zhi Ming Liao

Submitted in Partial Fulfillment
of the
Requirements for the Degree
Doctor of Philosophy

Supervised by
Professor Govind P. Agrawal

The Institute of Optics
The College
School of Engineering and Applied Sciences

University of Rochester
Rochester, New York

2001

dedicated to
Mom, Dad, ZJ, and Grandma

Curriculum Vitae

The author was born in Canton, China. He immigrated with his family to Florida when he was eleven. He learned English at Nova middle school and then graduated as the valedictorian of Lake Worth high school class of 1991. He enrolled at the University of Rochester as a Bausch-Lomb scholar and graduated with a degree in optical engineering and a minor in Electrical Engineering with High Distinction in 1995. He received the School of Engineering and Applied Science's Hook's award for displaying exemplifying interest in the engineering disciplines and for his active involvement in the various student engineering societies including the IEEE (president), OSA (vice-president), and Tau Beta Pi. Encouraged by the Optics faculty, he joined the PhD. program at the University of Rochester in the fall of 1995. He was awarded a Master of Science in Optics in 1996. During the course of his education at Rochester, he also spent summers working in Lawrence Livermore National Laboratory (1994 – 1996) and Los Alamos National Laboratory (1999) performing research ranging from implementing optical testing techniques to modeling soliton dynamics.

Publications

- Z. M. Liao and G. P. Agrawal, "Role of Distributed Amplification in Designing High Capacity Soliton Systems," *IEEE Photonics Technology Letters*, Submitted for Review (2000).
- Z. M. Liao and G. P. Agrawal, "Mode-Partition Noise in Fiber Lasers," *Electronics Letters*, **36**, 1188-1189 (2000).
- Z. M. Liao, C. J. McKinstrie, and G. P. Agrawal, "Importance of Prechirping in Constant-Dispersion Fiber Links with a Large Amplifier Spacing," *Journal of Optical Society of America B*, **17**, 514-518 (2000).
- Z. M. Liao and G. P. Agrawal, "High-Bit-Rate Soliton Transmission Using Distributed Amplification and Dispersion Management,"; *IEEE Photonics Technology Letters*, **11**, 818-820 (1999).
- J. Inman, S. Houde-Walter, B. McIntyre, Z. M. Liao, R. Parker, and V. Simmons, "Chemical Structure and the Mixed Mobile Ion Effect in Ag-for-Na Ion Exchange in Aluminosilicate Glasses," *Journal of Noncrystalline Solids*, **191**, 85-92 (1996).
- Z. M. Liao, S. J. Cohen and J. R. Taylor, "Total Internal Reflection Microscopy (TIRM) as a Nondestructive Subsurface Assessment Tool," *Proceedings of Annual Symposium on Optical Materials for High Power Lasers*, Boulder, CO. October 1994.

Presentations

- G. P. Agrawal and Z. M. Liao, "Mode-partition noise in fibre lasers," OSA Annual Meeting, Rhode Island, October 2000.
- Z. M. Liao and G. P. Agrawal, "Distributed Amplification," Invited talk, Corning, NY, June 2000.
- Z. M. Liao, "Implementation of Distributed Amplification for High Speed Soliton Transmission," Institute of Optics Industrial Associate's Meeting, Rochester, NY, October 1999.
- Z. M. Liao, C. J. McKinstrie, G. P. Agrawal "A Novel Operating Regime for Periodically Amplified Fiber Links: Role of Prechirping," OSA Annual Meeting, Santa Clara, CA, October 1999.
- Z. M. Liao and I. Gabitov, "Slow Dynamics of Optical Pulse in Optical Fibers," Summer seminar series, Los Alamos, NM, August 1999.
- Z. M. Liao and G. P. Agrawal, "Design of Soliton Communication Systems using Distributed Amplification," OSA Annual Meeting, Baltimore, MD, October 1998.

Acknowledgments

It may be challenging to fill 100 pages of technical material for this thesis, but it certainly would be a breeze to fill 100 pages to acknowledge all of the people who made this possible. Actually, the difficulty has been to reduce the list to a reasonable size, so I would like to apologize in advance to anyone I may have forgotten due to my deteriorating mental prowess. This is the price one must pay for a higher education. :-)

Mind: Since this is a scientific thesis, I would like to first thank those who have labored to educate me. I would like to acknowledge Dr. Taras I. Lakoba for his guidance in the realm of mathematics, Dr. Drew N. Maywar for being the best possible office-mate, and Dr. Rene Essiambre for introducing me to numerical simulations. For taking time off their busy lives to help proof read my thesis, I would like to thank the following individuals: Stephanie Chen, Falgun Patel, Drew Maywar, Gina Jones, Shafique Jamal and Kunal Kishore. I would also like to thank Professor Colin J. McKinstrie for his help with variational analysis. Last and certainly not the least, I am gratefully indebted to Professor Govind P. Agrawal, for his inhuman patience, boundless knowledge, and above all, kind guidance.

Body&Spirit: I would like to thank Joan Christian, Gayle Thompson, and all the staff at the Institute of Optics for making the place more like a home than a work place.

I like to thank my mentors: Simon Cohen for taking me under his wings at LLNL, Dr. Ildar Gabitov for his guidance at LANL, and Dr. Falgun Patel for instructing me the important technique of double-shaded boxes.

First of all, I would like to state that a moron does a body good. Without the morons, graduate school would not have been so enjoyable. I like to thank the Bean, Bhanu, Dave, KB, Gaby, Paul, Pete, Stephyjo and Steve for making Rochester a fun place to live !

For Stephanie Chen, whose advice, friendship, and yes, being a bully were, I am going have to create a new word here, "inrepayable", in the completion of this degree. I can't ever repay you, Steph, and I won't, so don't ask. :-)

My best bud, Anando Anwar Chowdhury, for always being there; for laughter, for understanding, for making me part of his family, and for being half of "zandy", a true kindred spirit.

Lastly, Christine Thao La for her dedication in making my graduate life as challenging as possible. She compensates that by breathing love into my life.

Soul: Mom, Dad, Jing and Grandma, the foundation in which everything in my life is based on.

Abstract

We study the design of fiber-optic transport systems and the behavior of fiber amplifiers/lasers with the aim of achieving higher capacities with larger amplifier spacing.

Solitons are natural candidates for transmitting short pulses for high-capacity fiber-optic networks because of its innate ability to use two of fiber's main defects, fiber dispersion and fiber nonlinearity to balance each other. In order for solitons to retain its dynamic nature, amplifiers must be placed periodically to restore powers to compensate for fiber loss. Variational analysis is used to study the long-term stability of a periodical-amplifier system. A new regime of operation is identified which allows the use of a much longer amplifier spacing.

If optical fibers are the blood vessels of an optical communication system, then the optical amplifier based on erbium-doped fiber is the heart. Optical communication systems can avoid the use of costly electrical regenerators to maintain system performance by being able to optically amplify the weakened signals. The length of amplifier spacing is largely determined by the gain excursion experienced by the solitons. We propose, model, and demonstrate a distributed erbium-doped fiber amplifier which can

drastically reduce the amount of gain excursion experienced by the solitons, therefore allowing a much longer amplifier spacing and superior stability.

Dispersion management techniques have become extremely valuable tools in the design of fiber-optic communication systems. We have studied in depth the advantage of different amplification schemes (lumped and distributed) for various dispersion compensation techniques. We measure the system performance through the Q factor to evaluate the added advantage of effective noise figure and smaller gain excursion.

An erbium-doped fiber laser has been constructed and characterized in an effort to develop a test bed to study transmission systems. The presence of mode-partition noise in an erbium-doped fiber laser was experimentally demonstrated. A numerical model has been developed using the Langevin rate equations and its predictions are in qualitative agreement with experimental data.

Table of Contents

1	Introduction	1
1.1	Motivation	1
1.2	Historical Overview	3
1.2.1	Fiber-Optic Communication Systems	3
1.2.2	Optical Solitons	5
1.3	Thesis Overview	7
1.3.1	Principle of Fiber-Optic Communication Systems	7
1.3.2	Outline	9
2	Theoretical Foundation	11
2.1	Introduction	11
2.2	Wave Propagation Equation	11
2.2.1	Dispersion	19
2.2.2	Fiber Loss	21
2.2.3	Nonlinear Schrödinger Equation	22

2.3	Optical Solitons	24
2.4	Split-Step Fourier Transform Method	26
2.5	Variational Technique	29
2.6	Summary	32
3	Chirped Solitons in Constant-Dispersion Fiber Links	33
3.1	Introduction	33
3.2	Guiding-Center Solitons	34
3.3	Pre-Chirped Solitons	37
3.3.1	Variational Results	38
3.3.2	Analytical Results	40
3.4	Numerical Results	41
3.5	Summary	47
4	Distributed Amplification in Constant-Dispersion Systems	49
4.1	Introduction	49
4.2	Erbium-Doped Fiber Amplifiers	50
4.3	Distributed Erbium-Doped Fiber Amplifiers	53
4.3.1	Modeling Gain in Distributed Fiber Amplifiers	53
4.3.2	Small-Signal Solution	54
4.3.3	Numerical Solution	56
4.4	Raman Amplifier	58

4.4.1	Small Signal Analysis	60
4.4.2	Numerical Results	60
4.5	Amplifier Performance	62
4.6	Summary	65
5	Dispersion-Management Systems	67
5.1	Introduction	67
5.2	Dispersion Managed Soliton	69
5.2.1	Variational Analysis	69
5.2.2	Two-Step Dispersion Map	70
5.2.3	Dense Dispersion Management	73
5.3	System Performance	75
5.3.1	Amplifier Noise	75
5.3.2	Numerical Results	76
5.4	Summary	81
6	Fiber Lasers	83
6.1	Introduction	83
6.2	Experimental Setup	83
6.2.1	Output Power	84
6.2.2	Frequency Characteristics	85
6.3	Mode-Partition Noise	86

6.3.1	Experimental Observation	87
6.3.2	Mode-Partition Noise Theory	88
6.4	Summary	91
7	Conclusions	93
7.1	Overview	93
7.2	Constant-Dispersion Fibers	93
7.3	Dispersion-Management Technique	96
7.4	Fiber-Laser Dynamics	97
7.5	Summary	97
	Bibliography	99
A	Calculating Pulse Parameters	105
A.1	Gaussian Pulse	105
A.2	Hyperbolic Secant Pulse	107
B	Bit-Error Rate	109

List of Tables

2.1	Parameters used in simulation of pulse broadening	20
2.2	Parameters used in simulation of pulse spectrum broadening	24
2.3	Parameters used in simulation of soliton propagation	26
3.1	Parameters used in simulation of soliton propagation	37
6.1	Parameters used in simulation of fiber laser dynamics	90

List of Figures

1.1	Capacity growth of fiber-optic communication systems.	5
1.2	Basic elements of a fiber-optic communication system	7
1.3	Optical bit stream using NRZ and RZ formats	8
2.1	Pulse spreading due to GVD	21
2.2	Pulse spreading due to GVD in the presence of fiber loss	22
2.3	Spectral broadening of optical pulse due to SPM	25
2.4	Soliton pulse propagation	27
2.5	Split-step Fourier transform method	28
3.1	Amplitude variations of lumped amplification with $L_A=20$ km and 0.2 dB/km loss.	36
3.2	Evolution of guiding-center soliton	38
3.3	Periodicity of soliton pulse through each amplifier unit	39
3.4	Power and chirp requirements for propagation	42
3.5	Pulse evolution over single amplifier period	44

3.6	Pulse evolution over single amplifier period	45
3.7	Pulse evolution over multiple amplifier periods	46
3.8	Pulse evolution over multiple amplifier periods	47
3.9	Poincaré map of pulse stability	48
4.1	Three level model of erbium-doped gain medium	50
4.2	Distributed-erbium doped amplifier link	53
4.3	Bi-directional pumping of d-EDFA	54
4.4	Analytical and numerical solution of the forward, backward, and total pump powers	57
4.5	Pump power needed for various dopant levels	58
4.6	Maximum net gain for various dopant levels	59
4.7	Pump power and gain variations of Raman amplifier	61
4.8	Pulse evolution in lumped and distributed amplification	63
4.9	Logarithmic plot of the pulse using distributed amplification	64
4.10	Pump power and gain variations of d-EDFA	65
5.1	Two-step dispersion map	70
5.2	Dense dispersion map	74
5.3	Eye diagram of a 20-Gb/s system	77
5.4	System performance of a 40-Gb/s DM soliton system using different amplification schemes.	79
5.5	Spatial gain distribution of different amplification schemes	80

5.6	System performance of a 80-Gb/s DM soliton system using different amplification schemes.	81
5.7	Pulse interaction for 80-Gb/s soliton system	82
6.1	Experimental configuration of the fiber laser	84
6.2	Output power vs. pump current for the fiber laser	85
6.3	Output power vs. pump power for the fiber laser	86
6.4	Spectrum of the pump output	87
6.5	Spectrum of the fiber laser output	88
6.6	Experimental observation of mode-partition noise	89
6.7	Simulation result of mode-partition noise	91

Chapter 1

Introduction

1.1 Motivation

The era of the information revolution is upon us. The internet has brought the world closer together. Although voice traffic continues to grow at merely 3 to 5% per year, the increase in data traffic will continue to expand global networks at an estimated rate of 10 to 25 times over the next few years [1]. This demand for high-bit-rate communication systems has heralded fiber-optical lightwave systems as the savior, primarily because of the extremely broad bandwidth associated with an optical carrier. This is because the frequency of an optical carrier (~ 100 THz) is five orders of magnitude greater than the frequency of a microwave carrier (~ 1 GHz) [2] and since the modulation bandwidth is usually limited to a small fraction of the carrier frequency in digital systems, this translates to roughly 100,000 times more capacity for a fiber optic communication system. Despite this tremendous increase in system capacity, it barely able to keep up with today's demand.

Optical fibers are considered by many as God-sent for optical communications because of their many wonderful features: wave-guiding, low loss, and small nonlinearity. However, as a system grows in capacity, its complexity also grows. Even though a

modern optical fiber suffers only a fraction of decibals (dB) per kilometer (km) of loss, system lengths of hundreds and thousands of kilometers will accumulate enough losses to demand the need of amplifiers. The introduction of erbium-doped fiber amplifiers (EDFAs) [3] in the early 1990s made it possible to support systems with capacity of tens and hundreds of gigabits per second (Gb/s) with an amplifier spacing of 50-100 km. Amplifiers need to be placed more frequently as system capacity increases when solitons are used since the dispersion length scales quadratically with soliton width. Thus, the demand on increasing capacity is causing the amplifier spacing to become shorter, which can drive the cost so high that the solution will become impractical. The placement of amplifier modules is therefore crucial in the design of high-capacity fiber optic systems.

Furthermore, the performance of these high-capacity systems are often limited by the lumped nature of the amplifiers. An alternative approach using distributed amplification has become an exciting new avenue to explore. Distributed amplification using stimulated Raman scattering (SRS) has already helped to produce terabits per second system capacity (Tb/s) as well as longer transmissions distances without regeneration [4–7]. In addition, the recent development of high power fiber/semiconductor pump lasers will make distributed amplification an even more attractive option for future systems. The synthesis of distributed amplification into existing system architecture with current technologies such as dispersion management and wavelength-division multiplexing (WDM) will bring forth the next generation of ultra-high-capacity fiber optic communication systems.

This thesis explores the placement and design of optical amplifiers in constant-dispersion systems as well as in dispersion management systems, and seeks to optimize

the existing technology and to advance future technologies in the design of ultra-high-capacity fiber-optic systems. A history of the evolution of optical communication is presented next.

1.2 Historical Overview

Solitons have a rich history that dates all the way back to the early 1800s even though fiber-optic communication systems have been in existence for less than 25 years. These temporally separated entities are on course to collide and create the next generation of ultra-high-capacity communication systems.

1.2.1 Fiber-Optic Communication Systems

The development of lasers in the 1960s and low loss fibers in the early 1970s made possible the first fiber-optic communication system in 1978. These systems were able to transmit signals at 100 Mb/s using multimode fibers operating near $0.85 \mu\text{m}$. Although the repeater spacing was less than 10 km, it was sufficiently large than the repeater spacing of the heritage coaxial system. This feature made fiber optic communication system an attractive alternative for the future — thus the first generation of fiber-optic systems was born [2].

The desire to reduce the number of regeneration units by increasing the repeater spacing of the first generation systems quickly lead to the second generation system in the early 1980s. The second generation system allowed for increased repeater spacing by operating the system at the lower loss regime near $1.3 \mu\text{m}$. Additional improvements were also made in optical fiber technology by the introduction of the single-mode fiber;

this soon propelled the system capacity to Gb/s with repeater spacings in excess of 50 km. The system operation wavelength was further moved to $1.55 \mu\text{m}$ to take advantage of the lowest fiber loss for the third generation system introduced in the late 1980s. The increased propagation distance allowed by lower fiber loss and the larger fiber dispersion at $1.55 \mu\text{m}$ introduced fiber dispersion as the next obstacle to tackle. The dispersion problem was eventually solved by using dispersion-shifted fibers and single longitudinal mode lasers to reduce the spreading of the transmitted pulse. Such systems can operate in excess of 10 Gb/s with repeater spacings as large as 100 km [2].

The early generations of fiber-optic systems relied on repeaters to compensate fiber loss through electrical amplification. These regeneration stations consisted of decoders to transform the information from an optical domain to an electrical domain, electronic amplifiers to reboost the signal, and transmitters to re-transform the information from the electrical domain back to the optical signal. This process was an expensive necessity. The development of EDFAs during the 1990s provided a breakthrough which allowed pulses to be optically amplified thus reducing the need of so many regeneration stations. This dramatically reduced the cost while provided a very dynamic and transparent solution. Optical amplifiers have paved the way to another ground-breaking technology — WDM. The WDM technique offered the ability to scale the system capacity via the same fiber by simply adding data channels using slightly different wavelengths [2]. The fourth generation systems boasted capacity of upwards of terabits per second (Tb/s) — yet, the demand is still increasing.

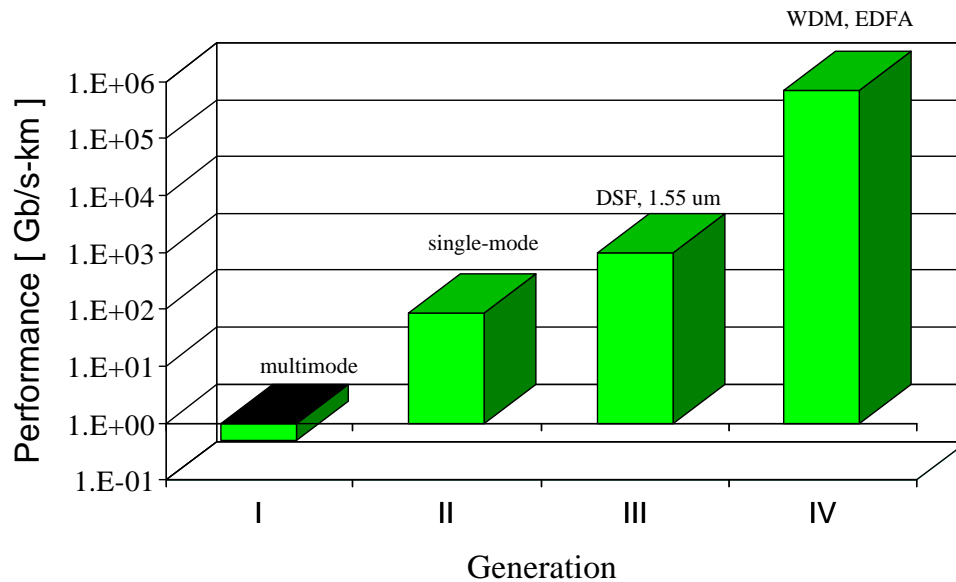


Figure 1.1: Capacity growth of fiber-optic communication systems.

1.2.2 Optical Solitons

Solitary water waves were first discovered by Scott Russell in 1834 and remained a mathematical curiosity for over 100 years. It was not until 1965 before the word “soliton” was coined by Zabusky and Kruskal [8]. The inverse-scattering method was used to solve the nonlinear Schrödinger equation in 1971 [9], but the concept of fiber solitons was not conceived until 1973 [10]. Then, it quickly became obvious that optical solitons would be extremely useful as information-carrying bits in a fiber-optic communication system.

The first experimental observation of solitons is attributed to Mollenauer et al. in 1980 [11]. The short optical pulses were generated by a color-center laser operating near $1.55 \mu\text{m}$ [12–14]. Ironically, without the availability of EDFAs, the first long-haul soliton transmission experiment was realized using Raman gain to compensate for fiber

losses [15]. Since then, tremendous strides have been made in soliton-communication systems by incorporating innovative technologies such as EDFAs, dispersion management, WDM, in-line filters, etc. [2]. Field trials of soliton communication systems first appeared in 1998 by Pirelli [16] and now, companies such as Algety Telecom has been formed explicitly to exploit soliton's advantages [1].

The semiconductor industry follows Moore's law to describe the rate of the growth of the processor speed. Moore's law states that in general, the speed of the processing chips doubles its system capacity every eight months. The capacity of public network traffic has been however, exceeding this rate and doubling about every six months [17]. While fiber loss has been addressed by the development of optical amplifiers (e.g. EDFA, Raman), the problem with fiber dispersion and fiber nonlinearity still remained. The next generation of fiber-optic communication system is focused on solving these issues. We believe that optical solitons are the ultimate solution, since they can effectively use the fiber nonlinearity to balance the accumulated dispersion. In order to maintain the soliton stability over large amplifier spacings and long distances, distributed amplification must be incorporated to minimize system perturbations. The purpose of this thesis is to contribute to the development of the next generation of high-capacity fiber-optic communication systems by studying how to design soliton systems with different dispersion management and amplification techniques.

1.3 Thesis Overview

1.3.1 Principle of Fiber-Optic Communication Systems

The simplest model of a lightwave system consists of a transmitter, a transmission medium such as an optical fiber, and a detector (see Figure 1.2). Information to be transmitted is digitized into 1's or 0's (also referred to as bits) and optical pulses representing this information is then send using a laser and a modulator. Semiconductor lasers are capable of emitting sufficient powers (~ 10 mW) and have a relatively high coupling efficiency ($\sim 50\%$ into single mode fiber) [2]. Consequently, semiconductor lasers are the sources of choice for long-haul communication systems.



Figure 1.2: Basic elements of a fiber-optic communication system

There are currently two formats for encoding optical bit streams, nonreturn-to-zero (NRZ) and return-to-zero (RZ) (see Figure 1.3). An optical pulse representing RZ encoding is shorter than NRZ pulse, and its amplitude returns to zero before the bit duration is over. For a NRZ pulse, the amplitude of a “1” does not return to zero during the bit duration; therefore, two successive 1s are merged into a pulse that is twice as long. Currently, the NRZ format is predominately used because of its intrinsically smaller signal bandwidth; however, for systems based on soliton principles, the RZ format must be used [2].

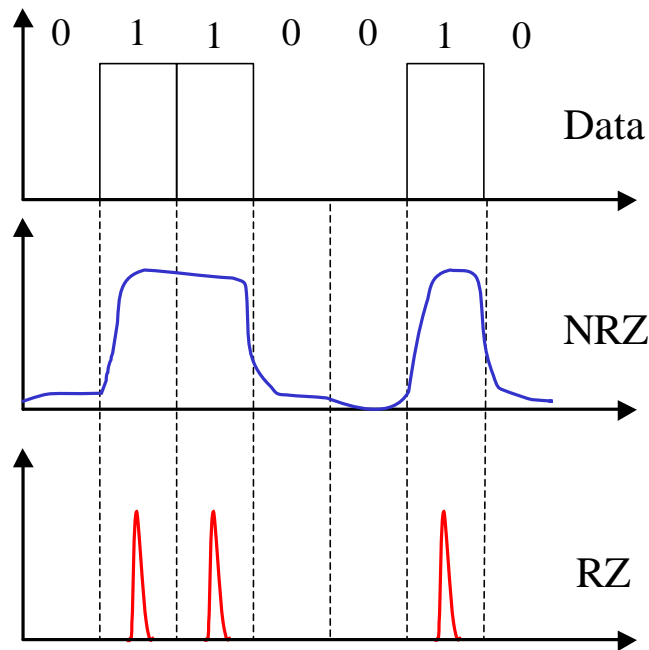


Figure 1.3: Optical bit stream using NRZ and RZ formats

The optical bit stream is transported through optical fibers from one location to another. The capacity of a fiber-optic communication system is designated by the number of bits it can send per second, or alternatively, by the inverse of the bit slot. Thus, a system transmitting 100-ps pulses using NRZ or 25-ps pulses using RZ (with pulse separation equal to four times the pulse width) will carry a single channel capacity of 10 Gb/s.

The receiver's role is to convert the optical signal received from the optical fiber back to the original electrical signal. Modern systems use the direct-detection scheme, which typically consists of a semiconductor detector, a clock-recovery circuit, and a decision-making circuit to identify bits as 1 or 0. The performance of fiber-optic

communication systems is characterized by the number of errors made per second as counted by its receiver circuit, or the bit-error rate (BER). Typically, a system is specified as having error-free transmission when it has BER of less than 10^{-9} [2]. With novel coding algorithms, systems can gain several dB in performance using forward error correction (FEC).

1.3.2 Outline

Chapter 2 provides the foundation of the theoretical and numerical analysis. We derive the nonlinear Schrödinger equation from Maxwell's equations and introduce the basic fiber properties and how they affect the pulse propagation. We will also present numerical and approximate analytical (variational analysis) techniques to solve the nonlinear Schrödinger equation. These will provide tools to simulate systems as well as to optimize parameters in system design.

Chapter 3 begins our investigation of designing soliton communication systems by examining the periodicity of constant-dispersion systems through variational analysis. We introduce the concept of a guiding-center soliton (GCS) and the limitations it imposes on the amplifier spacing of the system. We are then able to exploit the analytical results to use the chirp of soliton pulses to extend the amplifier spacing beyond the guiding-center soliton regime. We show through numerical simulations the effectiveness of the variational results and validate the technique as a valuable tool in exploring and optimizing the complex parameter space of a soliton communication systems.

Chapter 4 provides the foundation of implementing distributed amplification in fiber-optic communication systems. We first introduce the governing equations for distributed-EDFA as well as Raman amplification, and then provide some approxi-

mated analytical solutions to illustrate some basic principles such as pump depletion and gain saturation. These equations are solved numerically and the solution is then incorporated into the nonlinear Schrödinger equation to evaluate the effectiveness of distributed amplification.

Chapter 5 introduces the technique of dispersion management for combating the fiber dispersion problem. A two-step dispersion map as well as the novel dense dispersion map are introduced along with variational-analysis results in calculating the optimal launching condition for a given map. We also show how variational analysis has been applied to the study of dispersion management systems. We show how the system performance is characterized with the inclusion of noise, and assimilate different amplification schemes with dispersion-management techniques to investigate various design rules.

Chapter 6 characterizes the operation of a fiber laser. Specifically, it focuses on the mechanism of mode-partition noise in a fiber laser. We present the experimental setup and discuss the system operation of the fiber laser. We also present our theoretical formulation and examine the numerical results and compare them to experimental data.

Chapter 7 summarizes the main results and findings of the thesis and provides insights for future investigations.

Chapter 2

Theoretical Foundation

2.1 Introduction

The design of a fiber-optic communication system requires an understanding of the nonlinear propagation of optical pulses, with emphasis on fiber losses and fiber dispersion. In this chapter, we present equations that govern this process; namely, the nonlinear Schrödinger equation supporting picosecond pulses and higher order effects such as stimulated Raman scattering (SRS). Since the nonlinear Schrödinger equation cannot be solved in a closed form, numerical techniques such as the split-step Fourier transform method will be presented to help study it. Variational analysis will also be presented as a valuable analytical tool to give qualitative understanding of this complex process.

2.2 Wave Propagation Equation

As always, we begin our analysis of the optical signal propagation through an optical fiber with Maxwell's equations. Furthermore, we can safely assume that the optical fiber is a non-magnetic medium without any free surface charges. Maxwell's equations

are then given as (in SI units) [9]

$$\vec{\nabla} \times \vec{\mathcal{E}} = -\frac{\partial \vec{\mathcal{B}}}{\partial t}, \quad (2.1)$$

$$\vec{\nabla} \times \vec{H} = \frac{\partial \vec{D}}{\partial t}, \quad (2.2)$$

$$\vec{\nabla} \cdot \vec{D} = 0, \quad (2.3)$$

$$\vec{\nabla} \cdot \vec{\mathcal{B}} = 0, \quad (2.4)$$

where $\vec{\mathcal{E}}$ is the electric field, \vec{H} is the magnetic field, \vec{D} is the electric flux density, and $\vec{\mathcal{B}}$ is the magnetic flux density. The flux densities within an optical fiber can be written as

$$\vec{D} = \epsilon_o \vec{\mathcal{E}} + \vec{P}, \quad (2.5)$$

$$\vec{\mathcal{B}} = \mu_o \vec{H}, \quad (2.6)$$

where ϵ_o and μ_o are the vacuum permittivity and permeability respectively, and \vec{P} is the induced electric polarization.

The wave equation can be derived by first taking the curl of Eq. (2.1) and using Eq. (2.6) on the right hand side,

$$\vec{\nabla} \times \vec{\nabla} \times \vec{\mathcal{E}} = -\mu_o \frac{\partial}{\partial t} (\vec{\nabla} \times \vec{H}). \quad (2.7)$$

Substituting Eq. (2.2) to the right hand side and expanding the flux densities via

Eq. (2.5) results in the following form of the wave equation

$$\vec{\nabla} \times \vec{\nabla} \times \vec{\mathcal{E}} = -\frac{1}{c^2} \frac{\partial^2 \vec{\mathcal{E}}}{\partial t^2} - \mu_o \frac{\partial^2 \vec{P}}{\partial t^2}, \quad (2.8)$$

with the speed of light in vacuum defined as $c = 1/\sqrt{\epsilon_o \mu_o}$. The induced polarization can be separated into linear and nonlinear parts as

$$\vec{P}(\vec{r}, t) = \vec{P}_L(\vec{r}, t) + \vec{P}_{NL}(\vec{r}, t) \quad (2.9)$$

with linear and nonlinear induced polarizations defined as

$$\vec{P}_L(\vec{r}, t) = \epsilon_o \int_{-\infty}^{\infty} \chi^{(1)}(t-t') \cdot \vec{\mathcal{E}}(\vec{r}, t') dt', \quad (2.10)$$

$$\vec{P}_{NL}(\vec{r}, t) = \epsilon_o \iiint_{-\infty}^{\infty} \chi^{(3)}(t-t_1, t-t_2, t-t_3) : \vec{\mathcal{E}}(\vec{r}, t_1) \vec{\mathcal{E}}(\vec{r}, t_2) \vec{\mathcal{E}}(\vec{r}, t_3) dt_1 dt_2 dt_3, \quad (2.11)$$

where $\chi^{(1)}$ and $\chi^{(3)}$ are the first and third order susceptibility of the fiber respectively. The second order susceptibility $\chi^{(2)}$ is ignored since an optical fiber possesses inversion symmetry. Using the second derivatives of vector identities [18] and Eq. (2.3), the wave equation, Eq. (2.8) can be transform into

$$\nabla^2 \vec{\mathcal{E}} = \frac{1}{c^2} \frac{\partial^2 \vec{\mathcal{E}}}{\partial t^2} + \mu_o \frac{\partial^2 \vec{P}_L}{\partial t^2} + \mu_o \frac{\partial^2 \vec{P}_{NL}}{\partial t^2}. \quad (2.12)$$

In order to develop a propagation equation from Eq. (2.12), several important as-

assumptions must be made regarding the nonlinearity of the system [9]. We will make the following simplifications:

1. The nonlinear-induced polarization is small and can be treated as a perturbation.
2. The optical field can maintain polarization along fiber length, since this will allow the use of a scalar approach.
3. The optical field is quasi-monochromatic such that its spectral width $\delta\omega$ is small compared to its center frequency ω_o , i.e. $\delta\omega/\omega_o \ll 1$.

We will also use the slowly varying envelope approximation to separate the rapidly varying part of the field by rewriting the field as

$$\vec{\mathcal{E}}(\vec{r}, t) = \frac{1}{2} \hat{x} [E(\vec{r}, t) \exp(-i\omega_o t) + c.c.], \quad (2.13)$$

$$\vec{P}_L(\vec{r}, t) = \frac{1}{2} \hat{x} [P_L(\vec{r}, t) \exp(-i\omega_o t) + c.c.], \quad (2.14)$$

$$\vec{P}_{NL}(\vec{r}, t) = \frac{1}{2} \hat{x} [P_{NL}(\vec{r}, t) \exp(-i\omega_o t) + c.c.], \quad (2.15)$$

where *c.c.* stands for complex conjugate, \hat{x} is the polarization unit vector of the light assuming to be linearly polarized along the x axis, and $E(\vec{r}, t)$ is a slowly varying function with respect to optical carrier frequency, ω_o . We will often find it easier to work within the Fourier domain and will adopt the following notation for Fourier transforms

$$\tilde{E}(\vec{r}, \omega - \omega_o) = \int_{-\infty}^{\infty} E(\vec{r}, t) e^{i(\omega - \omega_o)t} dt. \quad (2.16)$$

In the Fourier domain, the linearly-induced polarization in Eq. (2.10) is simply

$$\tilde{P}_L(\vec{r}, \omega) = \epsilon_o \tilde{\chi}^{(1)}(\omega) \tilde{E}(\vec{r}, \omega). \quad (2.17)$$

The nonlinear-induced polarization can be also simplified by assuming that the nonlinear response is instantaneous such that Eq. (2.11) can be reduced to a delta function response,

$$\vec{P}_{NL}(\vec{r}, t) = \epsilon_o \chi^{(3)} : \vec{E}(\vec{r}, t) \vec{E}(\vec{r}, t) \vec{E}(\vec{r}, t), \quad (2.18)$$

where we use three vertical dots to denote the tensor nature of the third-order susceptibility. We can establish the nonlinear polarization contribution by simply treating the field as monochromatic waves [19]. We will treat all fields as scalar variables in the following derivation of the propagation equation.

$$E = E \cos(\omega_o t). \quad (2.19)$$

Then we can write the resulting nonlinear polarization

$$\begin{aligned} P_{NL} &= \epsilon_o \chi^{(3)} E^3 \cos^3(\omega_o t) \\ &= \epsilon_o \chi^{(3)} E^3 \left[\frac{1}{4} \cos(3\omega_o t) + \frac{3}{4} \cos(\omega_o t) \right]. \end{aligned} \quad (2.20)$$

The nonlinear-induced polarization is found to be oscillating at ω_o as well as at third-harmonic $3\omega_o$. However, the third-harmonic contribution is small for optical fibers and therefore can be ignored, further reducing the Eq. (2.18) to the following form

$$P_{NL}(\vec{r}, t) = \epsilon_o \epsilon_{NL} E(\vec{r}, t), \quad (2.21)$$

where ϵ_{NL} is the nonlinear contribution to the dielectric constant and can be deduced

from Eq. (2.20)

$$\epsilon_{NL} = \frac{3}{4}\chi^{(3)}|E(\vec{r}, t)|^2. \quad (2.22)$$

In order to solve the wave equation within the Fourier domain, we have to make the assumption that ϵ_{NL} is constant. This is justified through the fact that we make the slowly varying wave approximation and we are also treating P_{NL} as a perturbation [9]. The wave equation can then be reduced by taking the Fourier transform of Eq. (2.12) and using Eqs. (2.17) – (2.21) to

$$\nabla^2 \tilde{E} + \epsilon(\omega)k_o^2 \tilde{E} = 0, \quad (2.23)$$

where \tilde{E} is the electric field in the Fourier domain and the propagation constant $k_o = \omega/c$. Furthermore,

$$\epsilon(\omega) = 1 + \tilde{\chi}^{(1)}(\omega) + \epsilon_{NL} \quad (2.24)$$

is the dielectric constant including both linear and nonlinear contributions from the induced polarization.

The wave equation Eq. (2.23) can then be solved using the technique of separation of variables by rewriting the electric field as

$$\tilde{E}(\vec{r}, \omega - \omega_o) = F(x, y)\tilde{A}(z, \omega - \omega_o) \exp(i\beta_o z), \quad (2.25)$$

where $\beta_o = n\omega/c$ is the wave number. The separated equations are obtained by insert-

ing Eq. (2.25) into Eq. (2.23), resulting in

$$\frac{d^2 F}{dx^2} + \frac{d^2 F}{dy^2} + \left[\epsilon(\omega) k_o^2 - \tilde{\beta}^2 \right] F = 0, \quad (2.26)$$

$$2i\beta_o \frac{d\tilde{A}(z)}{dz} + (\tilde{\beta}^2 - \beta_o^2) \tilde{A} = 0, \quad (2.27)$$

where $\tilde{\beta}$ is the separation constant (eigenvalue). The equation for the modal distribution $F(r)$ can be solved by rewriting the dielectric constant as

$$\epsilon = (n + \delta n)^2 \approx n^2 + 2n \delta n. \quad (2.28)$$

where n is the index of refraction and δn is the nonlinear change of index as defined by

$$\begin{aligned} \delta n &= n_2 |E|^2 + \frac{i\alpha}{2k_o} \\ &= \frac{\Re(\epsilon_{NL})}{2n} + \frac{i\alpha}{2k_o}. \end{aligned} \quad (2.29)$$

with n_2 as the intensity-dependent index coefficient and α is the fiber loss coefficient. To first order (neglecting the nonlinear contribution), Equation (2.26) reduces to a well-known differential equation for the Bessel function by transforming to a cylindrical coordinate $F(x, y) = F(r) \exp(im\phi)$ and replacing ϵ by n^2 ,

$$\frac{d^2 F}{dr^2} + \frac{1}{r} \frac{dF}{dr} + \left[n^2 k_o^2 - \tilde{\beta}^2 - \frac{m^2}{r^2} \right] F = 0, \quad (2.30)$$

with the refractive index n of a fiber of core radius a given by

$$n = \begin{cases} n_1 & : r \leq a \\ n_2 & : r > a \end{cases} \quad (2.31)$$

The general solution in the core area of the fiber is the Bessel function consisting of a linear combination of Bessel and Neumann functions and is given by

$$F(r) = J_m(\kappa r), \quad r \leq a, \quad (2.32)$$

with $\kappa^2 = n_1^2 k_o^2 - \tilde{\beta}^2$ since the Neumann function is non-physical because of a singularity at $r = 0$ [9].

Equation (2.27) describes the propagation of the optical field within an optical fiber and can be reduced by using $\tilde{\beta}^2 - \beta_o^2 \approx (\tilde{\beta} - \beta_o)(\tilde{\beta} + \beta_o) \approx 2\beta_o(\tilde{\beta} - \beta_o)$. This is valid by choosing the eigenvalue $\tilde{\beta}$ to be close to β_o . Furthermore, $\tilde{\beta}(\omega)$ can be rewritten as

$$\tilde{\beta}(\omega) = \beta(\omega) + \Delta\beta \quad (2.33)$$

where $\Delta\beta$ is the nonlinear contribution to the eigenvalue and can be calculated by using the first-order perturbation theory. This is done by perturbing the system represented by Eq. (2.26) by using Eqs. (2.28) and (2.33), and replacing $F = F_0 + \delta F$. This results in the following expression for $\Delta\beta$,

$$\Delta\beta = \frac{k_0 \int \int_{-\infty}^{\infty} \delta n |F(x, y)|^2 dx dy}{\int \int_{-\infty}^{\infty} |F(x, y)|^2 dx dy}. \quad (2.34)$$

The propagation equation Eq. (2.27) then becomes

$$\frac{d\tilde{A}(z)}{dz} = i [\beta(\omega) + \Delta\beta - \beta_o] \tilde{A}. \quad (2.35)$$

2.2.1 Dispersion

Fiber dispersion is represented in Eq. (2.35) by the frequency dependent wave number $\tilde{\beta}(\omega)$. We can expand $\beta(\omega)$ in a Taylor series about the carrier frequency ω_o as

$$\beta(\omega) = \beta_o + (\omega - \omega_o)\beta_1 + \frac{1}{2}(\omega - \omega_o)^2\beta_2 + \frac{1}{6}(\omega - \omega_o)^3\beta_3 + \dots, \quad (2.36)$$

with

$$\beta_n = \left(\frac{d^n \beta}{d\omega^n} \right)_{\omega=\omega_o}. \quad (2.37)$$

In order to study the propagation of the field in the time domain, we must perform the inverse Fourier transform to Eq. (2.35) using the following relation

$$A(z, t) = \frac{1}{2\pi} \int_{-\infty}^{\infty} \tilde{A}(z, \omega - \omega_o) e^{-i(\omega - \omega_o)t} d\omega. \quad (2.38)$$

The resulting time domain propagation equation including up to the second order effect then becomes

$$\frac{\partial A}{\partial z} + \beta_1 \frac{\partial A}{\partial t} + \frac{i}{2} \beta_2 \frac{d^2 A}{dt^2} = i\Delta\beta A. \quad (2.39)$$

Table 2.1: Parameters used in simulation of pulse broadening

Parameter	Symbol	Value
Pulse shape	A	Gaussian
Pulse width	T_0	10 ps
Fiber dispersion	β_2	$-10 \text{ ps}^2/\text{km}$
Dispersion length	L_D	10 km

First order fiber dispersion β_1 defines the group velocity v_g of the pulse and second order dispersion β_2 , also known as group velocity dispersion (GVD), can cause pulse spreading because different spectral components will experience different group velocities. In studying pulse propagation, it is often convenient to measure time in the moving frame of the pulse through the following transformation

$$T = t - \beta_1 z = t - z/v_g. \quad (2.40)$$

The resulting equation then becomes

$$\frac{\partial A}{\partial z} + \frac{i}{2}\beta_2 \frac{d^2 A}{dT^2} = i\Delta\beta A. \quad (2.41)$$

A pulse launched into a dispersive medium usually does not maintain its shape and can become a disruptive force in fiber-optic communications systems. As the pulse is broadened its intensity degrades and crosstalk may develop with adjacent bit slots. In general, we can define the dispersion length $L_D = T_0^2/|\beta_2|$ as the length in which Gaussian pulse will spread to twice its initial pulse width, T_0 . Figure 2.1 shows the broadening of a Gaussian input pulse through one dispersion length assuming $\Delta\beta = 0$ using the parameters in Table 2.1.

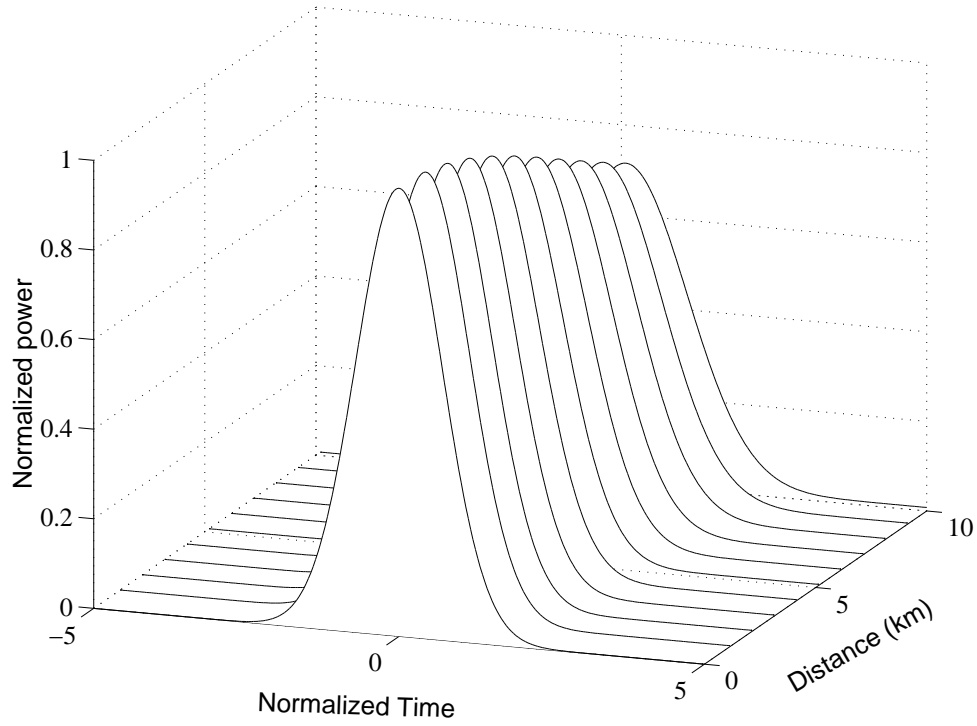


Figure 2.1: Pulse spreading due to GVD

2.2.2 Fiber Loss

Fiber loss is incorporated within the term $\Delta\beta$ in Eq. (2.41). We can rewrite the propagation constant in terms of index of refraction by noting that $\Delta\beta = k_0 \delta n$. Ignoring the first term of δn [Eq. (2.29)] for now (we will cover it in Section 2.2.3), substituting Eqs. (2.29) and (2.34) into Eq. (2.41) results in

$$\frac{\partial A}{\partial z} + \frac{i}{2}\beta_2 \frac{d^2 A}{dT^2} = -\frac{\alpha}{2} A. \quad (2.42)$$

Fiber loss is a major problem in fiber-optic communication systems because of the loss of signal power, which contributes directly to a high bit error rate. Figure 2.2 shows

how the addition of fiber loss, in conjunction with fiber dispersion, can further degrade the pulse intensity. The parameter used is the same as in Table 2.1 with the addition of $\alpha = 0.2$ dB/km.

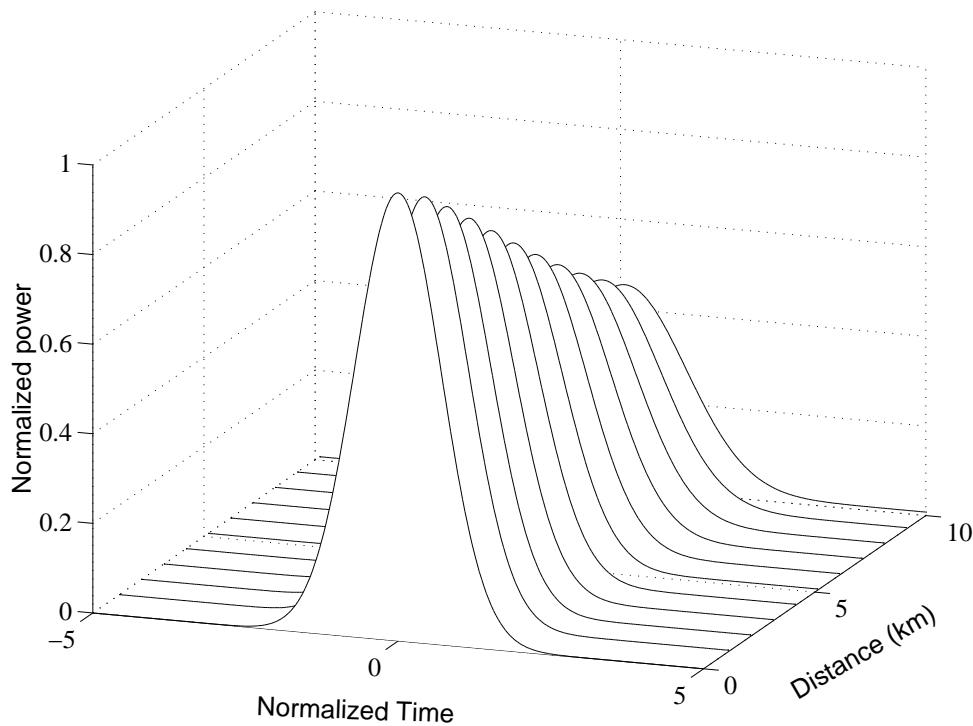


Figure 2.2: Pulse spreading due to GVD in the presence of fiber loss

2.2.3 Nonlinear Schrödinger Equation

The nonlinear Schrödinger equation (NSE) is obtained by adding the intensity-dependent index term to Eq. (2.42) by substituting both terms of Eqs. (2.29) and (2.34) into Eq. (2.41),

$$\frac{\partial A}{\partial z} + \frac{i}{2}\beta_2 \frac{d^2 A}{dT^2} + \frac{\alpha}{2}A = i\gamma|A|^2 A, \quad (2.43)$$

where the nonlinear coefficient γ defined as

$$\gamma = \frac{\omega_o n_2}{c A_{eff}}, \quad (2.44)$$

and the effective area defined as

$$A_{eff} = \frac{\left(\int \int_{-\infty}^{\infty} |F(x, y)|^2 dx dy \right)^2}{\int \int_{-\infty}^{\infty} |F(x, y)|^4 dx dy}. \quad (2.45)$$

By itself, nonlinearity can cause self-phase modulation (SPM) of the optical pulse. SPM is caused by the intensity dependence of the index of refraction which causes a time dependent nonlinear phase that leads to frequency chirp, a change of instantaneous optical frequency across the pulse from its center value ω_o . SPM induced chirp can cause spectral broadening (see Fig. 2.3) which can lead to pulse compression. Similar to the dispersion length, we can define a characteristic length of SPM (nonlinear length) by

$$L_{NL} = \frac{1}{\gamma P_o}, \quad (2.46)$$

where P_o is the peak power of the pulse.

There are other higher order nonlinear terms that we can add to the right hand side of Eq. (2.43). In high bit-rate soliton systems that require the use of extremely short optical pulses, a Raman effect on the pulse delay must be included in the nonlinear Schrödinger equation [9]

$$\frac{\partial A}{\partial z} + \frac{i}{2} \beta_2 \frac{\partial^2 A}{\partial T^2} + \frac{\alpha}{2} A = i\gamma \left[|A|^2 A - T_R A \frac{\partial |A|^2}{\partial T} \right]. \quad (2.47)$$

Table 2.2: Parameters used in simulation of pulse spectrum broadening

Parameter	Symbol	Value
Pulse shape	A	Hyperbolic secant
Pulse width	T_0	10 ps
Pulse power	P_s	30 mW
Dispersion length	L_D	1000 km
Nonlinear length	L_{NL}	10 km

2.3 Optical Solitons

We have seen in previous sections how fiber dispersion and fiber loss can distort the shape of the pulse, which can have an adverse effect on signal propagation for communication purposes. However, if we were to use fiber nonlinearity to counter-balance the fiber dispersion, a stable pulse can propagate undisturbed through the fiber — this is the concept of optical solitons.

It is useful to normalize the nonlinear Schrödinger equation, Eq. (2.43), by introducing

$$U = \frac{A}{\sqrt{P_o}}, \quad \zeta = \frac{z}{L_D}, \quad \tau = \frac{T}{T_o}. \quad (2.48)$$

The normalized nonlinear Schrödinger equation without the loss and the Raman term is given by

$$\frac{\partial U}{\partial \zeta} + \frac{i}{2} \text{sgn}(\beta_2) \frac{\partial^2 U}{\partial \tau^2} - iN^2 |U|^2 U = 0, \quad (2.49)$$

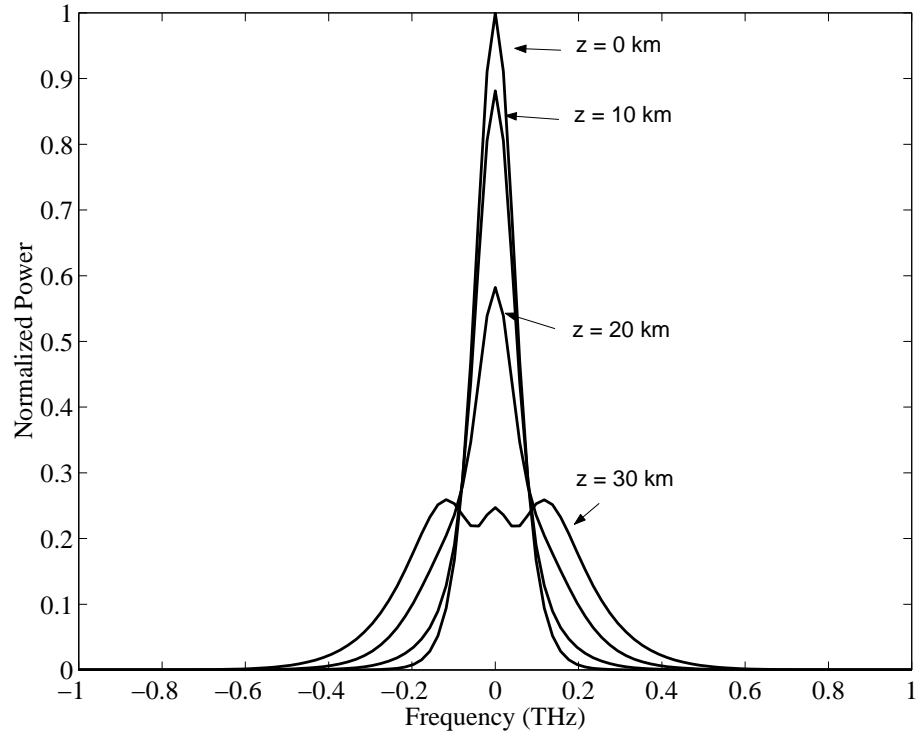


Figure 2.3: Spectral broadening of optical pulse due to SPM

where N is the soliton order and is defined by

$$N^2 = \frac{L_D}{L_{NL}} = \frac{\gamma P_o T_o^2}{|\beta_2|}. \quad (2.50)$$

Equation (2.49) can be solved by using the inverse scattering method [8] which consists of choosing a suitable scattering problem whose potential is the solution sought. The propagated field is reconstructed from the scattering data and the solution corresponds to $N = 1$ is called the fundamental soliton and can be written as

$$U(\zeta, \tau) = \text{sech}(\tau) \exp\left(\frac{i\zeta}{2}\right). \quad (2.51)$$

Table 2.3: Parameters used in simulation of soliton propagation

Parameter	Symbol	Value
Pulse shape	U	Soliton
Soliton order	N	1
Pulse width	T_0	10 ps
Fiber dispersion	β_2	$-10 \text{ ps}^2/\text{km}$
Dispersion length	L_D	10 km
Nonlinear parameter	γ	$3.36 (\text{W km})^{-1}$
Fiber loss	α	0 dB/km

As can be seen readily from Eq. (2.50), when $N = 1$, the dispersion length L_D exactly equals the nonlinear length L_{NL} , indicating that the solution exists when fiber nonlinearity exactly balances the fiber dispersion by choosing the appropriate launch power for a given fiber dispersion and pulse width. This is not too surprising since we have already seen how the pulse broadens due to GVD and compresses due to SPM. Fig. 2.4 shows the stable propagation of a soliton pulse over a dispersion length without any change in its shape using the parameters in Table 2.3.

2.4 Split-Step Fourier Transform Method

The inverse scattering method can solve the nonlinear Schrödinger equation only in some specific cases. Numerical methods are employed to study the nonlinear effects in optical fibers for most cases. Because of its speed, the most commonly used method is the split-step Fourier transform method, which takes advantage of finite-Fourier-transforms (FFT) algorithms [9].

The half-step Fourier transform methodology involves the separation of the equation into a differential part \hat{D} to be solved in the Fourier domain and a nonlinear part \hat{N}

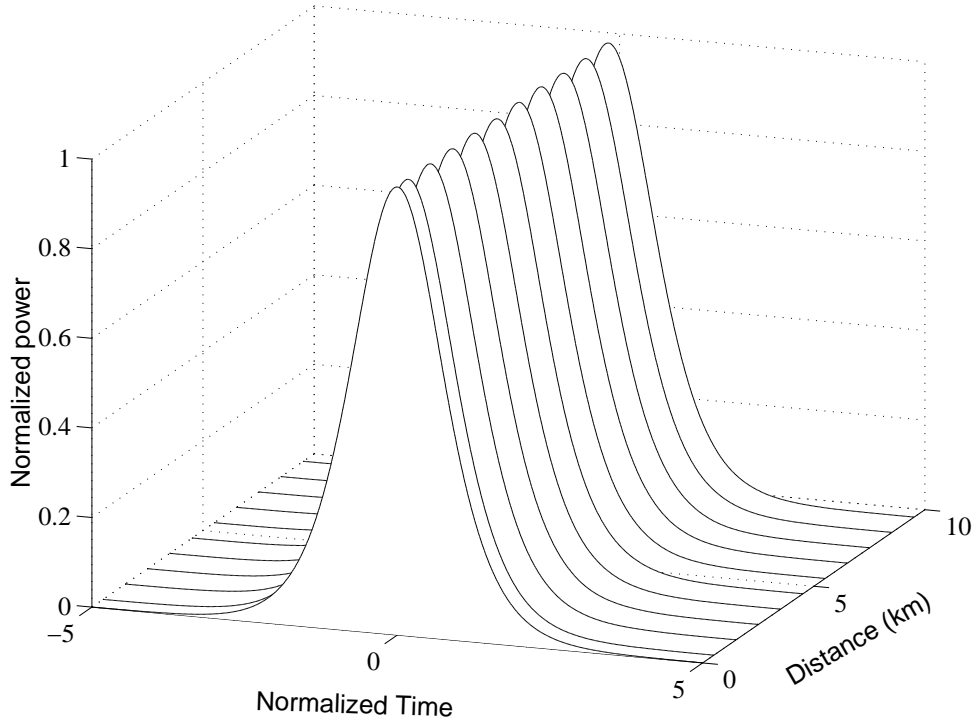


Figure 2.4: Soliton pulse propagation

to be solved in the time domain. This can be written mathematically as

$$\frac{\partial A}{\partial z} = (\hat{D} + \hat{N})A, \quad (2.52)$$

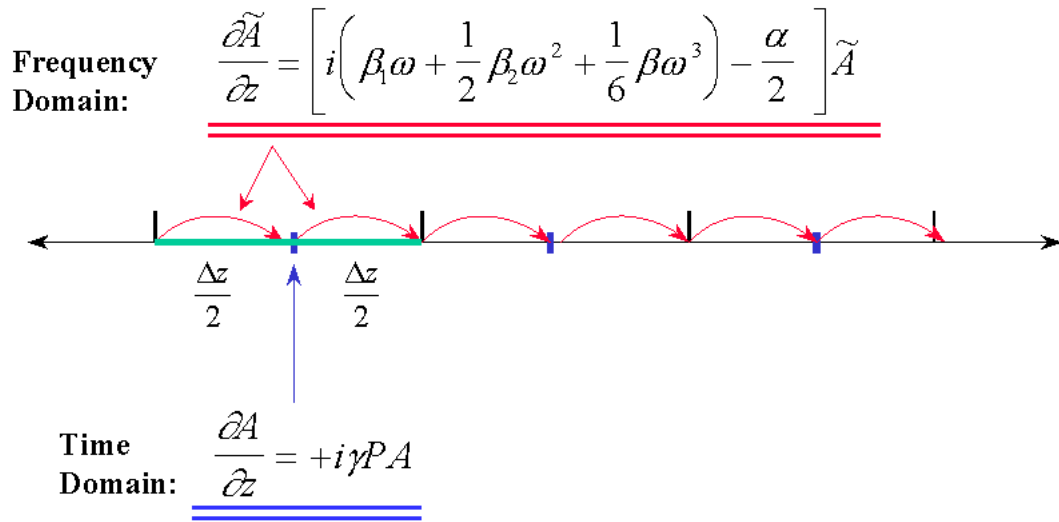
where the operators are given by

$$\hat{D} = -\frac{i}{2}\beta_2 \frac{\partial^2 A}{\partial T^2} - \frac{\alpha}{2}, \quad (2.53)$$

$$\hat{N} = i\gamma|A|^2 + \text{other nonlinear terms}. \quad (2.54)$$

The assumption made in using the split-step Fourier transform method is that even though dispersion and nonlinearity act concurrently over a small distance h , the dis-

persive and nonlinear effects can be assumed to act separately. The method is implemented by applying only the dispersive effect on the first half of the step, then applying the nonlinearity for the whole step (assuming the power is approximately constant over the step size, h), and finally re-applying the dispersive effect on the second half of the step. This is also referred to as the symmetric split-step Fourier transform method, (see Figure 2.5). Note that since the dispersion operator \hat{D} consists of differential operator,



independent of z , the exact solution is given by

$$A(z + h, T) = \exp\left((\hat{D} + \hat{N})h\right) A(z, T). \quad (2.56)$$

A comparison of the exact solution [Eq. (2.56)] with the approximate solution [Eq. (2.55)] using the Baker-Hausdorff formula shows that the error is on the order of h^3 [9].

2.5 Variational Technique

The propagation of soliton pulses in each fiber section between two consecutive amplifiers is described by the nonlinear Schrödinger equation, Eq. (2.49). The loss term can be eliminated with the following change of variables

$$A = B \exp(-\alpha z/2), \quad \gamma(z) = \gamma_0 \exp(-\alpha z), \quad (2.57)$$

where γ_0 is the nonlinear coefficient in the absence of loss. This reduces the nonlinear Schrödinger equation into the following form:

$$i \frac{\partial B}{\partial z} - \frac{1}{2} \beta_2 \frac{\partial^2 B}{\partial T^2} + \gamma(z) |B|^2 B = 0. \quad (2.58)$$

The effects of fiber loss are now included through the z dependence of γ .

Variational analysis provides approximate analytical results for features such as pulse compression, maximal pulse amplitude, and induced frequency chirp [20]. The nonlinear Schrödinger equation can be restated as a variational problem by casting it in

the form of the Euler-Lagrange equation

$$\frac{\partial}{\partial z} \left(\frac{\partial L}{\partial q_z} \right) + \frac{\partial}{\partial T} \left(\frac{\partial L}{\partial q_T} \right) - \frac{\partial L}{\partial q} = 0, \quad (2.59)$$

where q represents the field B or B^* , the subscripts T and z denote differentiation with respect to the appropriate variable, and the Lagrangian density L is given by [20]

$$L = -\frac{i}{2}(B^* B_z - B B_z^*) - \frac{1}{2} [\gamma(z)|B|^4 + \beta_2 |B_T|^2], \quad (2.60)$$

where a subscript denotes derivative with respect to that variable. Note that combining Eqs. (2.59) and (2.60) with $q = B^*$ produces Eq. (2.58).

To carry out the variational analysis, we average the Lagrangian density by integrating over time

$$\mathcal{L} = \int_{-\infty}^{\infty} L[T, q(z)] dT. \quad (2.61)$$

Integrating Eq. (2.59) over time, the reduced Euler-Lagrange equation becomes

$$\frac{d}{dz} \left(\frac{\partial \mathcal{L}}{\partial q_z} \right) - \frac{\partial \mathcal{L}}{\partial q} = 0. \quad (2.62)$$

To make further progress, we choose the following ansatz for the soliton shape and phase:

$$B(z, T) = a \operatorname{sech} \left(\frac{T}{T_o} \right) \exp \left(i\phi - \frac{iCT^2}{2T_o^2} \right), \quad (2.63)$$

where a is the amplitude, ϕ is the phase, C is the chirp, and T_o is the pulse width. All

of the soliton parameters except ϕ remain constant for a lossless fiber but are allowed to vary with z when solitons are amplified periodically to compensate for fiber losses. Performing the integral in Eq. (2.61) gives the following expression for the average Lagrangian density

$$\mathcal{L} = a^2 \left(2\phi_z T_o - \frac{\pi^2}{12} C_z T_o + \frac{\pi^2}{6} C T_{oz} \right) - \frac{2}{3} \gamma(z) a^4 T_o - \frac{\beta_2 a^2}{3T_o} \left(1 + \frac{\pi^2}{4} C^2 \right). \quad (2.64)$$

By combining Eqs. (2.62) and (2.64) with q representing any of the variables a , T_o , C , or ϕ , we obtain the following set of four ordinary differential equations governing variations of soliton parameters along the fiber link:

$$\frac{d(a^2 T_o)}{dz} = 0, \quad (2.65)$$

$$\frac{dT_o}{dz} = \frac{\beta_2 C}{T_o}, \quad (2.66)$$

$$\frac{dC}{dz} = \frac{4}{\pi^2} \gamma(z) a^2 + \frac{\beta_2}{T_o^2} \left(\frac{4}{\pi^2} + C^2 \right), \quad (2.67)$$

$$\frac{d\phi}{dz} = \frac{\beta_2}{3T_o^2} + \frac{5}{6} \gamma(z) a^2. \quad (2.68)$$

These equations are equivalent to solving the nonlinear Schrödinger equation within the variational approximation. Note however, that this approach is only approximate and does not account for characteristics such as radiative loss [21], damping of the amplitude oscillations, and changing of soliton shape [20]. It should be stressed that Eqs. (2.65) – (2.68) can also be applied for dispersion-managed solitons by making β_2 explicitly z -dependent. In the next chapter, we consider the case of constant-dispersion fibers first.

2.6 Summary

In this chapter, we presented the theory for nonlinear pulse propagation based on Maxwell's equations taking into account fiber dispersion, fiber losses, and fiber nonlinearity. We have also presented the optical soliton as a solution to the nonlinear Schrödinger equation that can be used advantageously in fiber optic communication systems. An efficient numerical algorithm is presented to effectively study the nonlinear pulse propagation. Furthermore, we presented the foundation of the variational method as an effective analytical tool in studying nonlinear propagation dynamics. This technique will be crucial in providing analytic insight in studying periodicity of constant-dispersion (Chapter 3) as well as dispersion-managed systems (Chapter 5).

Chapter 3

Chirped Solitons in Constant-Dispersion Fiber Links

3.1 Introduction

We introduced the concept of optical solitons in section 2.3 for transmitting information in an optical communication system. The ability of the soliton to maintain its shape as it propagates through an optical fiber, a dispersive and nonlinear medium, makes it an ideal choice in transmitting signals. Unfortunately, fiber loss reduces the nonlinearity needed to balance fiber dispersion, and a soliton can no longer be preserved. Optical amplifiers were developed to mitigate the problem of fiber loss and have been very successful. Lumped amplification systems place optical amplifiers periodically along the fiber link to compensate for the fiber loss. For cost effectiveness, it is necessary to have as large an amplifier spacing or conversely, as few amplifiers as possible.

The principal concept that has emerged in the context of lumped amplification is the path-averaged or guiding-center soliton [22–24]. This allows propagation of solitons through lossy fibers provided the amplifier spacing L_A is short compared to the dispersion length L_D . The soliton is launched with enough energy such that the path-

averaged peak power over one amplifier spacing is equal to the peak power needed for soliton propagation. However, this results in the need to limit L_A to a fraction of L_D ($L_A \ll L_D$), which in turn necessitates unreasonably short amplifier spacings (< 10 km) when operating at high bit rates. This limitation comes from the fact that the system is not perfectly periodic when L_A becomes comparable to or exceeds L_D . As a result, large perturbations generate spectral side bands and dispersive radiation which degrade the system performance [25–27]. Several techniques have been proposed to design soliton communication systems that can operate beyond the average-soliton regime [28–31]. However, their use often requires additional optical elements such as a fast saturable absorber [9]. We propose a way to extend the amplifier spacing to beyond the guiding-center soliton through pulse prechirping.

3.2 Guiding-Center Solitons

The normalized nonlinear Schrödinger equation including the effect of periodic optical gain provided by a series of inline optical amplifiers can be written as [2]

$$\frac{\partial U}{\partial \zeta} + \frac{i}{2} \text{sgn}(\beta_2) \frac{\partial^2 U}{\partial \tau^2} - iN^2 |U|^2 U = -\frac{\Gamma}{2} U + \left(\sqrt{G} - 1 \right) \sum_{n=1}^N \delta(\zeta - nz_A) U, \quad (3.1)$$

where $\Gamma = \gamma L_D$ is the normalized loss coefficient, $G = \exp(\Gamma z_A)$ is the amplifier gain, and z_A is the normalized amplifier length for the fundamental soliton ($N = 1$) in a anomalous dispersion fiber ($\beta_2 < 0$). Similar to the slowly varying envelope approximation of the previous chapter, we will separate the fast varying function that describes the soliton losses and amplifications (a) and the slowly varying function of the dispersion and nonlinear effect (u). The optical field can then be written as the

product of these functions

$$U(\zeta, \tau) = a(\zeta)u(\zeta, \tau). \quad (3.2)$$

After separating out the fast-varying processes, the resulting propagation equation is in the form of the lossless nonlinear Schrödinger equation, Eq. (2.49) after separating out the rapidly-varying processes,

$$\frac{\partial u}{\partial \zeta} + \frac{i}{2} \text{sgn}(\beta_2) \frac{\partial^2 u}{\partial \tau^2} - ia^2(\zeta)N^2|u|^2u = 0, \quad (3.3)$$

with $a(\zeta)$ obtained by solving the rapidly-varying dynamics of gain-loss evolution,

$$\frac{da}{d\zeta} = -\frac{\Gamma}{2}a + \left(\sqrt{G} - 1\right) \sum_{n=1}^N \delta(\zeta - nz_A)a. \quad (3.4)$$

Equation (3.4) can be easily solved with the result being an exponential loss with an abrupt amplification at $\zeta = z_A$ as can be seen in Figure 3.1.

The concept of guiding-center solitons relies on the fact that the amplitude variations are rapidly varying with the period $z_A \ll 1$. Since the solitons react on a much slower length scale, we can approximate $a^2(\zeta)$ by its average over the period. The solution to Equation (3.3) can be written as a combination of averaged solution (guiding-center soliton) \bar{u} and a perturbation δu , i.e. $u = \bar{u} + \delta u$. The resulting equation for the guiding-center soliton is then

$$\frac{\partial \bar{u}}{\partial \zeta} + \frac{i}{2} \text{sgn}(\beta_2) \frac{\partial^2 \bar{u}}{\partial \tau^2} - i \langle a^2(\zeta) \rangle N^2 |\bar{u}|^2 \bar{u} = 0, \quad (3.5)$$

with the perturbation small enough to be ignored for $z_A \ll 1$ [2]. For fundamental

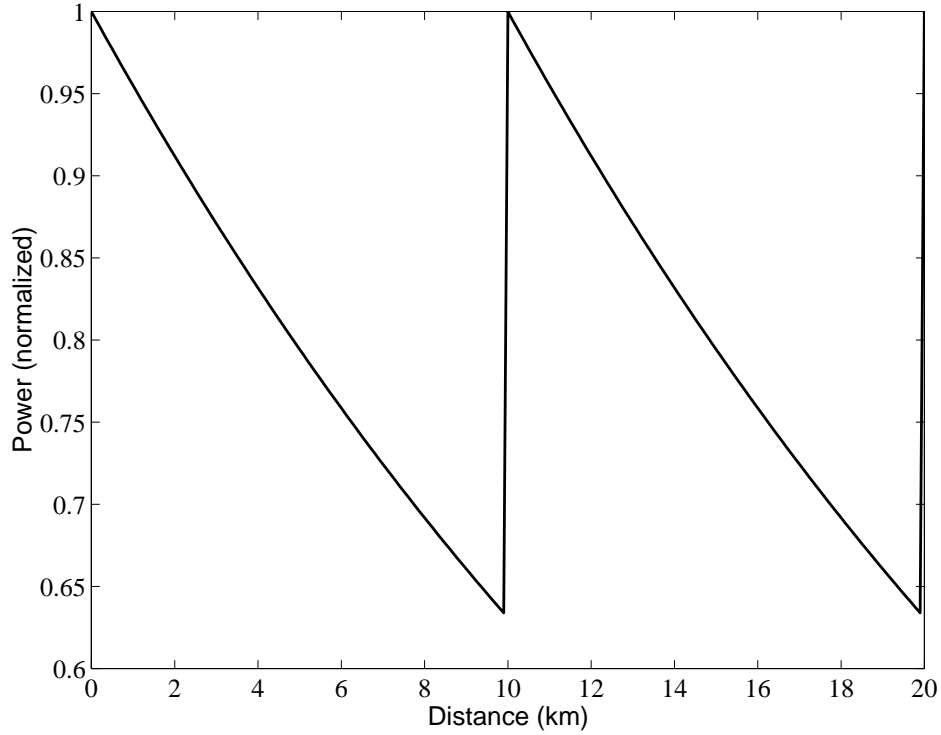


Figure 3.1: Amplitude variations of lumped amplification with $L_A=20$ km and 0.2 dB/km loss.

solitons to operate in the guiding-center soliton, input peak power of the pulse should be given such that $\langle a^2(\zeta) \rangle N^2 = 1$. For amplifier gain equal to fiber loss over the amplifier span, the peak power is given as

$$P_{in} = \frac{G \ln G}{G - 1} P_0, \quad (3.6)$$

where P_0 is the power required for the fundamental soliton in a lossless fiber. Figure 3.2 shows the evolution of a guiding center soliton through two amplifier stages with $z_A = 0.2$ (see Table 3.1). The figure clearly illustrates the effect of fiber loss which

Table 3.1: Parameters used in simulation of soliton propagation

Parameter	Symbol	Value
Pulse shape	U	Soliton
Soliton order	N	1.117
Pulse width	T_0	10 ps
Fiber dispersion	β_2	$-2 \text{ ps}^2/\text{km}$
Dispersion length	L_D	50 km
Nonlinear parameter	γ	$3.36 (\text{W km})^{-1}$
Fiber loss	α	0.2 dB/km
Amplifier spacing	L_A	10 km

causes pulse broadening but it also shows the ability of the pulse to retain its soliton nature through periodic amplification.

3.3 Pre-Chirped Solitons

A question one may ask is whether the periodicity of solitons (see Figure 3.3) can be restored even when $L_A \sim L_D$ by modifying the system design in an appropriate way. For example, the guiding-center soliton is launched with a unique peak power obtained by averaging the soliton energy over one amplifier spacing. However, the soliton is assumed to remain unchirped [22,32]. The trick is then to allow both the width and chirp of the soliton to vary in each fiber section between two amplifiers (similar concepts have been used in dispersion-managed solitons [33–38]). We use variational analysis to determine the optimal launch conditions for the guiding-center soliton (GCS) or path-averaged soliton (PAS). We require the pulse width and chirp to be periodic and determine the exact pre-chirping and peak power needed to maintain periodicity of soliton in periodically amplified fiber links. The use of prechirping provides a new

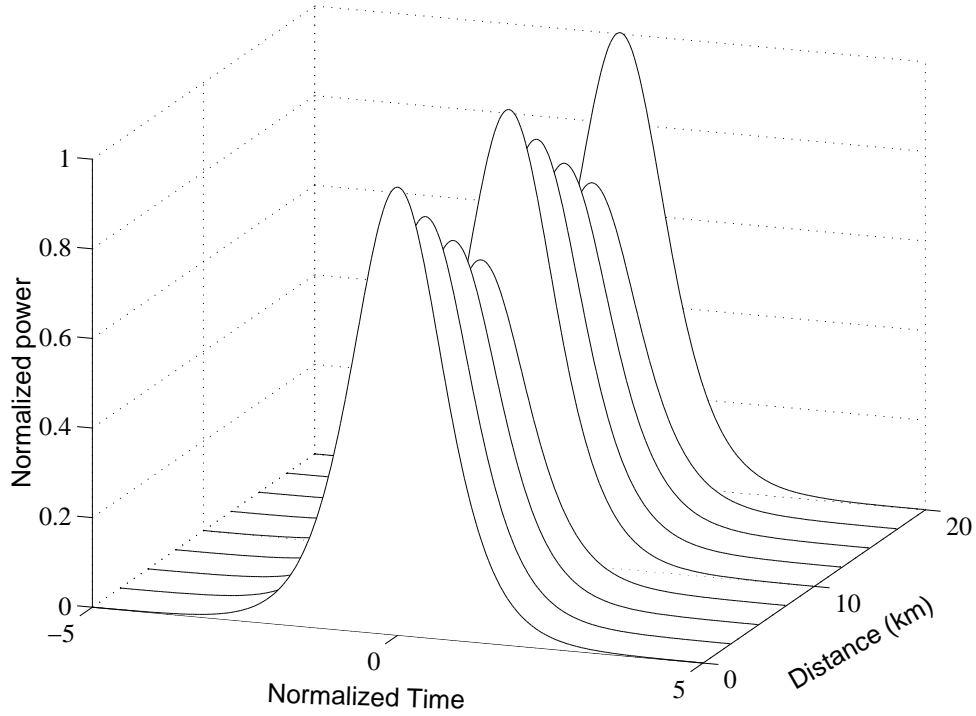


Figure 3.2: Evolution of guiding-center soliton

operating regime for such systems in which L_A can be comparable and even exceed L_D . This regime is especially useful at high bit rates ($B > 10$ Gb/s) for which the dispersion length becomes ~ 10 km. Furthermore, even though we focus on the case of constant-dispersion fibers, the new regime discussed here may find applications in the case of dispersion-managed lightwave systems.

3.3.1 Variational Results

Equation (2.65) shows the conservation of pulse energy $E_p = \int |B|^2 dt$ and relates the amplitude a of the pulse to its width T_o . We can write the relation as $a^2 = a_0^2 T_o(0)/T_o$ where a_0 and $T_o(0)$ are the initial pulse amplitude and width, respectively. As a result,

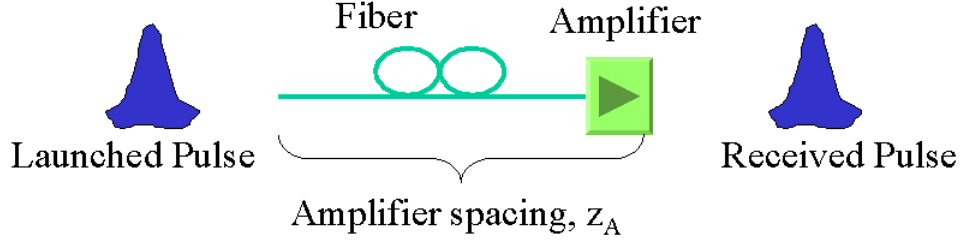


Figure 3.3: Periodicity of soliton pulse through each amplifier unit

ϕ is strictly determined by T_o , and the variational analysis is reduced to solving a pair of coupled ordinary differential equations for C and T_o only [Eq. (2.66) and (2.67)]. Furthermore, it is useful to introduce the normalized length $\xi = z/L_A$, and the normalized pulse width $W = T_o/T_o(0)$. Equation. (2.66) and (2.67) then become

$$\frac{dW}{d\xi} = -\frac{z_A C}{W}, \quad (3.7)$$

$$\frac{dC}{d\xi} = \frac{4z_A P_0 \exp(-\Gamma\xi)}{\pi^2 W} - \frac{z_A}{W^2} \left(\frac{4}{\pi^2} + C^2 \right). \quad (3.8)$$

where $\Gamma = \alpha L_A$, and $P_0 = \gamma_0 a_0^2 L_D$ is the normalized initial peak power. Our objective is to find a periodic solution of Eqs. (3.7) and (3.8) such that all soliton parameters (except ϕ) recover their initial values after one amplifier spacing. This periodicity condition can only be met under certain launch conditions. The optimal launch conditions are determined by solving Eqs. (3.7) and (3.8) with the boundary conditions

$$C(0) = C_0 = C(1), \quad W(0) = 1 = W(1). \quad (3.9)$$

3.3.2 Analytical Results

In general, Eqs. (3.7)–(3.9) should be solved numerically by considering different input values for the peak power P_0 , pulse width $T_o(0)$, and initial chirp C_0 . Because of the multidimensional nature of the parameter space, an exhaustive search for periodic solutions is quite time consuming. However, we can solve Eqs. (3.7) and (3.8) approximately by using a perturbation method in the regime $z_A \ll 1$. The natural parameter for perturbation expansion is z_A since C and W vary little along the fiber length for $z_A \ll 1$. Expanding C and W up to second-order in z_A , we can write

$$W = W_0 + W_1 z_A + W_2 z_A^2, \quad (3.10)$$

$$C = C_0 + C_1 z_A + C_2 z_A^2. \quad (3.11)$$

Since $C_0 = 0$ and $W_0 = 1$ (the lossless case), we obtain the following two equations by substituting Eq. (3.10) and (3.11) into Eq. (3.7) and (3.8) and collecting the terms in similar powers of z_A ,

$$\frac{dW_2}{d\xi} = -C_1, \quad (3.12)$$

$$\frac{dC_1}{d\xi} = \frac{4P_0 \exp(-\Gamma\xi)}{\pi^2} - \frac{4}{\pi^2}. \quad (3.13)$$

The width parameter W has no first-order corrections. These equations can be solved by direct integration to obtain $C_1(\xi)$ and $W_2(\xi)$. Applying the boundary condition $C_1(0) = C_1(1)$ sets the launch condition for peak power to be

$$P_0 = \frac{\Gamma}{1 - \exp(-\Gamma)} = \frac{G \ln G}{G - 1}. \quad (3.14)$$

Similarly, applying the boundary condition $W_2(0) = W_2(1)$ provides the input chirp

$$\begin{aligned} C_1(0) &= \frac{2}{\pi^2} - \left(\frac{4}{\pi^2} \right) \frac{\exp(-\Gamma) + \Gamma - 1}{\Gamma(1 - \exp(-\Gamma))} \\ &= \frac{4}{\pi^2} \left[\frac{1}{2} + \frac{(G - 1) - G \ln G}{\ln G(G - 1)} \right]. \end{aligned} \quad (3.15)$$

The peak-power condition, Eq. (3.14), is the same as that obtained by the guiding-center soliton theory [22] (also see Eq. (3.6)) assuming that an unchirped soliton is launched at the input end. The chirp condition, Eq. (3.15), is new and is obtained by requiring that the pulse width recovers its initial value periodically. We have seen that the variational analysis allows us to examine the conditions of periodicity for both the chirp and the width, resulting in an additional constraint in Eq. (3.15). We will refer these solitons as chirped path-average solitons.

3.4 Numerical Results

In this section we discuss the new operating regime of chirped solitons and compare it with the standard operating regime in which unchirped solitons are launched at the input end. The perturbation analysis of Section 3.3.1 provides an estimate of the launching parameter only for $z_A \ll 1$. However, we expect on physical grounds chirped solitons to be useful for designing high-speed periodically amplified fiber links even when z_A exceeds 1. The operating region in which the amplifier spacing is comparable or larger than the dispersion length ($z_A > 1$) can be studied by solving Eqs. (3.7) and (3.8) numerically.

To obtain the numerical solution, we use a root-finding algorithm to satisfy the boundary conditions imposed by Eq. (3.9). For definiteness, we choose $L_A = 40$ km

and $G = 10$ ($\Gamma = 2.3$) and find the optimum values of P_0 and $C(0)$ numerically for z_A in the range 0–2.5. Figure 3.4 compares the peak power P_0 needed for launching chirped (solid line) and unchirped (dashed line) soliton as z_A is increased from 0 to 2.5. In the regime $z_A \ll 1$, the launch power is virtually the same for both chirped and unchirped solitons; this result agrees with our perturbation analysis as well as with guiding-center soliton theory. As z_A increases, the chirped soliton requires slightly more power. However, the increase in peak power is less than 2% even for $z_A = 2.5$. Figure 3.4 shows the amount of prechirping required as a function of z_A . The input soliton needs to be prechirped more and more as amplifier spacing increases.

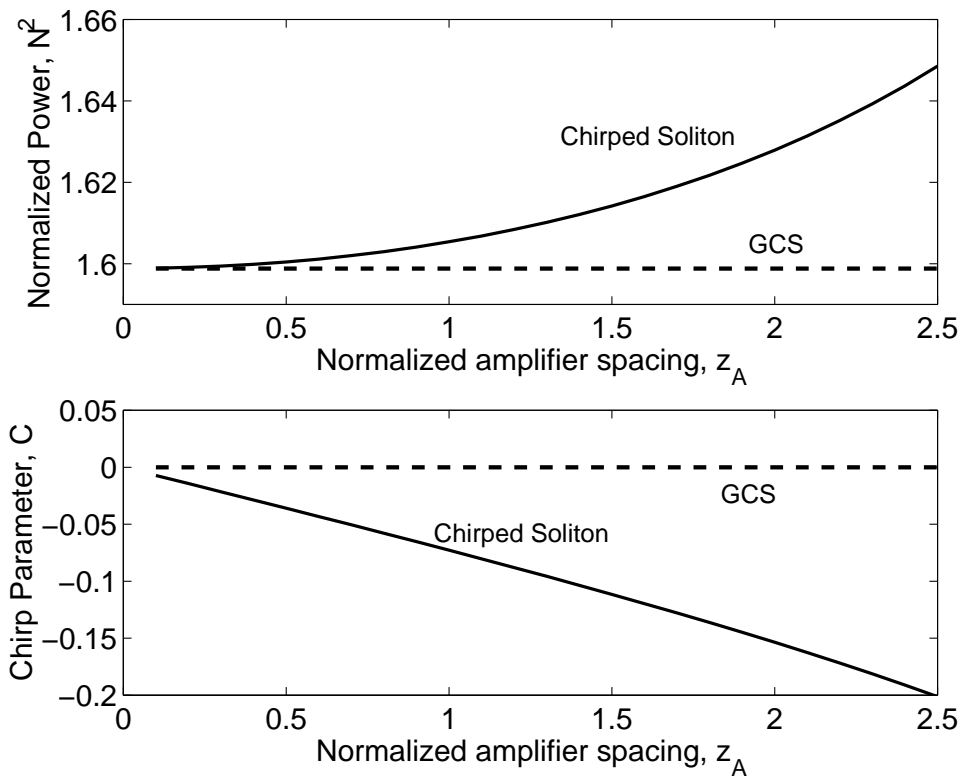


Figure 3.4: Comparison of launching peak power (top) and initial chirp (bottom) for chirped (solid curves) and unchirped (dotted curves) solitons or GCS as a function of normalized amplifier spacing when amplifiers with 10-dB gain ($\Gamma = 2.3$) are placed 40 km apart.

The need for negative prechirping can be understood by examining Eq. (3.8), which shows that $dC/d\xi$ contains a negative term (since $\beta_2 < 0$ for anomalous dispersion) and an exponentially decreasing positive term. Initially, the positive term dominates due to the high peak power, and the chirp increases with propagation. However, the nonlinear term is reduced because of fiber loss, and $dC/d\xi$ becomes negative, resulting in a downward concave trajectory. In addition the boundary condition Eq. (3.9) requires that

$$\int_0^1 C(\xi) d\xi = 0. \quad (3.16)$$

For a concave-down trajectory this integral relation can be satisfied only for negatively prechirped pulses [$C(0) < 0$] [see figure 3.6(b)].

Since both the soliton width and chirp are allowed to vary along z periodically in the new operating regime proposed here, it is important to consider the extent of variation in each fiber section between two amplifiers. Figures 3.5 and 3.6 show variation of pulse width and chirp along the fiber length for $z_A = 0.4$ and $z_A = 2.1$ respectively using launch conditions corresponding to a chirped (solid line) and an unchirped soliton (dashed line).

In the $z_A \ll 1$ regime, the chirp is fairly periodic in both cases. But since the unchirped soliton does not impose periodicity of the pulse width, soliton width is reduced by 1%. In contrast, the width recovers its initial value for the chirped soliton. In the $z_A > 1$ regime, however, the perturbation becomes too great for the unchirped soliton to maintain the periodic nature of the pulse width and chirp. As seen in Figure 3.6(a), the soliton width can vary as much as by 20% (dashed line) and is smaller by 10% after one amplifier spacing. In contrast, the chirped PAS recovers both pulse

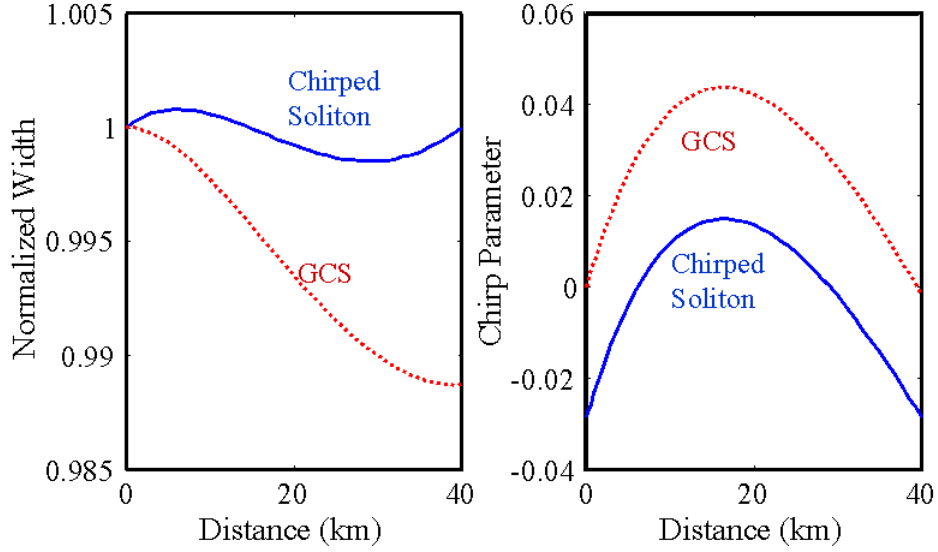


Figure 3.5: Evolution of pulse width and chirp over one amplifier stage for a chirped (solid curves) and an unchirped (dotted curves) soliton or GCS as predicted by variational analysis. Normalized amplifier spacing is $z_A = 0.4$.

width and chirp after each amplifier. Also, width variations are much smaller ($< 5\%$) for chirped solitons showing clearly that such solitons are not perturbed significantly even when $z_A > 1$.

In order to check the validity of variational analysis, Figure 3.7 and 3.8 are obtained using the same parameters as those used in Figure 3.5 and 3.6 except that the nonlinear Schrödinger equation is solved numerically over 20 amplification stages (total transmission distance of 800 km). The root-mean-square (RMS) width [2] (see Appendix) and chirp of the pulse are calculated numerically. We decided to estimate the RMS width since the shape of the pulse is not guaranteed to remain preserved even though variational analysis requires it. The chirp parameter is estimated by fitting a parabola to the phase profile in the vicinity $T = 0$ and noting from Eq. (2.63) that the quadratic term varies as $CT^2/2T_o^2$. Figure 3.7 and 3.8 show that the periodicity in C and T_o

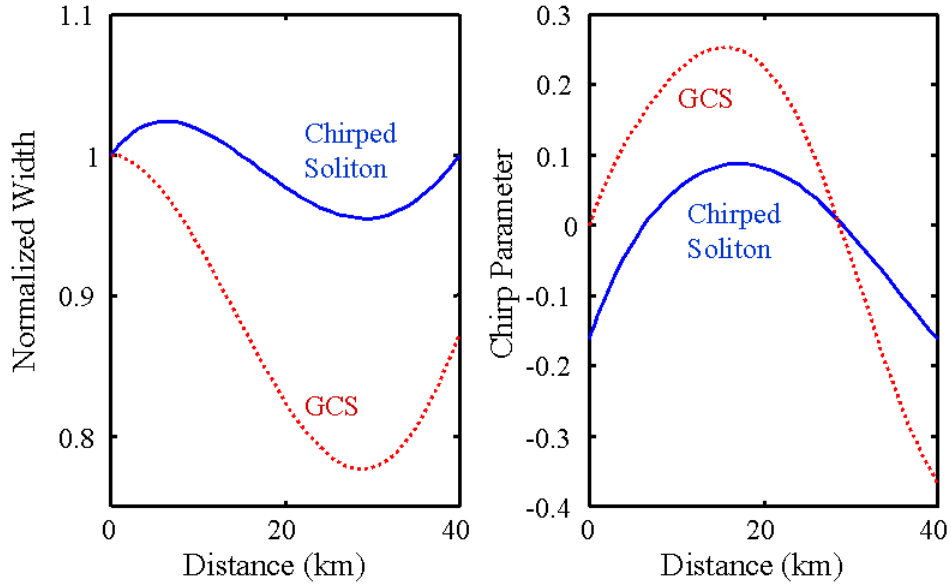


Figure 3.6: Evolution of pulse width and chirp over one amplifier stage for a chirped (solid curves) and an unchirped (dotted curves) soliton or GCS as predicted by variational analysis. Normalized amplifier spacing is $z_A = 2.1$.

is maintained only approximately over multiple amplifiers. For example, RMS pulse width varies 1% from amplifier to amplifier when $z_A = 0.4$, and variations become as large as 10% when $z_A = 2.1$. This is not surprising and indicates that the “sech” pulse shape is not the true pulse shape for the periodic solution of the nonlinear Schrödinger equation. As we noted earlier, variational analysis cannot accurately predict the soliton parameters once the shape of the soliton is not preserved. Figures 3.7(a) and 3.8(a) show that the RMS width varies less when a chirped soliton is launched. For instance, in the case $z_A = 2.1$, width of unchirped solitons exhibit more than 20% variation, whereas chirped solitons exhibit a maximum of 10% variation. This feature suggests that, in general, the use of prechirped solitons is likely to provide better system performance compared with unchirped solitons.

To explore the soliton-stability issue, we have plotted the chirp and width variations

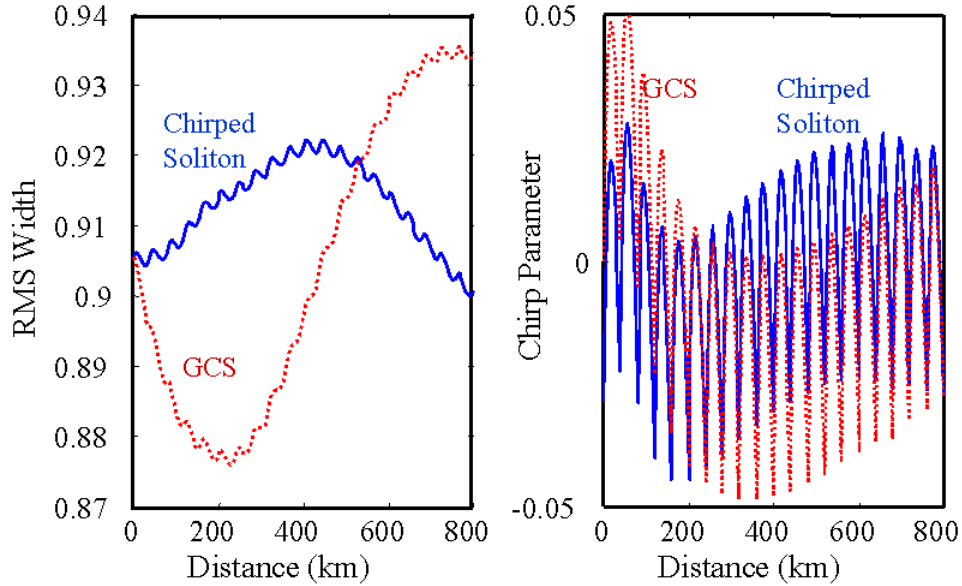


Figure 3.7: Same as in Fig. 3.5 except that soliton evolution over 20 amplification stages (total distance of 800 km) is shown by solving the NSE numerically.

in the two-dimensional phase space as a Poincaré map since such a map shows the phase-space region over which width and chirp vary along the fiber length. Figure 3.9 shows the Poincaré map for chirped and unchirped solitons over 100 amplifier spacing (4000 km). Ideally, if the system is perfectly periodic, we would expect all the points to coincide, resulting in a single dot in the plot. Our numerical results show that for both $z_A = 0.4$ and $z_A = 2.1$, the chirped soliton is more localized, implying that both the soliton width and chirp vary over a smaller range from one amplifier to the next. This behavior confirms our variational result that prechirping is necessary for stable propagation. Forysiak *et al.* [30] reached a similar conclusion using an operator-splitting technique.

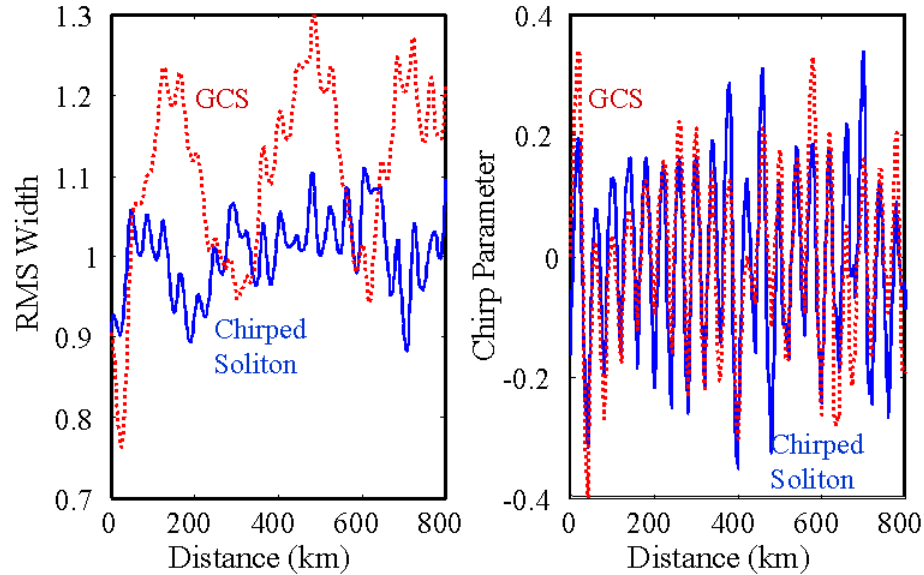


Figure 3.8: Same as in Fig. 3.6 except that soliton evolution over 20 amplification stages (total distance of 800 km) is shown by solving the NSE numerically.

3.5 Summary

Fiber-optic communication systems employ the technique of lumped amplification to compensate for fiber losses. In order to maintain soliton integrity in the presence of fiber losses, guiding-center soliton is used but the system is then limited in the amplifier spacing it can sustained. We have found a new operating regime for soliton transmission in periodically amplified lightwave systems. This regime requires launching of an initially chirped soliton. Our variational analysis recovers the guiding-center soliton result in the regime $z_A \ll 1$. By allowing both the pulse width and the chirp to vary over each amplifier section, we find that prechirping the pulse is necessary in order to sustain path-averaged solitons in the regime $z_A \sim 1$ in a periodically amplified optical communication system. We use the results of variational analysis to determine the amount of pre-chirping and initial peak power required to recover initial launch val-

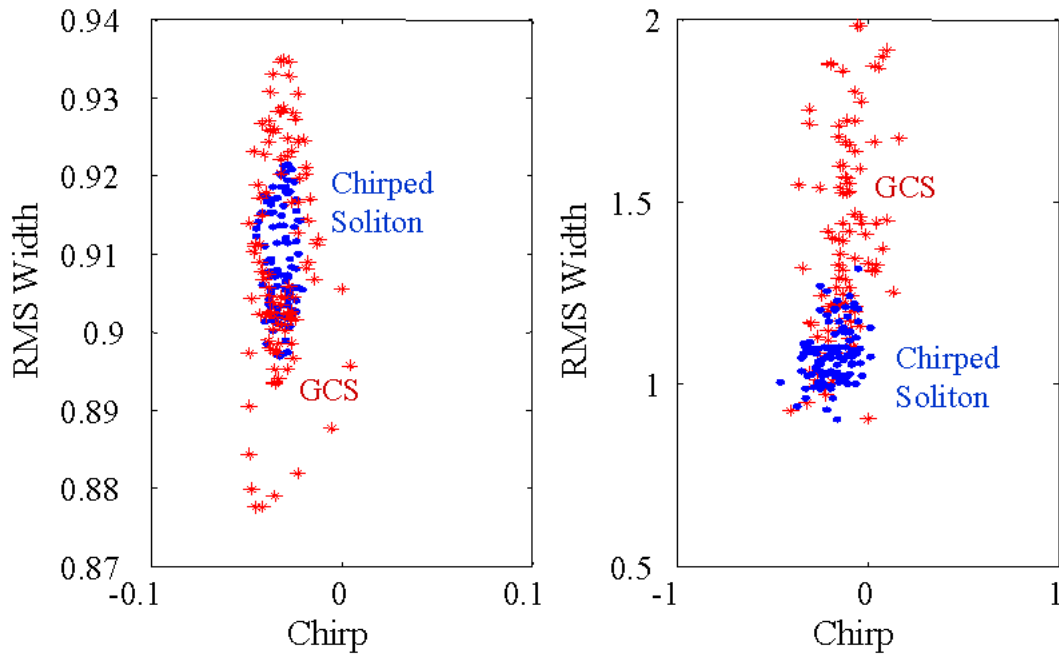


Figure 3.9: Poincaré map obtained by plotting soliton width and chirp at the end of each amplifier section for 100 amplification stages (4000 km) for unchirped or GCS (*) and chirped (●) soliton. For $z_A = 0.4$, nearly circular compact region shows the quasi-periodic nature of soliton evolution. For $z_A = 2.1$, soliton width and chirp vary over a wider region.

ues at each amplifier. Numerical solutions of the nonlinear Schrödinger equation show that the use of prechirped solitons improves stability since variations of pulse width and chirp over a large transmission distance are much smaller compared to guiding-center solitons. The new operating regime should be useful at high bit rates (> 20 Gb/s) by permitting amplifier spacing to become larger than the dispersion length. This technique is simple to implement because most pulses emitted by semiconductor lasers are chirped. In addition, correct prechirping can also be achieved through propagating the pulse through a correct length of optical fiber.

Chapter 4

Distributed Amplification in Constant-Dispersion Systems

4.1 Introduction

Soliton communication systems are leading candidates for long-haul lightwave transmission links because they offer the possibility of a dynamic balance between group-velocity dispersion (GVD) and self-phase modulation (SPM), the two effects that severely limit the performance of non-soliton systems [2,39]. Most system experiments employ the technique of lumped amplification and place fiber amplifiers periodically along the transmission line for compensating the fiber loss.

The limitation on the amplifier spacing imposed by lumped amplification was studied (see guiding-center soliton, section 3.2). This limitation can be overcome by prechirping the pulse (see Chapter 3) or by using distributed amplification [14]. In this scheme [40,41], the transmission fiber is pumped periodically, creating sufficient gain through either the presence of rare-earth erbium ions or using stimulating Raman scattering (SRS) for compensating the fiber loss. Since the gain is distributed throughout the fiber link and compensates the fiber loss locally all along the fiber, soliton peak-

power variations can be made much smaller compared with the lumped amplification scheme. Although one expects the pump-station spacing L_A to become comparable and even exceed L_D in the case of distributed amplification, a systematic comparison of the lumped and distributed amplification schemes is not available in the literature. Furthermore, shorter pulses needed at high bit rates are affected considerably by SRS, therefore the inclusion of SRS is essential in modeling high-bit-rate systems [9].

4.2 Erbium-Doped Fiber Amplifiers

Fiber-optic communication systems compensates for fiber losses through the use of EDFAs. An EDFA consists of regular silica fiber doped with erbium rare earth ions and is modeled as a three-level gain medium (see Figure. 4.1). Semiconductor lasers are

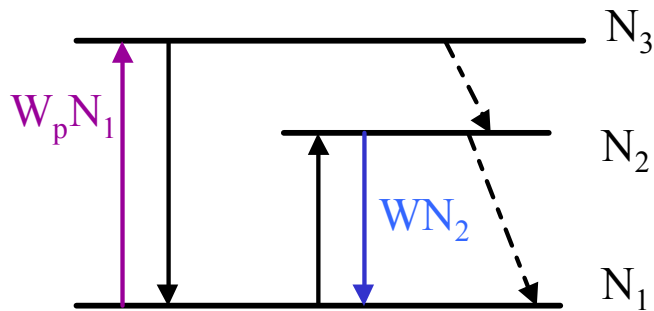


Figure 4.1: Three level model of erbium-doped gain medium

usually used as pump power sources to provide the population inversion necessary to achieve gain.

The rate equations for the three level system can be written down as follows:

$$\frac{dN_3}{dt} = W_p N_1 - N_3 \gamma_3 - W_p N_3 \quad (4.1)$$

$$\frac{dN_2}{dt} = N_3 \gamma_3 - W(N_2 - N_1) - N_2 \gamma_2 \quad (4.2)$$

$$\frac{dN_1}{dt} = N_2 \gamma_2 + W(N_2 - N_1) - W_p(N_1 - N_3), \quad (4.3)$$

Where N_1 , N_2 , and N_3 are the number of erbium ions in each of the respective energy levels, and $N_T = N_1 + N_2 + N_3$ is the total number of erbium ions (ions/ μm^3) in the fiber. The relaxation rate of the energy states (second and third level) are represented by γ_2 and γ_3 respectively, W and W_p are the photon density rates of the signal and the pump. The steady state solution of $\frac{dN_i}{dt} = 0$ (where $i=1, 2, 3$) reduces the rate equations (4.1) – (4.3) to the following equalities:

$$N_1 = \frac{N_3(\gamma_3 + W_p)}{W_p} \approx \frac{N_3 \gamma_3}{W_p} \quad (4.4)$$

$$N_2 = \frac{N_3 \gamma_3 + W N_1}{W + \gamma_2} \approx \frac{N_1(W + W_p)}{W + \gamma_2} \quad (4.5)$$

$$N_3 = \frac{N_1(W_p + W) - N_3 W_p}{W + \gamma_2} \approx \frac{N_1(W_p + W)}{W + \gamma_2}, \quad (4.6)$$

with the assumption that the third level decays faster than the pump absorption ($\gamma_3 \gg W_p$), and most of the ions are going to be in the ground state as compared to the upper state ($N_1 \gg N_3$). The population inversion ΔN can then be calculated from the above equations using $\Delta N = N_2 - N_1$

$$\Delta N = \frac{N_T(\gamma_3 W_p - \gamma_3 \gamma_2 - W_p \gamma_2)}{W(3W_p + 2\gamma_3) + 2W_p \gamma_2 + \gamma_3(W_p + \gamma_2)}. \quad (4.7)$$

For a rapid upper state relaxation ($\gamma_3 \gg \gamma_2, W_p$), Eq. (4.7) can be further reduced to

$$\Delta N = \frac{N_T(W_p - \gamma_2)}{2W + W_p + \gamma_2}. \quad (4.8)$$

The gain of the medium is the product of the absorption cross section and the population inversion so that

$$g = \sigma \Delta N = \frac{\sigma N_T(W_p - \gamma_2)}{2W + W_p + \gamma_2}. \quad (4.9)$$

Lumped amplification schemes using EDFA necessitates that the net gain of the amplifier exactly compensates for the fiber loss. To this end, the fiber is doped heavily and Eq. (4.9) is solved with respect to pump rate W_p such that sufficient gain is obtained, the stipulation being of course that the amplifier length L_A obeys the guiding-center soliton condition of section 3.2 or the prechirped path-average condition of section 3.3.

Even though the amplifier is intended to amplify a train of optical pulses, the communication system operates at very high bit rates with pulses in the order of picoseconds and because the fluorescence lifetime of the excited erbium ions is only order of ≈ 10 ms, we can write the signal and pump waves in the continuous wave (CW) regime [2].

The equations that describe the pump-signal interaction are given as

$$\frac{dP_p}{dz} = -(\sigma_p N_1 + \alpha_p) P_p, \quad (4.10)$$

$$\frac{dP_s}{dz} = (\sigma_s \Delta N - \alpha_s) P_s. \quad (4.11)$$

where P_p , P_s , σ_p , and σ_s are the pump and signal powers and transition cross sections respectively. The above equations are used to study the small-signal and large-signal

amplification and their predictions are accurate for our purposes. The gain of EDFA can be as high as 30 dB with only 30 m of erbium-doped fiber requiring only approximately 4 mW of pump power at $1.48 \mu\text{m}$ [2].

4.3 Distributed Erbium-Doped Fiber Amplifiers

Distributed erbium-doped fiber amplifiers (d-EDFA) basically replace the traditional set of transmission fiber and high-gain EDFA with a transmission fiber that is lightly doped with rare-earth erbium ions. The link then becomes essentially transparent when pumped from both directions (see Figure 4.2). Fiber transparency can be accomplished with various dopant concentrations, which can be used to adjust for minimum gain/loss perturbation for the soliton pulses.

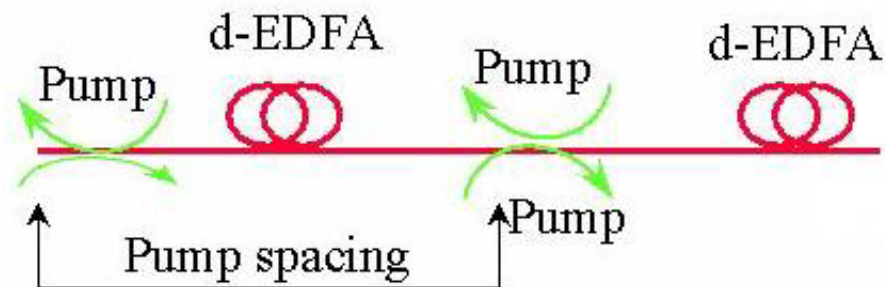


Figure 4.2: Distributed-erbium doped amplifier link

4.3.1 Modeling Gain in Distributed Fiber Amplifiers

Since d-EDFA is just an extension of EDFA, we can use the same three-level gain model from the previous section (Sec. 4.2). Since the erbium-doped fiber length is much

longer and we are trying to minimize gain/loss perturbation, the optimal pump scheme consists of bi-directional pumping [42] (see Fig. 4.3). We can study the evolution of

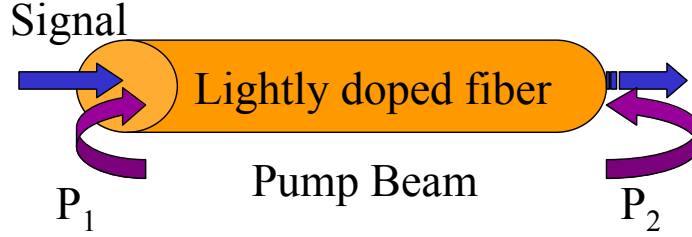


Figure 4.3: Bi-directional pumping of d-EDFA

forward and backward pump powers along with the signal power using the following set of three equations.

$$\frac{dP_f}{dz} = [-A N_1(z; P_f, P_b) - \alpha_p]P_f, \quad (4.12)$$

$$\frac{dP_b}{dz} = [A N_1(z; P_f, P_b) + \alpha_p]P_b, \quad (4.13)$$

$$\frac{dP_s}{dz} = [\sigma \Delta N(z; P_f, P_b) - \alpha_s]P_s. \quad (4.14)$$

which include the saturation of gain as well as pump depletion. P_f , P_b , and P_s are the forward, backward-pump and signal powers respectively.

4.3.2 Small-Signal Solution

Assuming small signal power, we can solve the above equations analytically by ignoring the first term in the pump power equation that represents the pump depletion due to absorption. Just keeping the fiber loss term of the pump powers, the forward and

backward pumped powers are given as

$$P_f(z) = P_i \exp(-\alpha_p z), \quad (4.15)$$

$$P_b(z) = P_i \exp[\alpha_p(z - L_A)], \quad (4.16)$$

where P_i is the initial pump power. The saturation power can be written in terms of the pump powers by noting that the signal and pump rate can be rewritten in terms of power

$$W = \frac{\sigma P}{E_o A_{eff}}. \quad (4.17)$$

Eq. (4.9) can then be rewritten as

$$g = \frac{g_o}{1 + P_s/P_{sat}}, \quad (4.18)$$

where the small signal gain g_o and the saturation power are define as

$$g_o = \frac{\sigma N_t(P_f + P_b + P_A)}{P_f + P_b + P_A}, \quad (4.19)$$

$$P_{sat} = \frac{1}{2} (P_f + P_b + P_A), \quad (4.20)$$

where $P_A = E_o A_{eff} \gamma_2 / \sigma$ represents the spontaneous emission, which contributes to the noise of the system.

4.3.3 Numerical Solution

Full solution can be obtained numerically by integrating Eqs. (4.12)–(4.14). Further simplification can be applied to reduce the complexity of the problem by noting that Eqs. (4.12)–(4.13) have the following equality

$$-\frac{1}{P_f} \frac{dP_f}{dz} = \frac{1}{P_b} \frac{dP_b}{dz}. \quad (4.21)$$

Simple algebraic manipulation yields the following relation between the forward and backward pump powers

$$\begin{aligned} \frac{d}{dz} [\ln(P_f) + \ln(P_b)] &= 0, \\ \frac{d}{dz} (P_f + P_b) &= 0, \\ P_f P_b &= C, \end{aligned} \quad (4.22)$$

where C is a constant that is the product of the forward and backward pump-powers. To summarize, the following constrains are used to solve coupled ordinary differential equations given by Eqs. (4.12)–(4.14):

$$P_f P_b = C, \quad (4.23)$$

$$P_f(z = 0) = P_b(z = L_A), \quad (4.24)$$

$$\int_0^{L_A} g(z) - \alpha_s dz = 0. \quad (4.25)$$

Figure 4.4 shows the comparison between the analytical and numerical solution of the pump power evolution, showing the role of pump absorption on a 100 km d-EDFA

amplifying an averaged signal power of 0.3 mW with losses of 0.2 dB/km for both pump and the signal. Note that even for such a small signal power, there is a noticeable

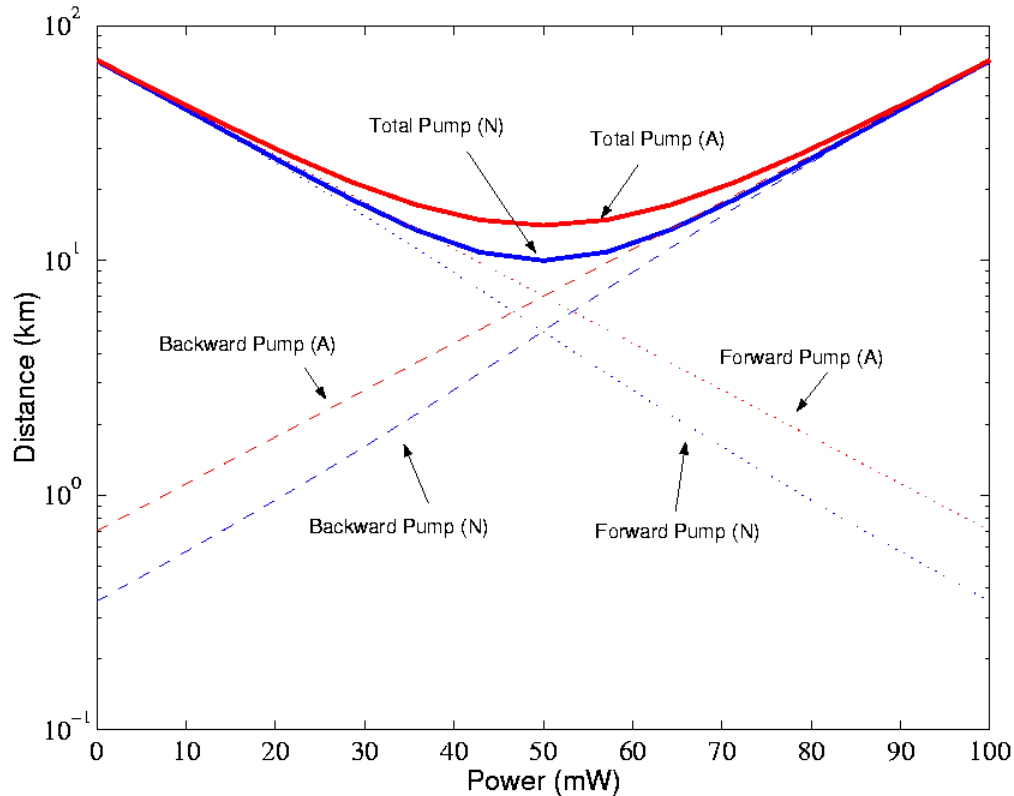


Figure 4.4: Analytical and numerical solution of the forward, backward, and total pump powers

differences in the pump power evolution which are due to the effect of pump depletion that was neglected in the analytical analysis. For systems using high power pulses or employing WDM technology, it is imperative that the effect of pump absorption due to signal-gain depletion be included. The results showed that a pump power of nearly 80 mW is required to amplify the signal using 100 km of d-EDFA fiber with a dopant density of $200 \text{ ions}/\mu\text{m}^3$. As the dopant density is increased, the pump power required is decreased (Figure 4.5). This comes from the fact that for low dopant densities, ad-

ditional pump power is needed to penetrate deeper into the erbium-doped fiber against pump power absorption and fiber loss. For higher dopant densities, enough gain can be garnished within a short span of erbium-doped fiber that additional power is not necessary. Unfortunately, because of the higher pump absorption caused by the higher dopant densities, the maximum gain experienced by the signal is also increased (see Figure 4.6).

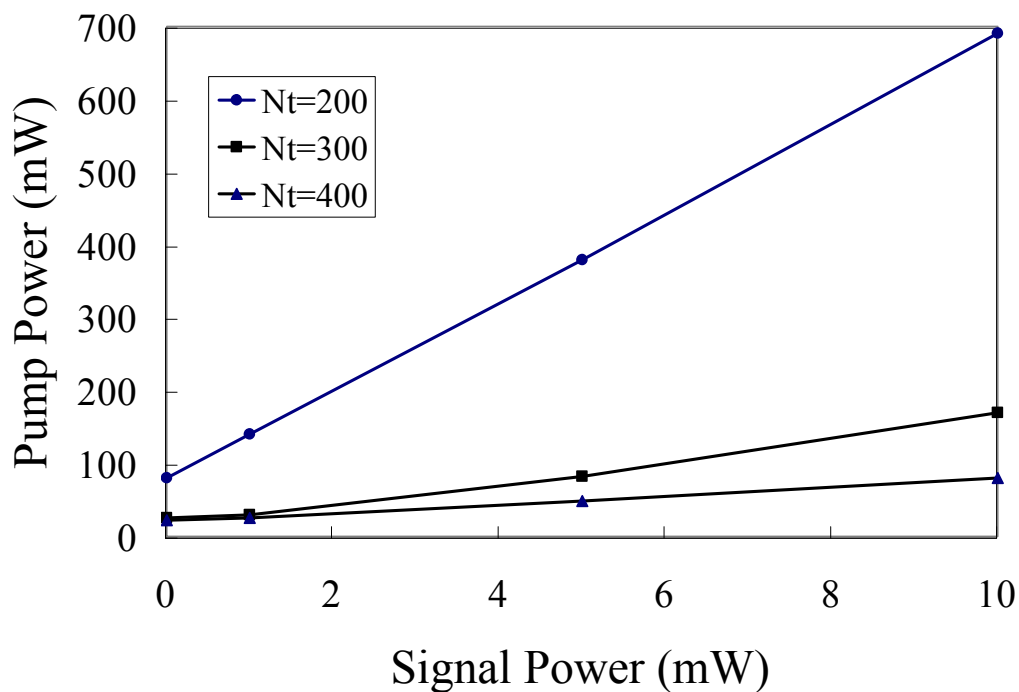


Figure 4.5: Pump power needed for various dopant levels

4.4 Raman Amplifier

Raman amplifiers use the nonlinear property of the fiber to convert pump light at one wavelength to signal gain at another wavelength. Unlike the d-EDFA, the transmission fiber is not modified with dopants but higher intensity pump powers are required to

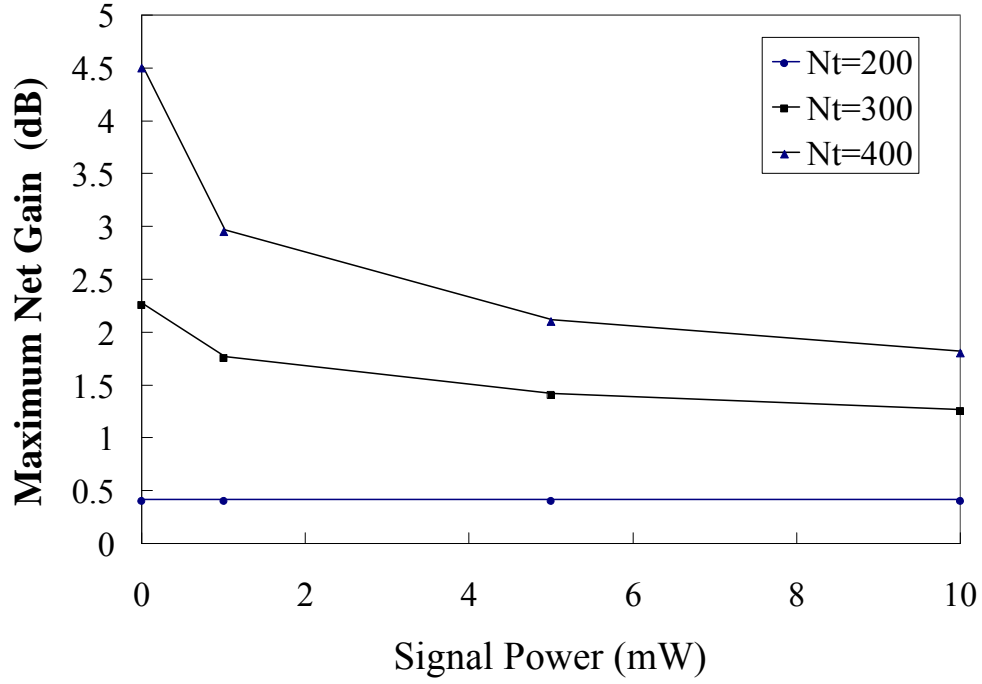


Figure 4.6: Maximum net gain for various dopant levels

initiate the nonlinear process. The Raman gain can be obtained by solving the following equations

$$\frac{dI_f}{dz} = -\frac{\omega_p}{\omega_s} g_R I_f I_s - \alpha_p I_f, \quad (4.26)$$

$$\frac{dI_b}{dz} = \frac{\omega_p}{\omega_s} g_R I_b I_s + \alpha_p I_b, \quad (4.27)$$

$$\frac{dI_s}{dz} = g_R (I_f + I_b) I_s - \alpha_s I_s, \quad (4.28)$$

where I_s , I_f and I_b are the signal and the forward and backward pump intensity respectively and g_R is the Raman gain coefficient. The frequency of the pump and signal is given by ω_p and ω_s .

4.4.1 Small Signal Analysis

We can solve Eqs. (4.26)-(4.28) analytically in the small-signal domain by assuming that the pump intensity is dominated by fiber losses. The forward and backward pump powers (note that we can convert intensity to power simply by using $P = I A_{eff}$) are given similarly by Eqs. (4.15)–(4.16). The pump parameter that we derived in Eq. (4.22) can also be applied to Raman amplification. Combining these equations, we can write the Raman gain as

$$g(z) = \frac{g_R}{A_{eff}} \left[P_i \exp(-\alpha_p z) + \frac{C}{P_i} \exp(\alpha_p z) \right]. \quad (4.29)$$

Imposing the equal pump condition and fiber transparency (see Eq. (4.23)) yields the following solution for the pump power needed

$$P_o = \frac{\alpha_s \alpha_p L_A A_{eff}}{2 g_R (1 - \exp(-\alpha_p L_A))}. \quad (4.30)$$

4.4.2 Numerical Results

The small signal approximation is valid for most single-channel systems since SRS is not a very efficient processes. For instance, even for average signals on the order of mW, the pump absorption due to signal-gain depletion is only on the order of

$$g_R A_{eff} I_s = 10^{-16} \left[\frac{\text{km}}{\text{W}} \right] \frac{10^{-3} [\text{W}]}{50 \times 10^{-18} [\text{km}^2]} \approx 0.01 \frac{\text{dB}}{\text{km}}, \quad (4.31)$$

which is much smaller than typical fiber loss 0.2 dB/km. Nevertheless, as in the case of d-EDFAs, the use of WDM technology greatly increases the total signal power that it

is often necessary to solve the equations exactly using numerical methods. The signal power as well as the forward and backward are solved simultaneously to obtain the gain

$$g(z) = \frac{g_R}{A_{eff}} [P_f(z) + P_b(z)]. \quad (4.32)$$

Figure 4.7 shows numerical result of the pump power evolution and the gain of a 100 km section of fiber compensated through bi-directional pumped Raman gain for low power signals. Note that the pump power needed is lower than a 100-km 200-ions/ μm^3

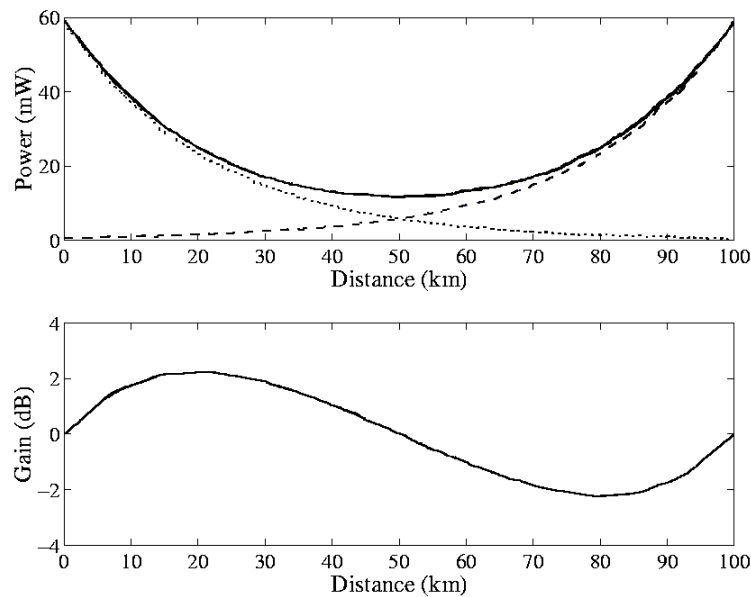


Figure 4.7: (Top) Numerical solution of forward (dotted line), backward (dashed line) and total pump power (solid line) of Raman amplifier. (Bottom) Numerical solution of gain variations of Raman amplifier

d-EDFA but its net gain is larger in comparison.

4.5 Amplifier Performance

We modify the generalized nonlinear Schrödinger equation, Eq. (3.1) to study the effect of using distributed amplification as

$$\frac{\partial U}{\partial \zeta} + \frac{i}{2} \text{sgn}(\beta_2) \frac{\partial^2 U}{\partial \tau^2} - iN^2 |U|^2 U = \left(g(\zeta) - \frac{\alpha}{2} \right) U - i\tau_R \frac{\partial |U|^2}{\partial \tau}, \quad (4.33)$$

with τ_R is the SRS coefficient and with lumped amplitude gain given by

$$g(z) = \left(\sqrt{G} - 1 \right) \sum_{n=1}^N \delta(\zeta - n\zeta_a). \quad (4.34)$$

Distributed amplification using d-EDFA and Raman gain is included by solving for the gain variation through Eq.(4.9) and Eq.(4.32) respectively. We used the split-step Fourier-transform method [9] to compare soliton propagation for lumped and distributed amplification schemes.

We first demonstrate the advantages offered by distributed amplification for a 20 Gb/s system having 100-km pump-station spacing, uniform dispersion with $\beta_2 = -0.5$ ps²/km, $\gamma = 3.36$ W⁻¹/km, $\tau_R = 3$ fs and $\alpha = 0.23$ dB/km at the operating wavelength near 1.55 nm. The soliton width should be a fraction of the 50-ps bit slot. We choose the input field $A(0, t) = \sqrt{P_0} \text{sech}(t/T_0)$ with $T_0 = 5$ ps ($T_{FWHM} = 8.8$ ps). The peak power P_0 corresponds to $N = 1$ for distributed amplification and $N = 2.307$ in the lumped amplification case as required in the average-soliton regime [2]. The dispersion length is 50 km for such a system, and the amplifier spacing is chosen to be 100 km both cases.

Figure 4.8(a) shows soliton evolution for the case of lumped amplification. Since

$L_A/L_D = 2$, the soliton develops significant dispersive waves after only 3 amplifiers and is distorted significantly after 6 amplification stages. Such a system cannot transmit

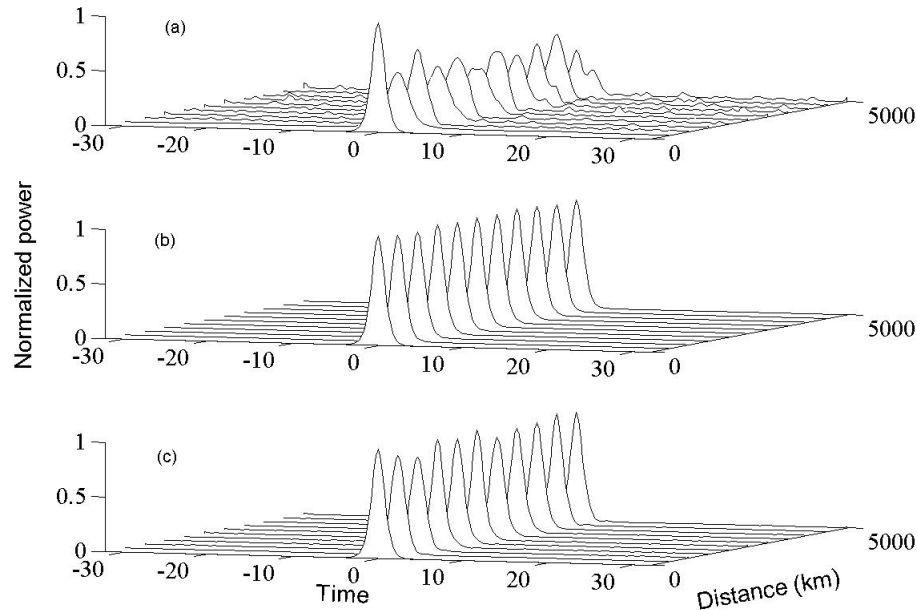


Figure 4.8: Comparison of (a) lumped, (b) d-EDFA, and (c) Raman amplification schemes for the case of a 20-Gb/s system designed with 100-km amplifier spacing.

the 20-Gb/s signal over more than 600 km. Figure 4.8(b) shows soliton evolution over 5000 km under identical operating conditions except for distributed amplification, with no visible sign of degradation. The optimum dopant density is found to be only 200 ions/ μm^3 when the fiber is bidirectionally pumped using equal pump powers of 79 mW at both ends. Figure 4.8(c) shows soliton evolution using Raman amplification. It uses slightly less pump power, roughly 60 mW at each end although it also supports soliton at the longer amplifier spacing; there were substantially more dispersive waves being generated. A logarithmic plot of the pulse power (Figure 4.9) shows the contribution of residual dispersive waves to remain below the 10^{-4} level even after 5000 km for d-

EDFA scheme while Raman amplification scheme has residual dispersion below 10^{-2} .

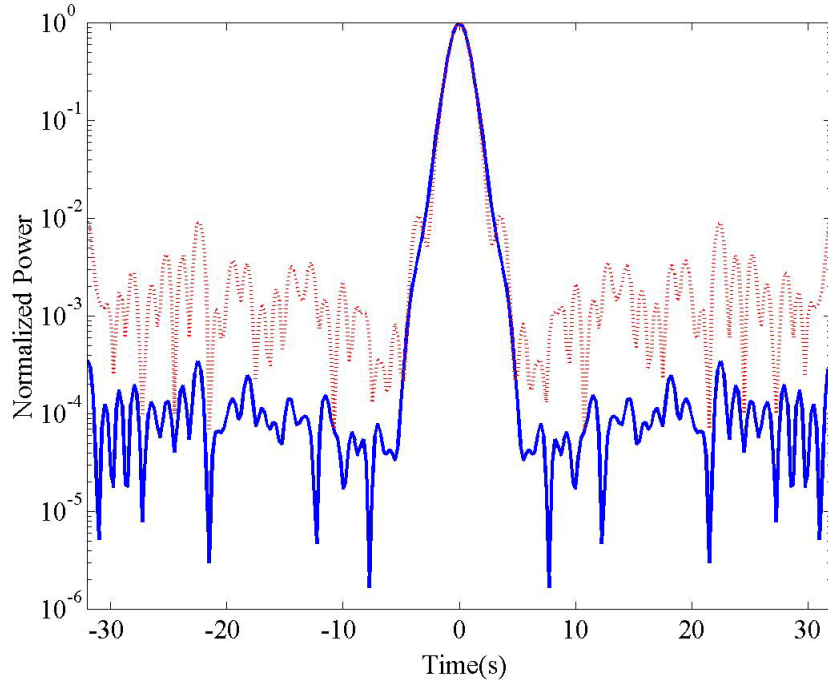


Figure 4.9: Level of dispersive wave using d-EDFA (solid line) and Raman amplification (dotted line)

The most important criterion for designing soliton systems with distributed amplification is to ensure that peak power varies as little as possible over each fiber span. Figure 4.10 shows the variation of pump power and the net signal gain defined as $G(z) = \exp(\int_0^z g(z) dz - \alpha z)$ over one fiber span for the results shown in Figures 4.8(b). Since $G(z) < 0.4$ dB, the soliton peak power varies less than 10%, compared with more than 20-dB variation occurring for lumped amplification or the 2 dB variation for Raman amplification (Figure 4.7). In general, peak-power variations become smaller as dopant density is reduced, but at the same time, required pump power increases [40]. In practice, one must choose the dopant density as small as possible for a given amount of pump power.

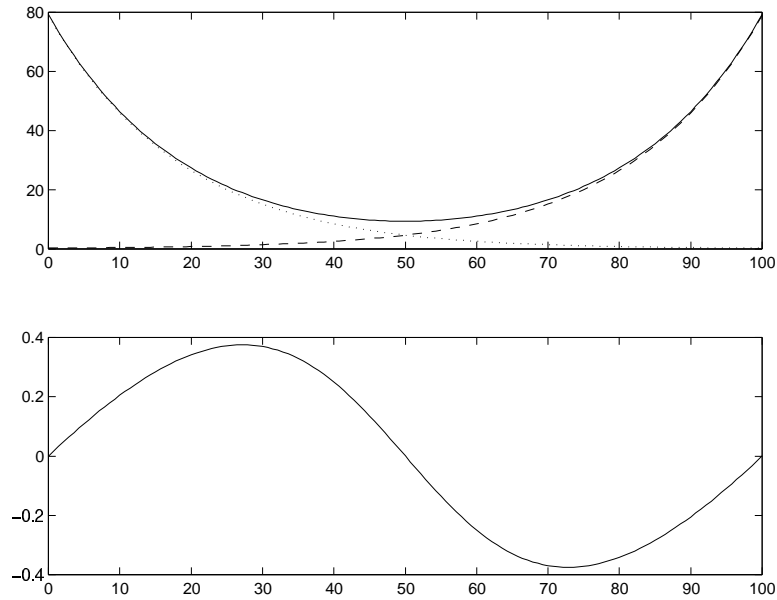


Figure 4.10: (Top) Numerical solution of forward (dotted line), backward (dashed line) and total pump power (solid line) of d-EDFA. (Bottom) Numerical solution of gain variations of d-EDFA

4.6 Summary

In this chapter, we set forth the models required to study distributed amplification using lightly-doped erbium ions as well as using distributed Raman gain. We present analytical solutions for the design of these distributed amplifiers in the small-signal regime. We also set forth the constraints needed to solve them numerically. In extending the guiding-center soliton limitation of the amplifier spacing, we found that distributed amplification can support solitons with amplifier spacing as large as $2L_D$. We also demonstrated through numerical simulation of the nonlinear Schrödinger equation that

distributed amplification can permit single-channel speeds of 20 Gb/s over transoceanic distances while maintaining 100 km spacing between pumping stations.

Chapter 5

Dispersion-Management Systems

5.1 Introduction

The two biggest obstacles in the design of high-capacity lightwave transmission systems are fiber loss and chromatic dispersion. It has been shown earlier that the use of distributed amplification can reduce the limitations of the guiding-center soliton amplifier spacing (see Chapter 4). Another way of solving the dispersion problem is through the use of dispersion management techniques. Thus far, the use of EDFAs in combination with dispersion management has produced commercial WDM systems having single-channel bit rates of up to 10 Gb/s with practical amplifier spacings. However, the increasing demand is pushing the industry toward systems with a capacity of a few Tbit/s. Keeping the current single-channel bit rate of 10 Gb/s would require hundreds of WDM channels in such systems. Increasing the single-channel bit rate to 40 and 80 Gb/s would reduce the number of multiplexed channels needed while simplifying the network management [43] by reducing the number of components required.

Soliton communication system is a natural candidate for long-haul, ultra-high-bit-rate lightwave transmission links, since the short pulse width required for high bit-rates will also induced large nonlinearity that must be accounted for. Solitons can effectively

use nonlinear SPM to dynamically balance GVD [2]. Most fiber-optic communication system experiments employ the technique of lumped amplification and place fiber amplifiers periodically along the link to compensate for the fiber loss. However, lumped amplification introduces large peak-power variations, which limit the amplifier spacing, L_A , to a fraction of the dispersion length L_D [2]. At high bit rates (> 20 Gb/s), the dispersion length can become quite small, making the use of lumped amplification impractical. For example, a recent experiment demonstrating a 40 Gb/s soliton system using dispersion management needed amplifier of 28 km [44]. Indeed, loss and gain perturbations along the fiber link are the most serious obstacle in designing practical soliton communication systems.

While many recent studies have considered novel dispersion maps and distributed amplification schemes [45–48], and a few studies even have examined the added stability of dispersion management with distributed amplification [46,47], a systematic study on the system level performance which includes the effect of ASE and incorporates both of these design features has not yet been performed. The performance of high-speed single-channel systems (operating at 40 and 80 Gb/s) with large amplifier spacings (100 km and 40 km, respectively) is examined in this thesis using several different hybrid amplification schemes. Two-step as well as dense dispersion-management configurations are used in conjunction with a variety of lumped and distributed amplification schemes. Specifically, the performance of lightwave systems using lumped amplifiers, hybrid amplifiers (backward-pumped Raman with EDFA), bidirectionally pumped Raman amplifiers (d-Raman), and distributed EDFA are compared.

5.2 Dispersion Managed Soliton

Dispersion Management uses spatially varying dispersion along the fiber to combat the effect of GVD. There are two basic techniques which consist of either using dispersion-decreasing fibers [9,49,50] or periodic dispersion maps. A dispersion decreasing fiber matches the dispersion of the fiber to the loss profile of the fiber. Such fibers are difficult to make and are not yet available commercially. The most popular technique of dispersion management by far is the use of a periodic dispersion map to compensate for GVD.

Substantial work has been done on the stability and the conditions of dispersion-managed solitons using a variety of techniques [51–58]. By far, the most commonly used technique has been the use of variational analysis [20,52,57]. The theoretical framework using variational analysis to calculate the amount of prechirping and launching power needed for stable pulse propagation is presented below.

5.2.1 Variational Analysis

Variational analysis is used to develop an approximate solution in a periodic dispersion map. It has been shown in Chapter 3 that prechirping is necessary for additional soliton control in establishing soliton periodicity. We also have seen that the creation of solitons necessitates a careful balance of nonlinearity and dispersion, so calculating the optimal launching power is also critical. Studies have shown that a detuning of the input soliton energy from its optimal value can generate dispersive-wave emission that can contribute to long-range soliton-soliton interactions [59,60].

5.2.2 Two-Step Dispersion Map

The nonlinear Schrödinger equation can be modified to account for the dispersion-variation by allowing the GVD to be a function of time. Equation (3.3) is generalized as

$$\frac{\partial U}{\partial z} + \frac{i}{2}\beta_2(z)\frac{\partial^2 U}{\partial T^2} - iG(z)\gamma|U|^2U = 0, \quad (5.1)$$

where $G(z)$ takes place of the fast-varying dynamics of gain-loss evolution a^2 , $\beta_2(z)$ is defined as

$$\beta_2(z) = \begin{cases} \beta_{21} & : 0 < \text{mod}(z, L_A) < L_1 \\ \beta_{22} & : 0 < \text{mod}(z, L_A) < L_{map} \end{cases} \quad (5.2)$$

where β_{21} , β_{22} , L_1 , and L_2 are the dispersion values and fiber section lengths of the two section of the fiber (see Figure 5.1) with differing signs of dispersion values ($\beta_{21} \beta_{22} <$

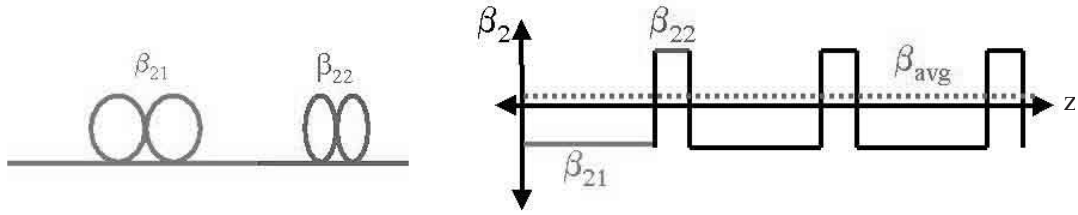


Figure 5.1: Two-step dispersion map

0). At the same time, the dispersion values sufficiently compensate each other such that

$$|\beta_{21} L_1| \approx |\beta_{22} L_2| \sim T_o^2, \quad (5.3)$$

where τ_o is the pulse width.

It is convenient to renormalize the system with respect to dispersion map L_{map} , normalized soliton energy U_o , and pulse [52],

$$\xi = \frac{z}{L_{map}}, \quad u = \frac{U}{U_o}, \quad \varsigma = \frac{T}{\sqrt{\frac{L_1 L_2 |\beta_{21} - \beta_{22}|}{L_{map}}}}. \quad (5.4)$$

This normalization allows us to rewrite the equation as follow

$$iu_\xi - \frac{1}{2}\beta_2(\xi) u_{\varsigma\varsigma} + \epsilon \left[\frac{1}{2}\bar{\beta}_2 u_{\varsigma\varsigma} + G(\xi)u|u|^2 \right] = 0 \quad (5.5)$$

where ϵ and the average dispersion, $\bar{\beta}_2$ are defined as

$$\epsilon = L_{map} \gamma |U_o|^2, \quad (5.6)$$

$$\bar{\beta}_2 = \frac{\beta_{21}L_1 + \beta_{22}L_2}{L_1 L_2 |\beta_{21} - \beta_{22}| |U_o|^2}. \quad (5.7)$$

Following the analysis set forth in 2.5, we will replace the soliton ansatz in Eq. (2.63) with a Gaussian ansatz of the form

$$u_o = \frac{A}{\sqrt{\left(1 + 2i \left(\frac{\Delta}{\varsigma_o^2}\right)\right)}} \exp\left(i\phi - \frac{i\varsigma^2}{\varsigma_o^2 + 2i\Delta}\right). \quad (5.8)$$

where A is the amplitude, ς_o is the initial normalized width, Δ is the normalized chirp parameter, and ϕ is the phase. The corresponding pulse parameter evolution is then

[52]

$$A^2 \varsigma_o = E = \text{constant}, \quad (5.9)$$

$$\frac{d\varsigma}{d\xi} = \frac{\sqrt{2}\epsilon G(\xi) E \varsigma_o \Delta(\xi)}{W^3(\xi)}, \quad (5.10)$$

$$\frac{d\Delta}{d\xi} = \epsilon \bar{\beta}_2 + \frac{\epsilon G(\xi) E [4\Delta^2(\xi) - \varsigma_o^4]}{2\sqrt{2}W^3(\xi)}, \quad (5.11)$$

with varying width defined as

$$W(\xi) = \frac{4\Delta^2 - \varsigma_o^4}{\varsigma_o}. \quad (5.12)$$

As in chapter 3, the periodicity condition can be imposed on the system as

$$\varsigma_o(\xi) = \varsigma(\xi + 1), \quad \Delta_o(\xi) = \Delta_o(\xi + 1) \quad (5.13)$$

with the new normalized width and chirp (also note that the length is now normalized to L_{map}). This is done by integration Eq. (5.10) and (5.11) from 0 to 1 and requiring them to be 0. With a simple change of variables using

$$\xi = \begin{cases} L_1(s + \frac{1}{2}) & : 0 < \xi < L_1 \\ L_1 + L_2(\frac{1}{2} - s) & : L_1 < \xi < 1 \end{cases} \quad (5.14)$$

the periodicity boundary condition yields the following constrains [52]:

$$\int_{-0.5}^{0.5} \frac{[s + \Delta_o + \frac{1}{2}] g(s) ds}{[\zeta_o^4 + 4(s + \Delta_o + \frac{1}{2})^2]^{\frac{3}{2}}} = 0, \quad (5.15)$$

$$\bar{\beta}_2 = \frac{\sqrt{2}A^2\zeta_o^4}{4} \int_{-0.5}^{0.5} \frac{[4(s + \Delta_o + \frac{1}{2})^2 - \zeta_o^4] g(s) ds}{[\zeta_o^4 + 4(s + \Delta_o + \frac{1}{2})^2]^{\frac{3}{2}}}, \quad (5.16)$$

where

$$g(s) = L_1 G\left(L_1(s + \frac{1}{2})\right) + L_2 G\left(L_1 + L_2(\frac{1}{2} - s)\right). \quad (5.17)$$

The normalized chirp Δ_o parameter is obtained by solving Eq. (5.15) and the normalized launching power A^2 is obtained by solving Eq. (5.16). The gain characteristics of the different amplification schemes can be easily incorporated through modifying Eq. (5.17).

5.2.3 Dense Dispersion Management

The strength of a DM map is defined as

$$S_{map} = \frac{|\beta_{21} L_1 - \beta_{22} L_2|}{\tau_{FWHM}^2}, \quad (5.18)$$

where τ_{FWHM} is the full width half maximum of the pulse and is related to the characterized pulse width τ_o by $\tau_{FWHM} \approx 1.665\tau_o$ for Gaussian pulses. This parameter characterizes the amount of perturbation a dispersion-varying medium has on the pulse. Typically, DM solitons are stable when $S_{map} < 3$ [52]. But as the single-channel bit rate is increased the pulse width decreases. This can dramatically increase the map

strength, especially if the map period, $L_{map} = L_1 + L_2$, (which until now is equivalent to the amplifier spacing) is kept relatively large. This will severely limit the amplifier spacing of high-bit rate systems. Dense DM map systems overcome this by allowing the amplifier spacing to contain multiple map periods ($L_A = M L_{map}$), where M is an integer. This allows the use of relatively tamed maps for pulse propagation at high bit rates while maintaining a large amplifier spacing (see Figure 5.2).

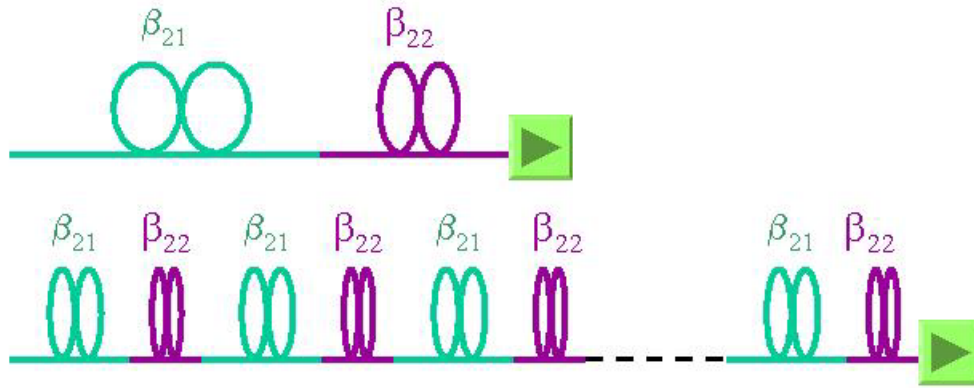


Figure 5.2: (Top) Two-step dispersion map. (Bottom) Dense dispersion map

The formula derived in the previous section is still valid in calculating the launching condition for dense DM map systems with only the gain needs to be modified. Equation (5.17) can be generalized as

$$g(s) = \sum_{m=0}^M \exp\left(\frac{-m \alpha L_{map}}{2}\right) \left[L_1 G\left(L_1\left(s + \frac{1}{2}\right)\right) + L_2 G\left(L_1 + L_2\left(\frac{1}{2} - s\right)\right) \right]. \quad (5.19)$$

5.3 System Performance

System performance can be gauged through observation of the received eye diagram. The eye diagram is a superposition of the pulse train in various combinations and gives in general an excellent indicator on the system performance. The more “open” the eye appears, the better the decision circuits can differentiate the “1” from the “0” bit and therefore, the less likely it is to make an error. It is beneficial to have a figure of merit to quantify the eye opening of the eye diagram for system performance characterization. The system performance is quantified through the use of the Q factor, which approximates the bit-error rate (BER) and is defined as (see Appendix B)

$$Q = \frac{I_1 - I_0}{\sigma_1 + \sigma_0} \quad (5.20)$$

where I_1 , I_0 , σ_1 and σ_0 are the intensity and the standard deviation of the received “1” and “0” of the bit pattern. In order to accurately calculate the Q, it is necessary to include the noise in the system.

5.3.1 Amplifier Noise

Amplified spontaneous emission (ASE) noise comes from the spontaneous emission amplified through cascade of optical amplifiers. The amount of ASE generated per a given bandwidth is given by

$$P_{ASE} = 2 n_{sp} h \nu \Delta \nu (G - 1) \quad (5.21)$$

where n_{sp} is the spontaneous emission factor, h is the Planck's constant, ν is the frequency, and $\Delta\nu$ is the bandwidth. The spontaneous emission factor can be written as a ratio of the ground and excited-level populations

$$n_{\text{sp}} = \frac{N_T - N_1}{N_T - 2N_1}, \quad (5.22)$$

which describes the amount of inversion of the system. Noise figure NF is often used when characterizing the noise performance of a system and it is defined as $NF = 10 \log(2 n_{\text{sp}})$. For fully-inverted amplifier, $N_1 = 0$, the n_{sp} is 1. Note that since the d-EDFA consists of long length of fiber, the NF changes as a function of distance [via. $N_1(z)$].

5.3.2 Numerical Results

In this section, 40 and 80 Gb/s systems using different amplification schemes and dispersion maps are examined using the Q factor to compare system performance. For a bit rate of 40 Gb/s, it is necessary to use a pulse width of only 2.5 ps ($T_{FWHM} = 4.4$ ps). Using the same design parameters as for the 20-Gb/s distributed amplification system in Chapter 4, the dispersion length is calculated to be only 12.5 km. To account for soliton interaction, a 64-bit pseudorandom sequence is used in numerical simulations. The two-bit-wide optical “eye diagram” (unfiltered) displayed in Figure 5.3(a) shows the combined effects of Raman-induced soliton self frequency shift (SSFS) and soliton interaction on the pulse train at a distance of 1000 km using lumped amplification excluding ASE. Clearly such a system will perform poorly in practice. We have

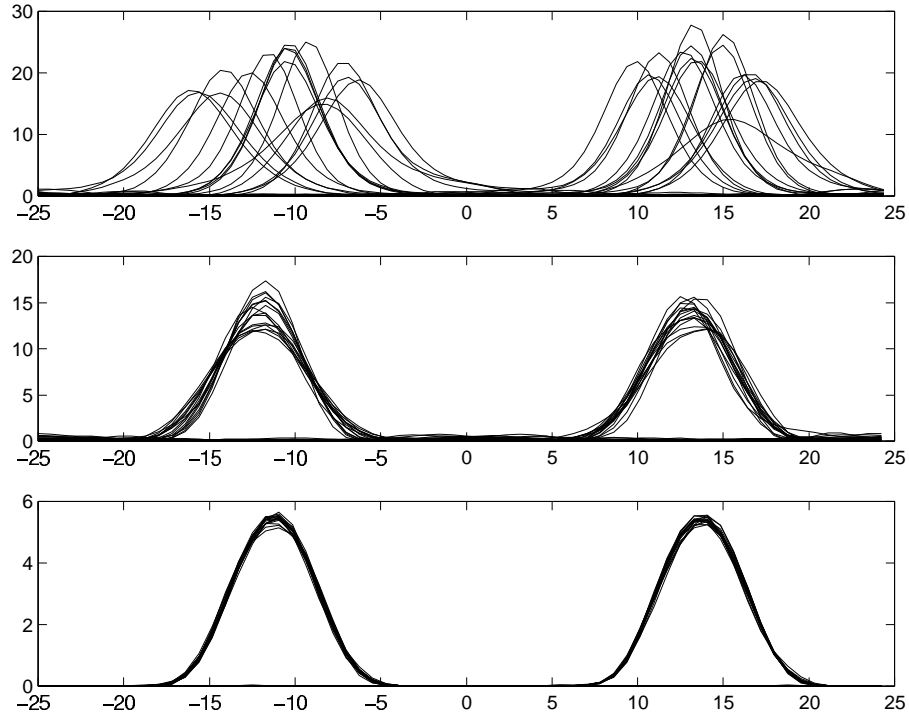


Figure 5.3: Two-bit-wide optical eye diagrams for a 40-Gb/s system without noise in three different operating conditions. (a) after 1000 km without DM. (b) after 5000 km with lumped amplification and DM. (c) After 5000 km with distributed amplification and DM.

found that both that both the SSFS and the soliton interaction problems can be solved by combining distributed amplification with dispersion management.

Figure 5.3(b) shows the eye diagram after 5000 km for a dispersion-managed (DM) system under identical operating conditions. The dispersion map consists of two 50-km fibers with $\beta_{21} = 0.3 \text{ ps}^2/\text{km}$ and $\beta_{22} = -0.38 \text{ ps}^2/\text{km}$, resulting in an average dispersion of $-0.04 \text{ ps}^2/\text{km}$ and a map strength $S_{map} = 1.75$ [52]. As evident in Figure 5.3(c), solitons barely move out of their time slot when distributed amplification is used with DM. The case of lumped amplifiers with DM was studied [44] and

it was found that both SSFS and soliton interaction are reduced in this case as well (Figure 5.3(b)) although system performance is better in the case of distributed amplification (Figure 5.3(c)).

Noise is included in the system by using a noise figure of 4.5 dB for EDFAs and 3 dB for Raman amplifiers. The launch power and initial chirp are calculated using the results of a variational analysis for dispersion-managed solitons. The distributed gain (for both d-EDFA and Raman amplifiers) is obtained numerically taking into account gain saturation and pump depletion. The results of the system simulation for different amplification schemes are shown in Fig. 5.4. where system performance as measured by Q is plotted vs. propagation distance. The maximum transmission can be deduced by noting that $Q = 6$ corresponds to BER of about 10^{-9} .

Figure 5.4 shows clearly the advantage of distributed amplification for high-speed lightwave systems. When lumped EDFAs are used, the transmission distance is limited to below 500 km, but increases to 3400 km for d-EDFA. Use of Raman amplification also improves the performance, although not as much as d-EDFA. The reason for this is that the design of a d-EDFA can be optimized by adjusting the dopant concentration. A Raman amplifier does not have this additional degree of freedom. The net gain over the 100-km amplifier span is only 0.5 dB for optimized d-EDFA but it increases to 6 dB for a distributed Raman amplifier and to over 15 dB for a hybrid amplification scheme (see Figure 5.5).

As the single-channel bit rate increases beyond 40 Gb/s, a reduced pulse width and a practical amplifier spacing combine to create a dispersion map that is too strong for stable propagation of solitons. A solution is provided by the technique of dense dispersion management [48] for which amplifier spacing is chosen to be a multiple of

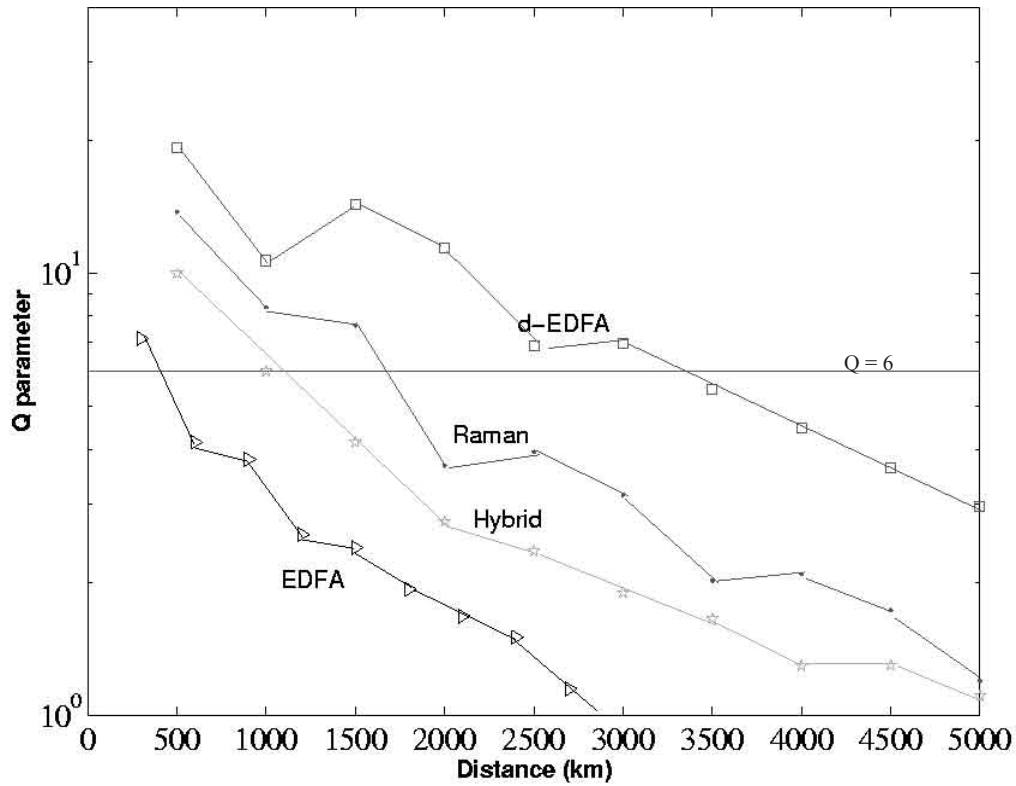


Figure 5.4: System performance of a 40-Gb/s DM soliton system using different amplification schemes.

the map period, which can be reduced to below 10 km. 2.93-ps pulses are launched into a dispersion map consisting of 2.231-km sections with $\beta_{21} = 3.2 \text{ ps}^2/\text{km}$ and $\beta_{22} = -3.2 \text{ ps}^2/\text{km}$, resulting in an average dispersion of $-0.013 \text{ ps}^2/\text{km}$ and a map strength of 1.65. The amplifier spacing of 40 km corresponds to 9 map periods. Figure 5.6 shows the performance of such an 80-Gb/s, multiple-cell soliton system for various amplification schemes. The results show again that the transmission distance can be increased using distributed amplification. Although one might expect the system performance (Q) to be a strictly monotonically decreasing function of distance, however, the system operates with two distinct dynamic time scales. There is a fast time scale that revealed the rapid oscillation of the pulse width and power due to periodic

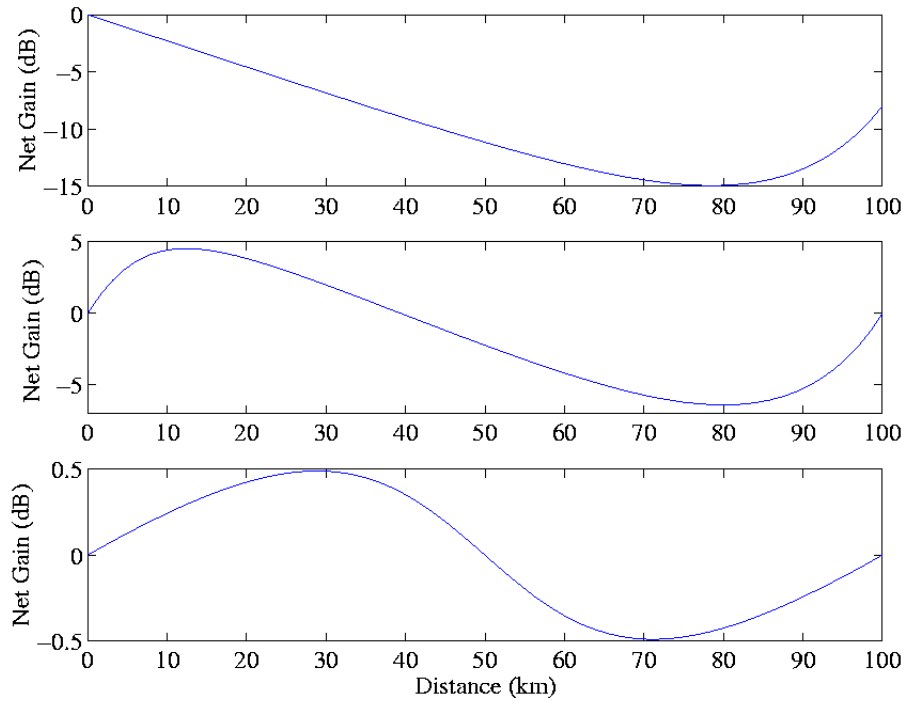


Figure 5.5: Net gain vs. distance for hybrid (top), distributed Raman (middle) , and distributed-erbium amplification schemes (bottom).

variations of the dispersion and amplification, and a second slow time scale that results from the combined effects of nonlinearity, residual dispersion, and pulse prechirping [61]. Nevertheless, it is clear from Figure 5.7, which plots the pulse evolution of a pair of solitons (corresponding to a pattern of 0 1 1 0) as it propagates through the system, that the advantage of the distributed amplification systems is to significantly reduce the effect of pulse to pulse interactions.

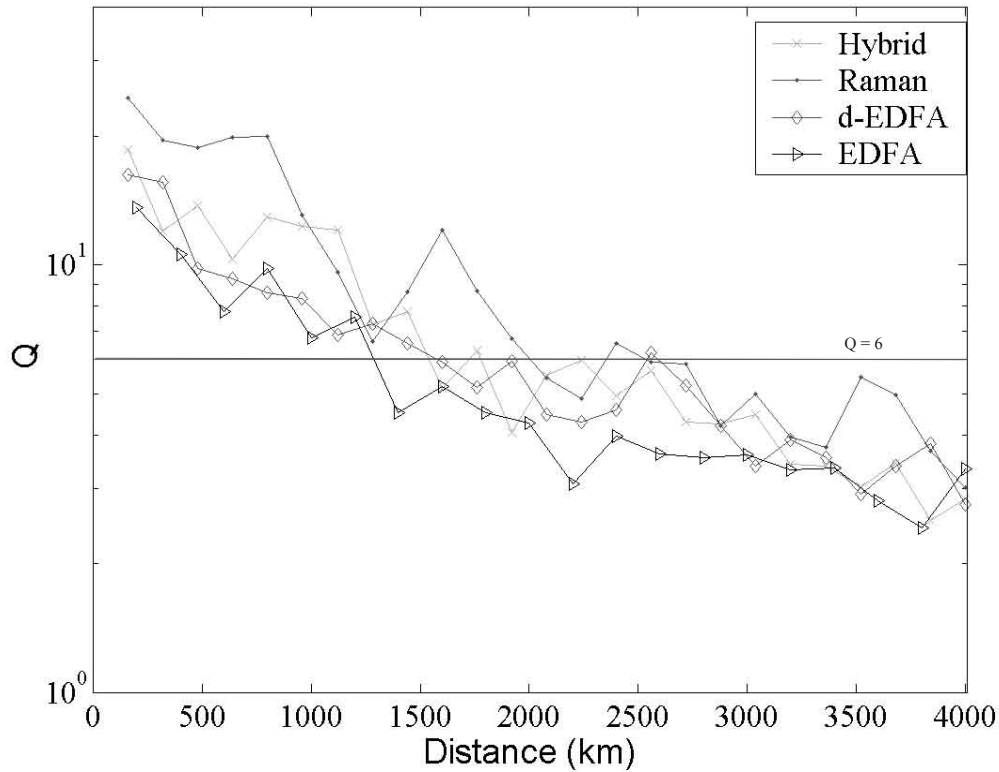


Figure 5.6: System performance of a 80-Gb/s DM soliton system using different amplification schemes.

5.4 Summary

Distributed amplification can increase the total transmission distance of ultra-high-bit-rate systems employing different dispersion maps. The improvement depends not only on the amplification scheme but also on details of the dispersion map. For systems limited by amplified spontaneous emission because of a relatively long amplifier spacing, the use of erbium doping provides best performance. Simulation results of 40 Gb/s systems using two-step dispersion map and 100 km amplifier spacing showed an increase of up to a factor of 7 in the maximum distance allowed by using d-EDFAs versus EDFAs. For systems limited by the map strength, the benefit of distributed amplification (Raman or erbium-doping) comes from the smaller net gain and a lower effective noise

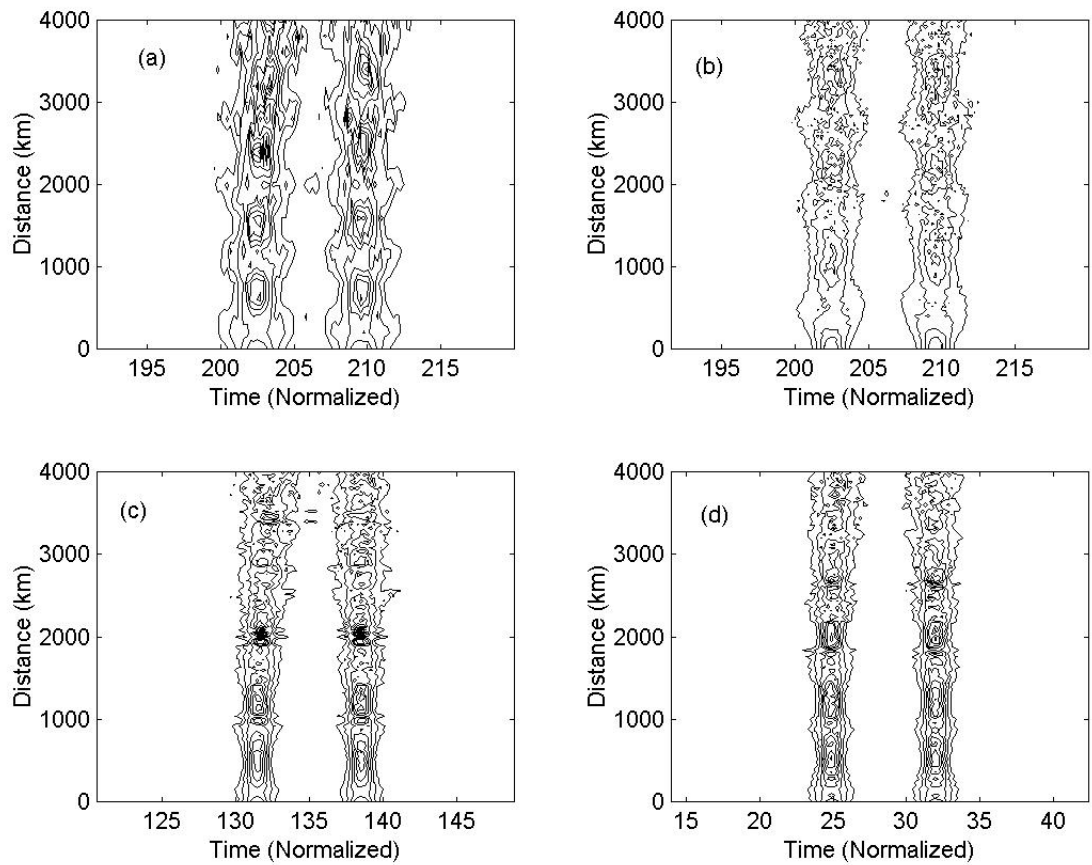


Figure 5.7: Pulse-to-pulse interaction for a 80-Gb/s soliton system using (a) EDFA, (b) hybrid, (c) distributed Raman, and (d) distributed erbium amplification schemes

figure. Simulation results of 80 Gb/s systems using dense dispersion map and 40 km amplifier spacing showed an increase of up to a factor of 2 in the maximum distance allowed by using d-EDFAs versus EDFAs.

Chapter 6

Fiber Lasers

6.1 Introduction

Ideally, we would like to compare the results of our numerical simulations with experimental transmission systems. Unfortunately, such systems are expensive and hard to come by. In an effort to establish a transmission system from the ground up, we have focused much of our experimental efforts to the understanding and characterization of fiber lasers, which can be used as transmitters, the first building block of a fiber-optic communication systems.

6.2 Experimental Setup

The ring-cavity of our fiber laser (see Fig. 6.1) consists of 7.2 m of erbium-doped fiber and 11.1 m of standard fiber, resulting in a total cavity length of 18.3 m [see Figure 6.1] [62]. A 980-nm pump laser diode (LD) (Lasertron QLM9S470) injects light through a 980/1550-nm WDM coupler; it couples about 95% of the pump light into the cavity. The output coupler transmits approximately 10% of the bidirectional circulating powers

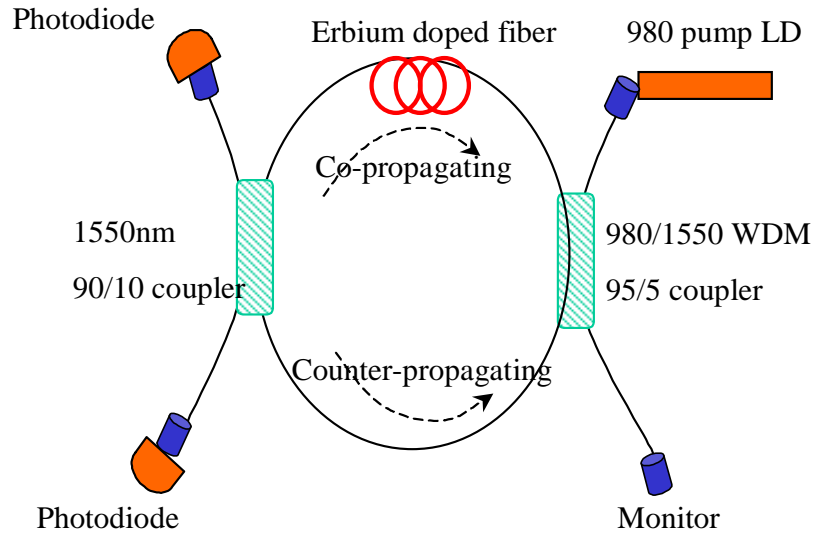


Figure 6.1: Experimental configuration of the fiber laser

per round trip. Each end of the output coupler is connected to a large-area germanium photoreceiver (New Focus Model 2033).

6.2.1 Output Power

We first measured the output power from the fiber laser through the monitor (P_{monitor}), and the sum of the co-propagating and counter-propagating ports (P_{tot}) as a function of the pump current. As is evident from Figure 6.2, the threshold for the 980-nm pump LD (which is measured through the monitor port) is 20 mA. The power emitted by the fiber laser in each counter propagating direction is observed through the output port of the 90/10 1550 nm coupler. The threshold for the fiber laser is measured to be 30 mA, which translate roughly to 5 mW of pump power at 980 nm. The slope efficient is about

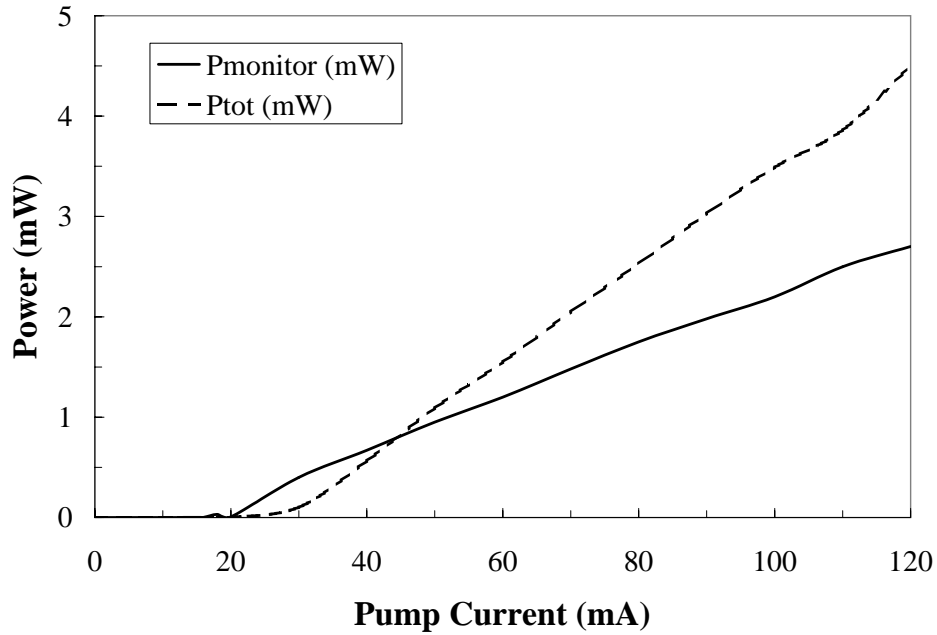


Figure 6.2: Output power vs. pump current for the fiber laser

10% for the fiber laser (see Figure 6.3). The temperature controller is set to 25° C for these measurements.

6.2.2 Frequency Characteristics

The spectrum of both the pump LD and the fiber laser was measured using a CVI monochromator. The spectrum of the pump LD was measured from the monitor port (see Figure 6.1). As can be seen in Figure 6.4, the spectrum is actually center around 976 nm with a full width close to 4 nm. The output of the fiber laser is shown in Fig. 6.5, the spectrum consists of many modes with a dominated mode centered around 1559.7 nm.

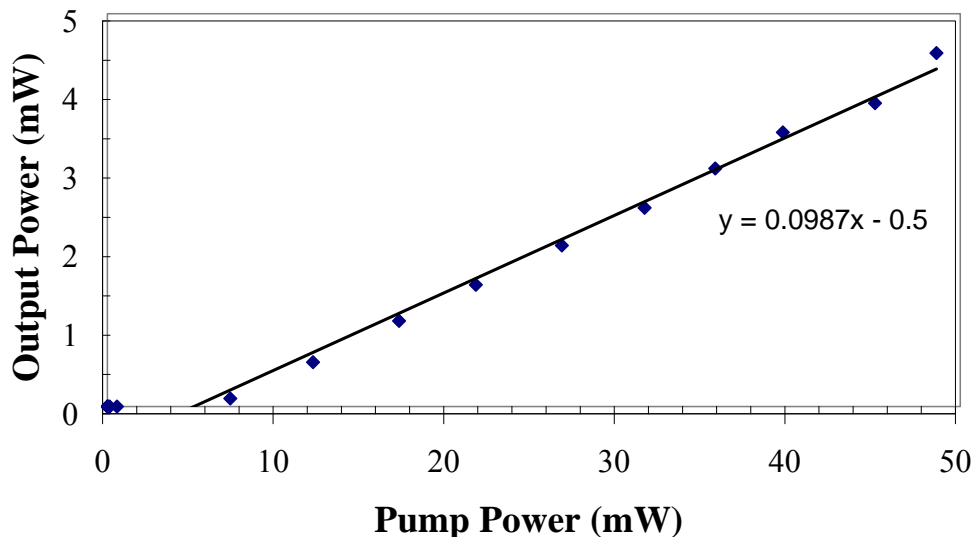


Figure 6.3: Output power vs. pump power for the fiber laser

6.3 Mode-Partition Noise

Mode-partition noise has been observed in a variety of lasers including semiconductor lasers [63,64], gas lasers [65], and dye lasers [66]. In semiconductor lasers, mode-partition noise arises from competition among multiple longitudinal modes. Mode-partition noise can also occur when cavity design forces co and counter-propagating modes to compete for the same gain. In particular, bidirectional-ring dye lasers have been found to exhibit random on-off switching between the two counter-propagating modes of the cavity such that whenever one mode turns on, the other turns off completely [66]. This phenomenon is attributed to the strong mode coupling that can occur in a homogeneously-broadened gain medium [67]. Fiber lasers are made using silica fibers whose core is doped with rare-earth ions, together with other codopants such as aluminum and germanium. Depending on the proportion of codopants, the gain spec-

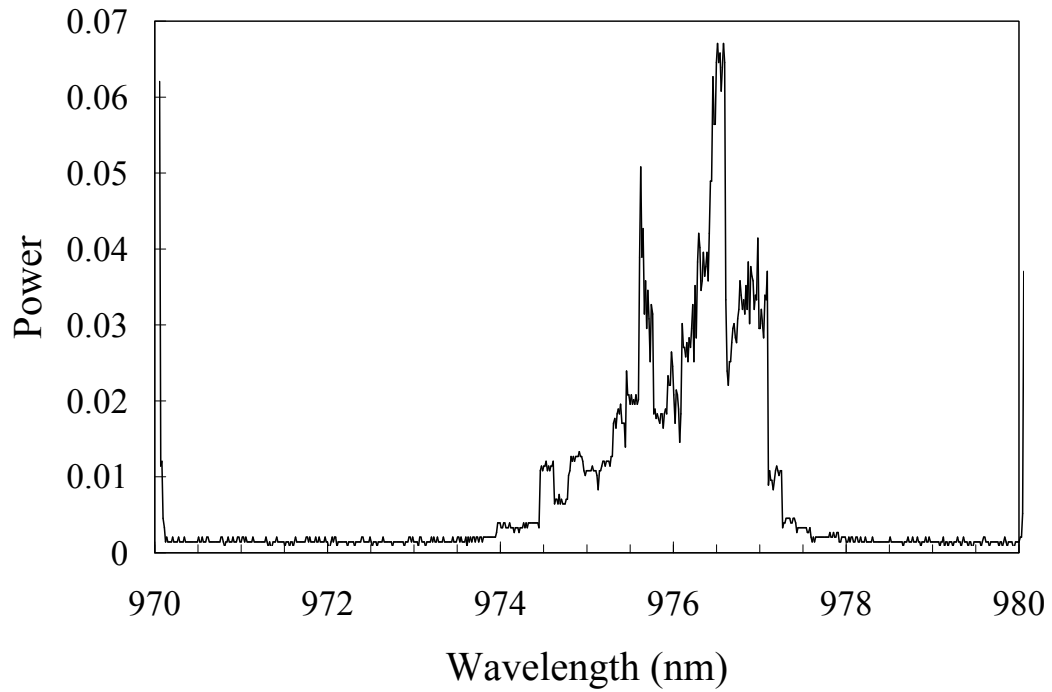


Figure 6.4: Spectrum of the pump output

trum of fiber lasers can be dominated by homogeneous or inhomogeneous broadening [68]. In this section, we present the experimental evidence of mode-partition noise in fiber lasers. We have also developed a theoretical model, based on the Langevin rate equations, whose predictions agree well with our experimental results.

6.3.1 Experimental Observation

Temporal evolution of the photoreceiver signals is monitored using an oscilloscope. Since we do not use an intracavity isolator, the laser emits light in both the clockwise and counter-clockwise directions. Figure 6.6 shows the output powers for the two directions when the laser is pumped 2.6 times above its threshold. The two modes are almost perfectly anti-correlated; an increase in the power of the one mode corresponds

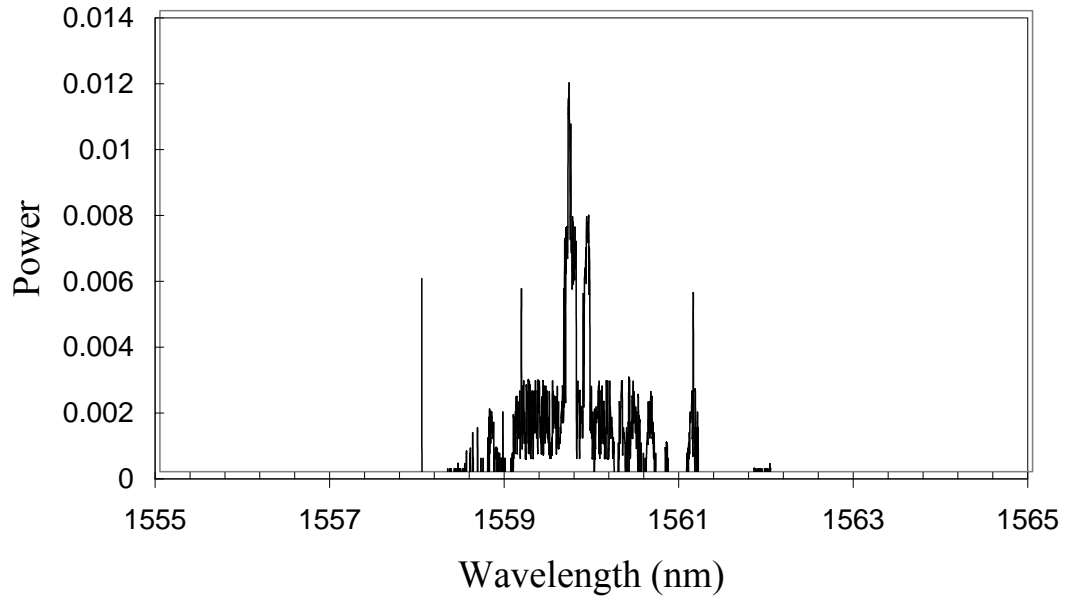


Figure 6.5: Spectrum of the fiber laser output

to a decrease in the other. The sum of the powers remains nearly constant, except for small fluctuations occurring at the relaxation oscillation frequency (≈ 29 kHz). The individual powers on the other hand, fluctuate on a rather slow time scale (~ 0.1 s). These fluctuations are due to mode-partition noise induced by cross-gain saturation. This interpretation is confirmed by the theoretical model presented next. Figure 6.6 is a snapshot of the temporal evolution of the signal on a 20 second time interval.

6.3.2 Mode-Partition Noise Theory

We use the standard three-level rate-equation model but simplify it by assuming rapid transfer of the pumped population to the excited state. The resulting rate equations with

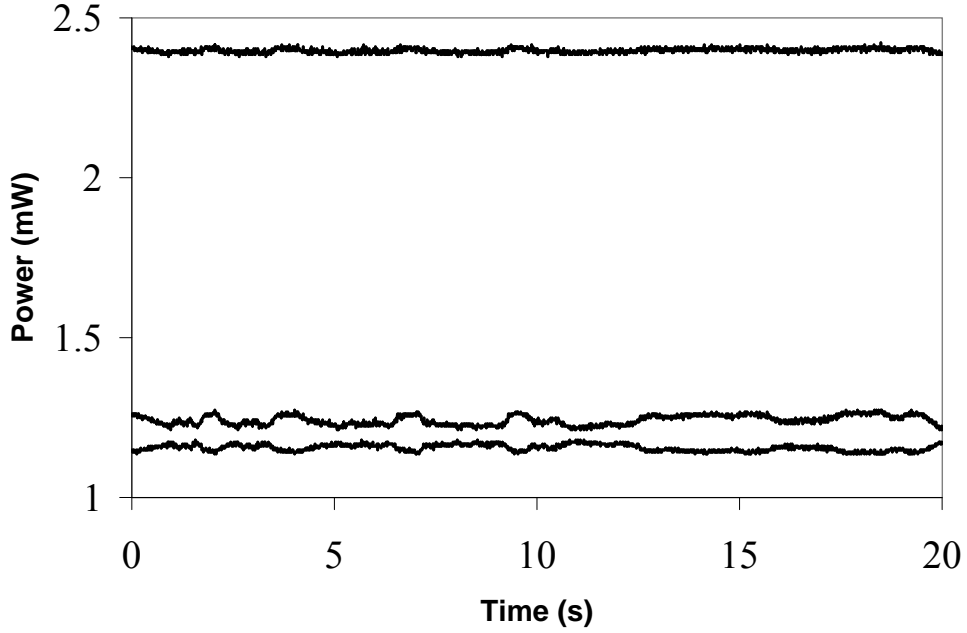


Figure 6.6: Output power of fiber laser for clockwise mode (middle), counter-clockwise mode (bottom), and sum of the two modes (top)

added Langevin noise terms can be written as [69]

$$\dot{P}_1 = (BN - \gamma)P_1 + R_{sp} + F_1(t), \quad (6.1)$$

$$\dot{P}_2 = (BN - \gamma)P_2 + R_{sp} + F_2(t), \quad (6.2)$$

$$\dot{N} = W_p(N_T - N) - 2(P_1 + P_2)BN - (N + N_T)/T_1, \quad (6.3)$$

where P_1 and P_2 are the number of photons in the co- and counter-propagating modes, respectively, and N represents the population-inversion level. The cavity-decay rate γ is related to the photon lifetime τ_p as $\gamma = 1/\tau_p$. The rate of spontaneous emission is taken to be $R_{sp} = n_{sp}BN$, where n_{sp} is the inversion parameter, and B is related to the rate of stimulated emission. In Eq. (6.3), W_p is the pump rate, N_T is the total number

Table 6.1: Parameters used in simulation of fiber laser dynamics

Parameter	Symbol	Value
Average photons in the clockwise mode	P_1	4.056×10^9
Average photons in the counter-clockwise mode	P_2	3.314×10^9
Population inversion density	N	$4 \times 10^{23} m^{-3}$
Total dopant density	N_T	$1 \times 10^{25} m^{-3}$
Rate of cavity decay	γ	$4.14 \times 10^6 s^{-1}$
Population relaxation time	T_1	$1 \times 10^{-2} s$
Pump photon rate	W_P	$390 s^{-1}$
Effective active volume	V_a	$2.256 \times 10^{-11} m^3$
Rate of stimulated emission	B	$4.588 \times 10^{-7} s^{-1}$

of dopants, and T_1 is the fluorescence time. The coupling between P_1 and P_2 is solely due to cross-gain saturation resulting from gain sharing.

The Langevin noise sources $F_1(t)$ and $F_2(t)$ are responsible for fluctuations in P_1 and P_2 , respectively. They vanish on average ($\langle F_i(t) \rangle = 0$). Assuming noise to be Markoffian (white noise), we use [69]

$$\langle F_i(t)F_j(t') \rangle = 2D_{ij}\delta(t - t'), \quad (6.4)$$

where $i, j = 1, 2$. The diffusion coefficient are related to the rate of spontaneous emission as

$$D_{11} = R_{sp}\bar{P}_1, \quad D_{22} = R_{sp}\bar{P}_2, \quad D_{12} = 0, \quad (6.5)$$

where \bar{P}_1 and \bar{P}_2 are the average steady-state values.

The stochastic rate equations Eq. (6.1)–(6.3) are solved numerically using parameter values appropriate to our fiber laser (a noise figure of 3.4 dB corresponding to

$n_{sp} = 1.1$ is assumed). Figure 6.7 shows a 5 second section of the time series simulated numerically. Comparing Fig. 6.6 and 6.7, we see that our model reproduces all qualitative features of the mode-partition noise observed experimentally. This agreement

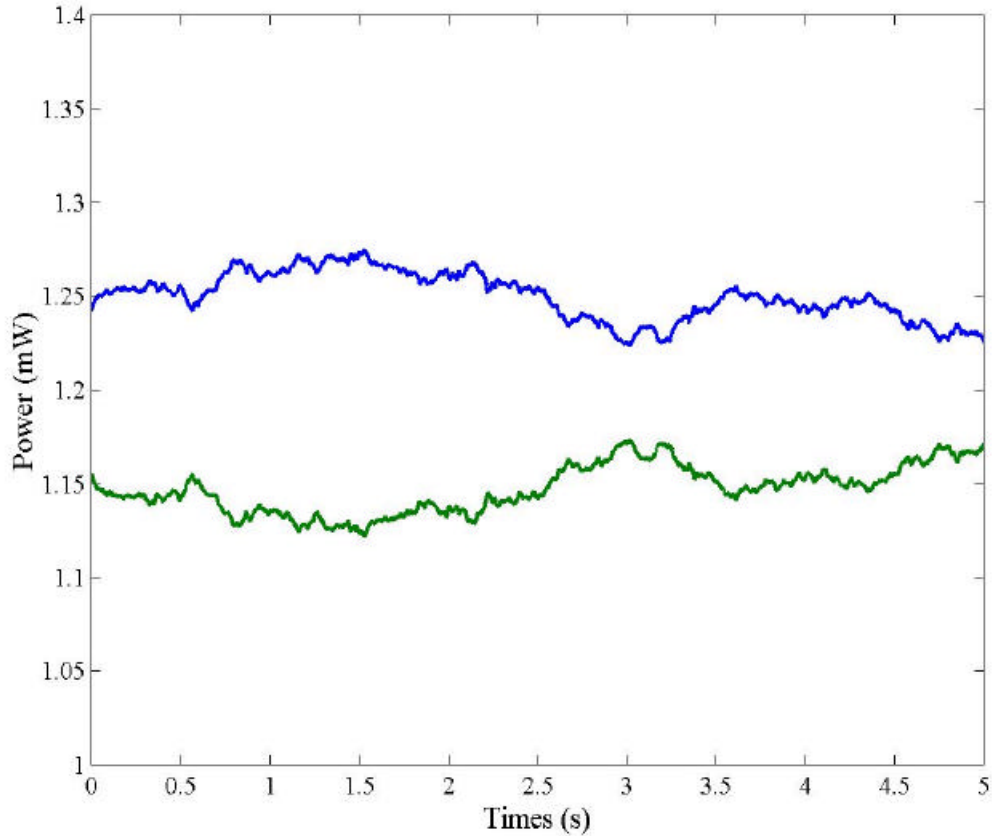


Figure 6.7: Numerical simulation of output powers in clockwise (top curve) and counter-clockwise (bottom curve) directions.

confirms that the anticorrelation seen in Fig. 6.6 has its origin in cross-gain saturation.

6.4 Summary

We have built and characterized an erbium-doped fiber laser pumped by a 980 nm LD.

We observed a threshold of 20 mA for the pump LD and 30 mA for the fiber laser.

With respect to the pump light, the lasing threshold was measured to be 5 mW. The slope efficiency of the fiber laser was found to be 10%. The spectrum of the fiber laser was measured to be centered at 1559.7 nm with a linewidth of approximately 2 nm. We have also experimentally observed mode-partition noise in a fiber laser. We have developed a rate-equation model that is capable of reproducing the experimentally observed behavior. We did not observe complete on-off switching similar to that observed in dye lasers [66]. We believe that the inhomogeneous broadening of the gain spectrum in our fiber laser leads to weak mode coupling. It is well known that codopants such as aluminum can make the gain spectrum nearly homogeneously broadened. Such fiber lasers may exhibit complete on-off switching.

Chapter 7

Conclusions

7.1 Overview

This thesis developed several techniques and concepts that will help shape the next generation of high-capacity fiber-optic communication systems. The principal target has been to increase the amplifier spacing through various techniques in present and future systems. In this chapter, we will expand and elaborate on the three main research areas covered in this thesis: design of constant dispersion system, design of dispersion management systems, and fiber laser dynamics. In each section, we will summarize our findings and provide additional insights for future research.

7.2 Constant-Dispersion Fibers

For a constant-dispersion system, soliton evolution through a lossy medium can be described by the guiding-center soliton theory. This allows stable propagation of soliton pulses provided that the fiber loss is compensated and the amplifier spacing is a fraction of the the dispersion length. Extending the amplifier spacing can be achieved in two ways: providing an additional degree of freedom in the guiding center soliton theory

to relax the amplifier-spacing constraint or to replace the large perturbation of lumped amplification by distributed amplification.

In Chapter 3, we used the variational analysis to solve the periodicity condition for pulse propagation in a lumped-amplification system by allowing both the pulse width and the chirp to change over the amplifier spacing. We were able to recover the input power condition as prescribed by the guiding-center soliton theory in the small amplifier spacing regime ($L_A \ll L_D$) while, at the same time, predict the additional power and the initial chirp needed for the large amplifier regime ($L_A \geq L_D$). Our numerical results show a much greater stability for systems operating at amplifier spacing exceeding those valid for the guiding-center solitons.

Amplifier spacing can also be extended by noting that the amplifier spacing constraint is a result of the large perturbation caused by the use of lumped amplifiers which give a large kick to the system within a very small distance (the longer the amplifier spacing, the larger the gain needed to compensate for fiber loss). In Chapter 4, we have seen that the use of distributed amplification can make the fiber appear transparent to the optical pulses. We use distributed erbium-doped fiber amplifiers as well as Raman gain to design distributed-amplification systems. The optimal pump configuration is bidirectional pumping as it allows a more uniform gain distribution for the system. Unlike the distributed Raman amplifiers, d-EDFA has an additional degree of freedom which allows the amplifier to be designed with minimal gain excursion. The penalty to pay for the low gain excursion is the higher pump power needed for d-EDFA. Although at high dopant concentration, less pump power is needed for loss compensation since the pump power does not need to penetrate deep into the fiber and work as hard (because the high dopant is able to provide a large gain in a short span close to the pump). Of

course, there is a limit — at too low a dopant density, no amount of pump power is able to compensate for the fiber loss at the signal and the pump wavelengths. For a 100-km distributed amplifier, gain excursion using a d-EDFA only experienced 0.4 dB by using a dopant density of $200 \text{ ions}/\mu\text{m}^3$ while distributed Raman amplifiers experienced 2-dB gain excursion (as compared to lumped amplifiers of 20 dB gain excursion). The pump power at each direction needed for d-EDFA was nearly 80 mW, slightly larger than the pump power needed for distributed Raman (60 mW). Backward-pumped Raman gain has already attracted considerable attention for current system designers to achieve extra system margin; it will be only a matter of time before system complexity can only be solved through distributed-amplification solutions.

Our study has shown the advantage of prechirping and distributed amplification in extending the amplifier spacing in high-bit-rate single-channel constant-dispersion soliton communication systems. On a practical note, prescribing precise chirp at the launching of a pulse is not a trivial issue, although chirp can be provided by simply propagating the pulse through a fixed length of fiber, because measurements of fiber length or GVD in the field are not precise enough. Further studies on the sensitivity of the initial input parameters vs. the system stability will provide critical information on the feasibility of this technique. The capacity of the system can be greatly increased if WDM technology is employed. Further investigation is needed to study the effect of prechirping and distributed amplification in a WDM system. Our analysis has already shown that the small-signal analytical solution is insufficient to describe the gain distribution; the presence of multiple channels in a WDM system will surely present similar challenges since the sum of the channel powers can easily exceed 40 mW. Furthermore, the presence of constant, undiminished power at each of the channels along

the transmission line can further increase the nonlinear penalties such as cross-phase modulation (XPM) and four-wave mixing (FWM) [9].

7.3 Dispersion-Management Technique

In Chapter 5, we presented the technique of dispersion management in soliton transmissions. The two-step dispersion map allows compensation of chromatic dispersion through the use of fibers with normal and anomalous GVD. For ultra-high-bit-rate systems, it was necessary to use multiple dispersion maps within an amplifier spacing to keep the map strength low enough for stable pulse propagation. We have also gathered current amplifier technologies as well as developed future technologies such as d-EDFA and bi-directional pumped Raman amplifiers in conjunction with dispersion management in an effort to study the advantages of using each kind of amplifier.

Since distributed amplifiers offer better noise performance for systems limited by noise, distributed amplification was able to outperform other schemes (lumped amplification and hybrid amplification) by being able to transmit over seven times the distance for a 40 Gb/s system. However, for systems limited by dispersion map, distributed amplification was not able to offer as much advantage. Nonetheless, a lower gain excursion, and therefore a smaller soliton-soliton interaction effect, can also improve the system performance of distributed amplifiers over lumped amplifiers, by roughly increasing the transmission distance by a factor of 3 times over a 80 Gb/s system. The effect of collision-induced timing jitter in dispersion-managed systems has been shown to degrade the system performance in WDM systems. This has been attributed to the asymmetric collisions at the amplifier nodes; it would be of extreme interest to study how this effect changes with distributed-amplification schemes. Dispersion-managed

solitons have also been shown to be able to reduce the Gordon-Haus timing jitter because of the ability of the dispersion to create a potential trapping for the soliton pulses. Further studies of this effect in conjunction with distributed amplification will also be fruitful.

7.4 Fiber-Laser Dynamics

In Chapter 6, we characterized the operation of a fiber laser in an ongoing effort to build a transmitter for a fiber-optic transmission system. The threshold as well as the spectrum properties of the pump LD and the fiber laser was measured. We also experimentally demonstrated mode-partition noise in a fiber laser. The theoretical model was successful in duplicating the phenomenon. It is well known that the complete on-off switching that has been reported for dye lasers is an effect of the homogeneous nature of the gain medium; the lack of this similar phenomenon in the fiber laser can be attributed to the inhomogeneous broadening of the gain spectrum. Since fibers with codopants such as aluminum has been known to be able to make the fiber nearly homogeneous, it would be worthwhile to test the above hypothesis by duplicating the experiment with aluminum-doped fiber lasers.

7.5 Summary

As evident in the previous chapters, this thesis seeks to explore the issues in expanding amplifier spacing for a wide range of soliton-communication systems while maintaining or surpassing the system performance. We can summarize the contribution of this work to the development of soliton-communication system as follows:

- Expanded on Guiding-center soliton theory by prechirping the pulse, which provides an additional degree of freedom for satisfying the periodicity conditions.
- Demonstrated a new regime of operation beyond that of Guiding-center solitons where $L_D \geq L_A$.
- Predicted the ability of distributed amplification to extend the performance beyond the Guiding-center soliton where $L_D \geq L_A$.
- Predicted an improvement in the system performance (through greater transmission distance) with the use of distributed amplification in a two-step dispersion managed system because of a better noise figure.
- Predicted an improvement in the system performance (through greater transmission distance) with the use of distributed amplification in a dense dispersion managed system because of a smaller gain excursion.
- Constructed and characterized the operation threshold and the spectrum properties of an erbium-doped fiber laser.
- Experimentally demonstrated and theoretically verified the effect of mode-partition noise in fiber lasers.

These advances have significantly advanced the theory and design of high-capacity soliton transport systems, especially in the realm of distributed amplification.

Bibliography

- [1] Technical report, Merrill Lynch: Global Fundamental Equity Research Department (unpublished).
- [2] G. P. Agrawal, *Fiber-Optic Communication Systems*, 2 ed. (John Wiley & Sons, Inc., New York, 1991).
- [3] T. Li, "The impact of optical amplifiers on long-distance lightwave telecommunications," Proc. IEEE. **81**, 1568 (1993).
- [4] T. N. Nielsen *et al.*, "3.28-Tb/s (82x40 Gb/s) transmission over 3x1000 km nonzero-dispersion fiber using dual C- and L-band hybrid Raman/erbium-doped inline amplifiers," Opt. Fiber Confer. **Postdeadline Papers**, PD23 (2000).
- [5] T. Ito, K. Fukuchi, Y. Inada, T. Tsuzaki, M. Harumoto, and M. Kakui, "3.2 Tb/s – 1500 km WDM transmission experiment using 64 nm hybrid repeater amplifiers," Opt. Fiber Confer. **Postdealing Papers**, PD24 (2000).
- [6] A. K. Srivastava *et al.*, "Ultra-dense terabit capacity WDM transmission in L-band," Opt. Fiber Confer. **Postdealine Paper**, PD27 (2000).
- [7] T. Terahara, T. Hoshida, J. Kumasako, and H. Onaka, "128x10.66 Gbit/s transmission over 840-km standard SMF with 140-km optical repeater spacing (30.4-dB loss) employing dual-band distributed Raman amplification," Opt. Fiber Confer. **Postdeadline Papers**, PD28 (2000).
- [8] N. Zabusky and M. D. Kruskal, "Interaction of solitons in collisionless plasma and the recurrence of initial states," Phys. Rev. Lett. **15**, 240 (1965).
- [9] G. P. Agrawal, *Nonlinear Fiber Optics*, 3 ed. (Academic Press, San Diego, 2001).
- [10] A. Hasegawa and F. Tappert, "Transmission of stationary nonlinear optical pulses in dispersive dielectric fibers," Appl. Phys. Lett. **23**, 142 (1973).
- [11] L. Mollenauer, R. H. Stolen, and J. P. Gordan, "Experimental observation of pi-

- cosecond pulse narrowing and solitons in optical fibers,” *Phys. Rev. Lett.* **45**, 1095 (1980).
- [12] A. Hasegawa, “Amplification and reshaping of optical solitons in a glass fiber IV: Use of the stimulated raman process,” *Opt. Lett.* **8**, 650 (1983).
- [13] L. F. Mollenauer, R. H. Stolen, and M. N. Islam, “Experimental demonstration of soliton propagation in long fibers: Loss compensated by raman gain,” *Opt. Lett.* **10**, 229 (1985).
- [14] L. F. Mollenauer, J. P. Gordon, and M. N. Islam, “Soliton propagation in long fibers with periodically compensated loss,” *IEEE J. Quantum Electron.* **22**, 157 (1986).
- [15] L. F. Mollenauer and K. Smith, “Demonstration of soliton transmission over more than 4000 km in fiber with loss periodically compensated by Raman gain,” *Opt. Lett.* **13**, 675 (1988).
- [16] P. Andrekson, “Soliton tests show promise for dense wdm systems,” *Laser Focus* 145 (1999).
- [17] Technical report, Morgan Stanley Dean Witter (unpublished).
- [18] D. J. Griffiths, *Introduction to Electrodynamics*, 2 ed. (Prentice-Hall, Englewood Cliffs, 1989).
- [19] R. W. Boyd, *Nonlinear Optics* (Academic Press, New York, 1992).
- [20] D. Anderson, “Variational approach to nonlinear pulse propagation in optical fibers,” *Phy. Rev. A* **27**, 3135 (1983).
- [21] W. L. Kath and N. F. Smyth, “Soliton evolution and radiation loss for the nonlinear Schrödinger’s equation,” *Phy. Rev. E* **51**, 1484 (1995).
- [22] A. Hasegawa and Y. Kodama, “Guiding-center soliton in optical fibers,” *Opt. Lett.* **24**, 1143 (1990).
- [23] L. F. Mollenauer, S. G. Evangelides, and H. A. Haus, “Long-distance soliton propagation using lumped amplifiers and dispersion shifted fiber,” *J. Lightwave Technol.* **9**, 194 (1991).
- [24] K. J. Blow and N. J. Doran, “Average soliton dynamics and the operation of soliton systems with lumped amplifiers,” *IEEE Photon. Technol. Lett.* **3**, 369 (1991).

- [25] S. M. J. Kelly, "Characteristic sideband instability of periodically amplified average soliton," *Electron. Lett.* **28**, 806 (1992).
- [26] N. J. Smith, K. J. Blow, and I. Andonovic, "Sideband generation through perturbations to the average soliton model," *J. Lightwave Technol.* **10**, 1329 (1992).
- [27] J. P. Gordan, "Dispersive perturbations of solitons of the nonlinear Schrödinger equation," *J. Opt. Soc. Am. B* **9**, 91 (1992).
- [28] N. J. Smith and N. J. Doran, "Picosecond soliton transmission using concatenated nonlinear optical loop-mirror intensity filters," *J. Opt. Soc. Am. B* **12**, 1117 (1995).
- [29] M. Matsumoto, H. Ikeda, T. Uda, and A. Hasegawa, "Stable soliton transmission in the system with nonlinear gain," *J. Lightwave Technol.* **13**, 658 (1995).
- [30] W. Forysiak, N. J. Doran, F. M. Knox, and K. J. Blow, "Average soliton dynamics in strongly perturbed systems," *Opt. Comm.* **117**, 65 (1995).
- [31] R. J. Essiambre and G. P. Agrawal, "Soliton communication beyond the average-soliton regime," *J. Opt. Soc. Am. B* **12**, 2420 (1995).
- [32] A. Hasegawa and Y. Kodama, "Guiding-center soliton," *Phys. Rev. Lett.* **24**, 1143 (90).
- [33] T. Okamawari, Y. Ueda, A. Maruta, Y. Kodama, and A. Hasegawa, "Interaction between guiding centre solitons in a periodically compensated optical transmission line," *Electron. Lett.* **33**, 1063 (1997).
- [34] Y. Kodama and A. Maruta, "Optimal design of dispersion management for a soliton-wavelength-division-multiplexed system," *Opt. Lett.* **22**, 1692 (1997).
- [35] I. Morita, M. Suzuki, N. Edagawa, K. Tanaka, S. Yamamoto, and S. Akiba, "Performance improvement by initial phase modulation in 20 Gbit/s soliton-based RZ transmission with periodic dispersion compensation," *Electron. Lett.* **33**, 1021 (1997).
- [36] H. Sugahara, T. Inoue, A. Maruta, and Y. Kodama, "Optimal dispersion management for wavelength-division-multiplexed RZ optical pulse transmission," *Electron. Lett.* **34**, 902 (1998).
- [37] T. Georges and B. Charbonnier, "Reduction of the dispersive wave in periodically amplified links with initially chirped solitons," *IEEE Photon. Technol. Lett.* **9**, 127 (1997).

- [38] F. Favre, D. Guen, and T. Georges, "Experimental evidence of pseudoperiodical soliton propagation in dispersion-managed links," *J. Lightwave Technol.* **17**, 1032 (1999).
- [39] A. Hasegawa and Y. Kodama, *Solitons in Optical Communications* (Clarendon, Oxford, 1995).
- [40] K. Rottwitt, J. H. Povlsen, and A. Bajarklev, "Long-distance transmission through distributed erbium-doped fibers," *J. Lightwave Technol.* **11**, 2105 (1993).
- [41] A. Altuncu *et al.*, "20 Gbit/s error-free transmission over 68 km distributed-erbium doped fibre amplifier," *Electron. Lett.* **32**, 233 (1996).
- [42] K. Rottwitt, A. Bjarklev, J. H. Povlsen, O. Lumholt, and T. P. Ramussen, "Fundamental design of a distributed erbium-doped fiber amplifier for long-distance transmission," *J. Lightwave Technol.* **10**, 1544 (1992).
- [43] Y. Miyamoto, "40-Gbit/s transport system: Its WDM upgrade," *Tech. Dig. OFC ThW4*, 323 (2000).
- [44] I. Morita, K. Tanaka, N. Edagawa, S. Yamamoto, and M. Suzuki, "40 Gbit/s single-channel soliton transmission over 8600 km using periodic dispersion compensation," *Electron. Lett.* **34**, 1863 (1998).
- [45] D. S. Govan, W. Forysiak, and N. J. Doran, "Long-distance 40-Gbit/s soliton transmission over standard fiber by use of dispersion management," *Opt. Lett.* **23**, 1523 (1998).
- [46] Z. M. Liao and G. P. Agrawal, "High-bit-rate soliton transmission using distributed amplification and dispersion management," *IEEE Photon. Technol. Lett.* **11**, 818 (1999).
- [47] S. Turitsyn, M. Fedoruk, W. Forysiak, and N. Doran, "Dispersion-management in fiber communication lines using Raman amplification," *Opt. Comm.* **170**, 23 (1999).
- [48] A. H. Liang, H. Toda, and A. Hasegawa, "High-speed soliton transmission in dense periodic fibers," *Opt. Lett.* **24**, 799 (1999).
- [49] A. J. Stentz, R. W. Boyd, and A. F. Evans, "Dramatically improved transmission of ultrashort solitons through 40 km of dispersion-decreasing fiber," *Opt. Lett.* **20**, 1770 (1995).
- [50] R. J. Essiambre and G. P. Agrawal, "Timing jitter of ultrashort solitons in

- high-speed communication systems. I. General formulation and application to dispersion-decreasing fibers,” *J. Opt. Soc. Am. B* **14**, 314 (1997).
- [51] A. Hasegawa, Y. Kodama, and A. Maruta, “Recent progress in dispersion-managed soliton transmission technologies,” *Opt. Fiber Technol.* **3**, 197 (1997).
- [52] T. I. Lakoba, J. Yang, D. J. Kaup, and B. A. Malomed, “Conditions for stationary pulse propagation in the strong dispersion management regime,” *Opt. Comm.* **149**, 366 (1998).
- [53] T. I. Lakoba and D. J. Kaup, “Hermite-Gaussian expansion for pulse propagation in strongly dispersion managed fibers,” *Phy. Rev. E* **58**, 6728 (1998).
- [54] J. Kutz and P. Wai, “Gordan-Haus timing jitter reduction in dispersion-managed soliton communications,” *IEEE Photon. Technol. Lett.* **10**, 702 (1998).
- [55] S. Turitsyn, V. Mezentsev, and E. Shapiro, “Dispersion-managed solitons and optimization of the dispersion management,” *Opt. Fiber Technol.* **4**, 384 (1998).
- [56] I. Gabitov, E. Shapiro, and S. Turitsyn, “Optical pulse dynamics in fiber links with dispersion compensation,” *Opt. Comm.* **134**, 317 (1997).
- [57] S. Turitsyn *et al.*, “Variational approach to optical pulse propagation in dispersion compensated transmission systems,” *Opt. Comm.* **151**, 117 (1998).
- [58] I. Gabitov, T. Schafer, and S. Turitsyn, Technical Report No. LAUR-99-4752, Los Alamos National Laboratory (unpublished).
- [59] M. Romagnoli and L. Socci, “Long-range soliton interactions in dispersion-managed links,” *Opt. Lett.* **23**, 1182 (1998).
- [60] S. Kumar, A. Hasegawa, and Y. Kodama, “Adiabatic soliton transmission in fibers with lumped amplifiers: Analysis,” *Opt. Lett.* **14**, 888 (1997).
- [61] S. Turitsyn and A. Aceves, “Average dynamics of the optical soliton in communication lines with dispersion management: Analytical results,” *Phy. Rev. E* **58**, 48 (1998).
- [62] L. Liou, *Temporal, Spectral, and Noise Characteristics of Erbium-Doped Fiber Amplifiers and Lasers*, Ph.D. thesis, University of Rochester, 1995.
- [63] G. P. Agrawal and N. K. Dutta, *Semiconductor lasers*, 2 ed. (Van Nostrand Reinhold, New York, 1993).

- [64] J. Law and G. P. Agrawal, "Mode-partition noise in vertical-cavity surface-emitting lasers," *IEEE Photon. Technol. Lett.* **4**, 437 (1997).
- [65] A. Valle, A. Mecozzi, L. Pesquera, M. Rodriguez, and P. Spano, "Transient statistics of two-mode gas ring lasers," *Phys. Rev. A* **3**, 2426 (1993).
- [66] L. Mandel and E. Wolf, *Optical Coherence and Quantum Optics* (Cambridge University Press, New York, 1995).
- [67] M. Sargent, M. Scully, and W. Lamb, *Laser physics* (Addison-Wesley Publishing Company, Reading, 1974).
- [68] P. C. Becker, N. A. Olsson, and J. R. Simpson, *Erbium-Doped Fiber Amplifiers: Fundamentals and Technology* (Academic Press, San Diego, 1999).
- [69] G. P. Agrawal, "Mode-partition noise and intensity correlation in a two-mode semiconductor laser," *Phys. Rev. A* **7**, 2488 (1988).
- [70] G. P. Agrawal, *Applications of Nonlinear Fiber Optics* (Academic Press, San Diego, 2001).

Appendix A

Calculating Pulse Parameters

Throughout this thesis, we are required to study pulse dynamics in various scenarios. It is therefore necessary to numerically calculate certain pulse characteristics in order to ascertain the stability and periodicity of the pulse. Even though we primarily study the dynamics of soliton pulses, it has been found that dispersion managed solitons have attributes much more like a gaussian pulse than to a hyperbolic secant shape. The primary attributes that we are interested are pulse width, center, and chirp. We will therefore discuss the mathematics of how to calculate these characteristics for both soliton as well as gaussian pulses.

A.1 Gaussian Pulse

The field of a gaussian pulse can be expressed as

$$q(t) = A_o \exp\left(-\frac{(t - t_c)^2}{2T_o^2}\right) \exp\left(-\frac{iC}{2T_o^2}(t - t_c)^2\right), \quad (\text{A.1})$$

with t_c as the pulse center and A_o as the pulse amplitude. The intensity is therefore

$$|q(t)|^2 = A_o^2 \exp\left(-\frac{(t - t_c)^2}{T_o^2}\right). \quad (\text{A.2})$$

It is advantageous to define the following property of the pulse through the calculation of the moments of the pulse as given by

$$\sigma_n = \frac{\int_{-\infty}^{\infty} t^n |q(t)|^2 dt}{\int_{-\infty}^{\infty} |q(t)|^2 dt} \quad (\text{A.3})$$

where σ_n is the n th order moment of the pulse with $n = 1, 2, \dots$

The energy of the pulse by the following relations

$$\begin{aligned} E_p &= A_o^2 \int_{-\infty}^{\infty} \exp\left(-\frac{(t-t_c)^2}{T_o^2}\right) dt \\ &= \sqrt{\pi} T_o A_o^2. \end{aligned} \quad (\text{A.4})$$

Similarly, the center of the pulse can be calculated by noticing that the first moment of the pulse is given by

$$\begin{aligned} \sigma_1 &= \frac{1}{E_p} A_o^2 \int_{-\infty}^{\infty} t \exp\left(-\frac{(t-t_c)^2}{T_o^2}\right) dt \\ &= t_c. \end{aligned} \quad (\text{A.5})$$

The RSM width is calculated using $\langle \sigma_2 \rangle - \langle \sigma_1 \rangle^2$ with σ_2 given as

$$\begin{aligned} \sigma_2 &= \frac{1}{E_p} A_o^2 \int_{-\infty}^{\infty} t^2 \exp\left(-\frac{(t-t_c)^2}{T_o^2}\right) dt \\ &= \frac{T_o^2}{2} + t_c^2. \end{aligned} \quad (\text{A.6})$$

The quadratic chirp of the pulse can be extracted using the following formula which

can be written in terms of second moment of the pulse,

$$\begin{aligned}
\Psi &= \frac{i}{2E_p} \int_{-\infty}^{\infty} (t - t_c) [q q^*_{T} - q^* q_T] dt \\
&= \frac{-C}{E_p T_o^2} \int_{-\infty}^{\infty} (t - t_c)^2 \exp\left(-\frac{(t - t_c)^2}{T_o^2}\right) dt \\
&= \frac{-C}{E_p T_o^2} (E_p \sigma_2 - 2E_p t_c \sigma_1 + E_p t_c^2) \\
&= \frac{-C}{T_o^2} (\sigma_2 - 2t_c \sigma_1 + t_c^2) \\
&= -\frac{C}{2}.
\end{aligned} \tag{A.7}$$

A.2 Hyperbolic Secant Pulse

The field of a hyperbolic secant pulse (soliton) can be expressed as

$$q(t) = A_o \operatorname{sech}\left(\frac{t - t_c}{T_o}\right) \exp\left(-\frac{iC}{2T_o^2}(t - t_c)^2\right), \tag{A.8}$$

The intensity is therefore

$$|q(t)|^2 = A_o^2 \operatorname{sech}^2\left(\frac{t - t_c}{T_o}\right). \tag{A.9}$$

The characteristic width of the pulse can also be related to the zero moment σ_0 of the pulse by the following relations

$$\begin{aligned}
E_p &= A_o^2 \int_{-\infty}^{\infty} \operatorname{sech}^2\left(\frac{t - t_c}{T_o}\right) dt \\
&= 2T_o A_o^2.
\end{aligned} \tag{A.10}$$

Similarly, the center of the pulse can be calculated by noticing that the first moment of the pulse is given by (via u substitution)

$$\begin{aligned}\sigma_1 &= \frac{1}{E_p} A_o^2 \int_{-\infty}^{\infty} t \operatorname{sech}^2 \left(\frac{t - t_c}{T_o} \right) dt \\ &= t_c.\end{aligned}\tag{A.11}$$

The second moment is calculated to be

$$\begin{aligned}\sigma_2 &= \frac{1}{E_p} A_o^2 \int_{-\infty}^{\infty} t^2 \operatorname{sech}^2 \left(\frac{t - t_c}{T_o} \right) dt \\ &= \frac{\pi^2 T_o^2}{12} + t_c^2.\end{aligned}\tag{A.12}$$

The quadratic chirp of the pulse can be extracted using the following formula which can be written in terms of second moment of the pulse,

$$\begin{aligned}\Psi &= \frac{i}{2E_p} \int_{-\infty}^{\infty} (t - t_c) [q q^*_{T} - q^* q_T] dt \\ &= -\frac{C}{T_o^2 E_p} \int_{-\infty}^{\infty} (t - t_c)^2 \operatorname{sech}^2 \left(\frac{t - t_c}{T_o} \right) dt \\ &= \frac{-C}{T_o^2} (\sigma_2 - 2t_c \sigma_1 + t_c^2) \\ &= -\frac{\pi^2 C}{12}.\end{aligned}\tag{A.13}$$

Appendix B

Bit-Error Rate

In Chapter 5, we first introduced the parameter Q which approximates bit-error rate (BER) to qualify system performance. We will now provide a more in depth derivation of calculating BER [70].

BER is an excellent measurement of the system performance because it quantifies the probability in which an error is made in the decision system. The error is often due to the presence of various noises in the system. As a result, BER typically has a strong dependence on the signal to noise ratio (SNR) of the signal received. A BER of 10^{-9} corresponds to 1 error per 10^9 bits. Error-free transmission is often referred to as having BER less than 10^{-9} , although modern systems often require BER to be less than 10^{-12} . In a binary coding system, BER is merely the sum of probabilities of identifying 1 bit as 0 bit and vice versa. Mathematically, it is expressed as

$$\text{BER} = p(1) P(0/1) + p(0) P(1/0), \quad (\text{B.1})$$

where $p(1)$ and $p(0)$ is the probability of receiving 1 and 0 bits respectively. $P(0/1)$ is the conditional probability of assigning a 0 bit to the signal when in actuality a 1 bit is

received and $P(1/0)$ is the conditional probability of assigning a 0 bit to the signal when in actuality a 1 bit is received.

In calculating the BER, two assumptions are made. First, it is safe to assume that in any given pattern, the probability of receiving 1 and 0s is about the same. As such, we can equate $p(0) = p(1) = 0.5$. The second assumption involves the probability density function of the random process of received signals. For most systems not dominated by inter-symbol interference (ISI), we can assume the random process to be Gaussian with different average and variance for the 1 and 0 bits, i.e.,

$$p(m) = \frac{1}{\sigma_m \sqrt{2\pi}} \exp \left[-\frac{(I - I_m)^2}{2\sigma_m^2} \right] \quad (\text{B.2})$$

with I_m and σ_m corresponding to the average current and variance for 1 or 0 bits, depending on $m = 0$ or 1. Now we can evaluate the two conditional probabilities in Eq. (B.1) as

$$P(0/1) = \frac{1}{\sigma_1 \sqrt{2\pi}} \int_{-\infty}^{I_D} \exp \left[-\frac{(I - I_1)^2}{2\sigma_1^2} \right] dI \quad (\text{B.3})$$

$$P(1/0) = \frac{1}{\sigma_0 \sqrt{2\pi}} \int_{I_D}^{\infty} \exp \left[-\frac{(I - I_0)^2}{2\sigma_0^2} \right] dI, \quad (\text{B.4})$$

where I_D is the threshold setting between deciding whether a received signal is 1 or 0 bit. The above integral is in the form of the complementary error function defined by

$$\text{erfc} = \frac{2}{\sqrt{\pi}} \int_x^{\infty} \exp(-y^2) dy. \quad (\text{B.5})$$

Evaluating Eqs. (B.3)–(B.4) using Eq. (B.5) simplify Eq. (B.1) into

$$\text{BER} = \frac{1}{4} \left[\text{erfc} \left(\frac{I_1 - I_D}{\sigma_1 \sqrt{2}} \right) + \text{erfc} \left(\frac{I_D - I_0}{\sigma_0 \sqrt{2}} \right) \right]. \quad (\text{B.6})$$

It suffices to say that all system designers wish to minimize BER. Optimizing BER with respect to the only free variable left, I_D , yielded the following expression (creating our new parameter, Q)

$$\frac{I_1 - I_D}{\sigma_1} = \frac{I_D - I_0}{\sigma_0} \equiv Q. \quad (\text{B.7})$$

Under this condition, it is straight forward to write the decision threshold as

$$I_D = \frac{\sigma_0 I_1 + \sigma_1 I_0}{\sigma_0 + \sigma_1}, \quad (\text{B.8})$$

and Q as

$$Q = \frac{I_1 - I_0}{\sigma_1 + \sigma_0}. \quad (\text{B.9})$$

This reduces the equation for BER as follows,

$$\text{BER} = \frac{1}{2} \text{erfc} \left(\frac{Q}{\sqrt{2}} \right) \approx \frac{\exp(-Q^2/2)}{Q\sqrt{2\pi}}, \quad (\text{B.10})$$

where the approximated is reasonably accurate for $Q > 3$.